Master Thesis

New cleavable moieties for biodegradable photopolymers

performed at
Institute of Applied Synthetic Chemistry
TU Wien

under the supervision of

Univ. Prof. Dipl.-Ing. Dr.techn. Robert Liska

and

Univ.Ass. Dipl.-Ing. Dr.techn. Stefan Baudis

by

Barbara Dellago, BSc

01126632

Herzgasse 62/11, 1100 Wien

Vienna, 2019

DANKSAGUNG

An dieser Stelle möchte ich meinen Dank aussprechen, da mich während meiner Arbeit viele Personen begleitet und unterstützt haben.

Zuallererst möchte ich mich bei Prof. Robert Liska bedanken, da er mir Möglichkeit gegeben hat, meine Arbeit in seiner Arbeitsgruppe durchzuführen und mir es mir ermöglicht hat an diesem interessanten Thema zu arbeiten. Er hatte immer ein offenes Ohr und stets fachliche Ratschläge, wofür ich ihm danken möchte.

Weiteres gilt mein Dank dir, Stefan, für die kompetente Betreuung dieser Arbeit. Du hast durch produktive Denkanstöße einen wertvollen Beitrag zu dieser Arbeit geleistet.

Ein herzliches Dankeschön gebührt Labor H25, welches ein großartiges Arbeitsklima geschaffen hat. Insbesondere möchte ich dir, Hofi, danken. Du hast mich von Anfang an herzlichst aufgenommen, hast mich in meinen Hoch und Tiefs immer unterstützt und stets motivierende Worte für mich.

Johannes (Hansi), du hattest immer einen fachlichen Rat für mich und warst zu jeder Zeit hilfsbereit. Außerdem möchte ich mich für die vielen Gespräche, auch außerhalb des Arbeitsumfeldes, bedanken.

Der gesamten Arbeitsgruppe der FBMC möchte ich meinen riesigen Dank aussprechen. Ihr habt mich von Beginn an herzlich miteinbezogen und wart für zahlreiche, abwechslungsreiche und unvergessliche Abende verantwortlich. Ich bin froh, Teil dieser einzigartigen Arbeitsgruppe zu sein.

Des Weiteren möchte ich meiner ganzen Familie danken, die mich mein ganzes Leben unterstützt haben. Insbesondere meinem Bruder, der immer an meiner Seite stand und mich überhaupt erst der Chemie näherbrachte.

Zuletzt gebührt ein enormer Dank meinen Eltern, die mir immer alle Freiheiten und Möglichkeiten gegeben haben, das Studium und alle meine Träume zu verwirklichen. Euch widme ich diese Arbeit.

=

KURZFASSUNG

In den letzten Jahrzehnten hat sich gezeigt, dass die moderne Medizin zu einer deutlich höheren Lebenserwartung und besseren Lebensqualität führt. Dabei kommt es jedoch zu altersbedingten Problemen, wie zu Erkrankungen des Herz-Kreislauf-Systems aber auch des Bewegungsapparates. Aus diesem Grund ist es das Ziel der Medizintechnik und aktueller Biowissenschaften, solcher Erkrankungen durch Tissue Engineering (TE) mit künstlichen Materialien zu heilen. Solche Biomaterialien sollten eine gute Biokompatibilität sowie eine gute biologische Abbaubarkeit aufweisen.

Ein Großteil der bisher eingesetzten Biomaterialien basiert auf Polyestern. Diese sind jedoch als Materialien, insbesondere für Knochenersatzmaterialien, nur bedingt geeignet. Osteoklasten bauen Knochen unter sauren Bedingungen ab, wobei die oben genannten Ester jedoch unter diesen Bedingungen nur sehr langsam abbauen. Daher werden Alternativen für esterfunktionelle Biomaterialien gesucht, die eine verbesserte Bioabbaubarkeit unter saurem Milieu aufweisen.

In dieser Arbeit werden verschiedene Spiroacetale als Bausteine für solche Biomaterialien vorgestellt. Neben diesen, die bereits als recht stabil bekannt sind, wurden auch lineare und zyklische Acetale synthetisiert und hinsichtlich ihrem Abbau im Vergleich zu Estern bewertet. Die Abbauuntersuchungen an den Modellverbindungen zeigten, dass die letztgenannten Acetale ein 80 bis 200-mal rascheres Abbauverhalten als entsprechende Ester aufweisen. Basierend auf diesen Ergebnissen wurden photopolymerisierbare Monomere mit Acetalbausteinen entworfen, synthetisiert und mittels RT-NIR-Photorheologie untersucht. *In vitro* Studien zeigten eine rasche biologische Abbaubarkeit, welche das Potenzial von Acetalen in Biomaterialien zur Knochenregeneration bestätigten.

ABSTRACT

During the last decades, modern medicine leads to increased life expectancy and better quality of life. However, age-related problems such as cardiovascular diseases or problems of the musculoskeletal system arose. For this reason, the goal in life sciences, especially in the field of tissue engineering (TE) is to counteract these consequences with artificial materials. One of the main factors of these materials is that they should have a good biocompatibility as well as biodegradability.

A vast majority of biomaterials used up to now are based on polyesters. However, these are only useful to a limited extent as materials especially for bone graft substitutes. Osteoclasts degrade bone under acidic conditions and the aforementioned esters only cleave very slowly in this environment. Therefore, alternatives for ester functionalities, which show enhanced biodegradability under acidic conditions, are of interest.

Herein, we present different spiroacetals as building blocks for biomaterials, which are already known as quite stable. Linear as well as cyclic acetals were synthesized and evaluated regarding their degradation behavior compared to esters. The degradation studies of the model compounds show that the last mentioned acetals have a 80-200 times faster degradation behavior than accordingly esters. Based on these results, photopolymerizable monomers with acetal building blocks were designed, synthesized and investigated via RT-NIR photorheology. A high reactivity and subsequent biodegradability were confirmed in *in vitro* tests, which elucidates the potential of acetals in biomaterials for bone regeneration.

Table of Content

INTRODUCTION

1. Bone-Skeletal System

The human adult skeleton usually consists of between 206 and 213 bones. These can be divided into two areas, the so-called axial skeleton and the appendicular skeleton. [1, 2] The human skeleton is adapted to its function. It not only gives the body its stability, but also is responsible for the protection of the vital internal organs from injury and for mineral storage, especially calcium and phosphate. After all, the skeletal system is the production site for most blood cells. [2-4]

The bone consists of 50-70% extracellular matrix (ECM, largely mineralized) [3], organic matrix (20-40%), water (5-10%), lipids (<3%) and cells. Hydroxyapatite [$Ca_{10}(PO_4)_6(OH)_2$] is the most common mineral. [1, 5] In addition, small amounts of carbonates, magnesium and acidic phosphates with missing hydroxyl groups occur. The crystals of the hydroxyapatite are very small, less crystalline and carbonate-substituted, which makes them soluble and thus supports the mineral metabolism. [1] In contrast, the organic matrix consists of fibrous proteins. About 90% of these are composed of type I collagens and the remaining 10% of non-collagenous proteins. [5]

The bone composition (porosity, mineralization, etc.), but also the structural orientation (trabecular or cortical bone architecture, collagen fiber orientation, etc.) affect the mechanical properties of the bone. [6] The bone material properties are important to the strength of the bone and are responsible for the mechanical rigidity, load-bearing strength and stiffness. [6, 7] Elasticity and flexibility of the bone are given by the organic matrix. [1]

It makes sense to divide the more than 200 bones of the human bodies according to their shape in bone types: Long, short, flat and irregular bones. [2] These are divided again into two different bone types regardless of their shape. It is distinguished between compact (or cortical) and spongy (cancellous or trabecular) bone. As can be seen from the names, the difference between these two structures lies in their density but the chemical composition is identical. [2, 7] Cortical bone, which comprises 80% of the skeleton, has a porosity of 3 to 12%. Cancellous bone represents 20% of the skeletal mass and the porosity ranges from 50-90%. [1, 6] For larger bones, only the outer layer is made up of dense bone tissue. Their thickness varies depending on the functional requirement. On the other hand, the much larger portion inside

the bone consists of delicate trabeculae, the cancellous bone. [4] Both layers are made of osteons. These in turn consist of bundled osteoblasts and osteocytes, which are arranged around the Haversian canal. Volkmann's canals connect the osteons. [2] The general structure of bone separated in its layer and the organization of compact and spongy bone can be seen in Figure 1.

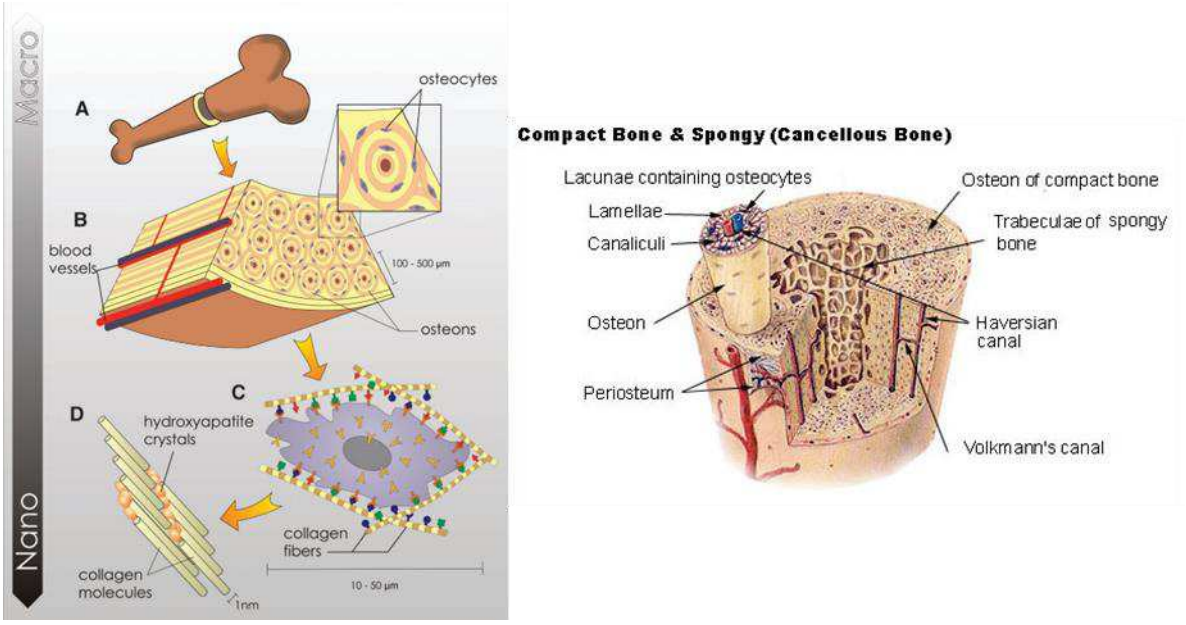

Figure 1: Hierarchical organization of bones from macro to nanoscales (left). Bone has a heavily calcified and compact outer layer (A), which includes a larger number of cylindrical Haversian systems or osteons (B). The resident cells are coated in cell membrane receptors that respond to specific binding sites (C) and the clearly defined nanoarchitecture of the surrounding extracellular matrix (D). [8] Compact and spongy bone (right). [2]

Regardless of the type of bone, bone is formed during growth, but also after damage. Four different cells are responsible for the degradation of damaged bone and bone formation, respectively. [2, 6] The **osteoblasts** are bone-forming cells. They are important for the construction and remodelling of the bone matrix. Collagen is formed, calcium phosphates and calcium carbonates are secreted into the interstitial space by these cells. The minerals crystallize along the collagen fibers due to their poor solubility. Mature bone cells are osteoblasts, which lose their cell division ability and are now called **osteocytes**. Finally, the tissue hardens and thus forms the finished, very resilient bone matrix. This process of ossification takes several months to many years depending on the type of bone. Because of this, children have a softer, more flexible skeleton compared to adults. [2, 4] The antagonists of the osteoblasts/osteocytes are the **osteoclasts**. They break down and resorb bone, resulting in reconstruction phases of the skeleton, e.g. in growth phases, but also in the healing phase after fractures. They are lowering the pH and this acidic environment helps to mobilize the

bone mineral. [9] Erosive pits on the bone surface, known as “Howship’s lacuna”, are created. [2, 4, 10-12]

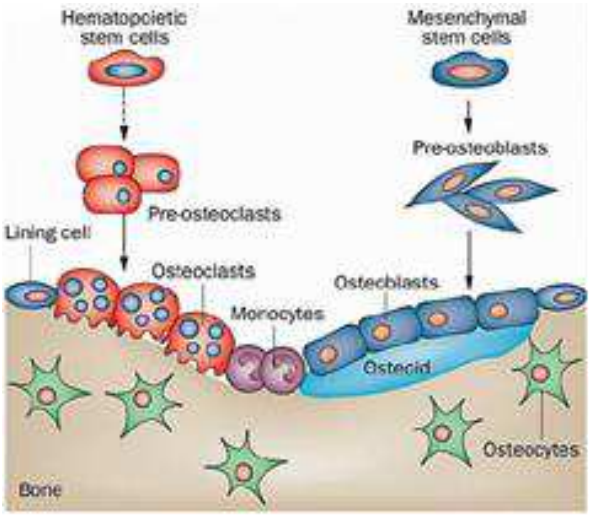

Figure 2: Classification of bone cells based on source, resorption, and formation function (right). [13]

The **bone-lining cells** are modified osteoblasts. They are attached on the inactive bone surface and form a protective layer. [14] These cells regulate the influx and efflux of mineral ions into and out of the bone. [15] Bone tissue is maintained by a dynamic equilibrium between osteoblasts and osteoclasts. The interaction and all the classifications are shown in Figure 2. The new bone is mechanically stronger and help to preserve bone strength. [2] Summarized, the remodeling of bone includes three consecutive phases: resorption, reversal, and formation. The first phase, the resorption phase, continues for about two weeks. There, the osteoclasts acidify the attached interface. The bone matrix gets dissolved and it results in deep cavities. Followed by the reversal phase, which last up to four to five weeks. During this phase, the resorbed surface is prepared for the following phase. The formation may continue for four months until the new bone structural unit is completely created. [3]

If the bone has been damaged, the natural bone formation can be additionally supported. The damage or loss of bone is treated by surgical reconstructions or mechanical devices. [16] If it is necessary to treat the loss of bone, implants can be used. These artificial bone grafts need specific characteristics, which are described by three essential elements (osteoinduction, osteoconduction and osseointegration). The process by which the osteogenesis is promoted is specified by osteoinduction. Osteoconduction describes the bone growth on a surface. Is a surface osteoconductive it permits growth on the surface or down into channels or into pores. [17] The final bonding between the host bone and grafting material during bone regeneration is called osseointegration. [18] A number of bone diseases, like fractures, arthritis,

osteoporosis, infections, but also tumors, lead to considerable loss of bone. Depending on the disorder and treatment methods, different types of transplantation can be considered. If the bone grafts are reused from one's own body, one speaks of **autografts**. **Allografts** are taken from a cadaver of the own species, whereas **xenografts** are taken from another species. Furthermore, there are **synthografts**, which are artificially made grafts. [5, 6] However, these transplantation methods involve some imperfect solutions. The procedure of harvesting bone grafts is complicated and painful. In addition, donor site morbidity can occur and surgical process need a long recovery period. [5] Additionally, autologous bone is a limited resource as it is not always of sufficient size. [18] Moreover, the time at which the grafts can be preserved outside the body, is limited. For allogeneic graft, the risk of disease transmission exists and there is no guarantee that the body will accept this graft. [16, 18] The acceptance is also for xenografts a huge problem. The surgical intervention and rejection can be reduced by using artificial grafts avoiding the need to harvest tissue. Moreover, the likelihood of rejection or transmission of disease is cut down, compared to allogeneic grafts. The health care costs can be reduced significantly with these materials. Therefore, they are a popular alternative.

2. Tissue Engineering and Regenerative Medicine (TERM)

The ideal bone substitute has biomimetic properties and is patient specific. Essential properties of the material are biocompatibility, osteoconductivity and degradability. However, most of the synthetic materials used, are poorly or not at all resorbable. [19] Nevertheless, synthetic devices provide the maximum scope for size and shape to fill bone voids. For the reconstruction or replacement of diseased or injured bone, the ideal synthetic bone devices have a number of important features: The scaffold should have a biocompatible matrix, which can be easily formed to the desired shape. In addition, the matrix should be porous in order to allow cells to colonize the scaffold and thus ensure bone formation. [20] As soon as the natural bone growth process begins, the transplanted bone is at least partially resorbed. Resorption can be enhanced by increased porosity of the implant material to allow vascularization of the new tissue. [5, 20]

Recent research place a scope on the development of new materials for tissue engineering application. Tissue engineering combines medicine, chemistry and mechanical engineering to develop functional substitutes for damaged tissue. [16, 21] This interdisciplinary field provides solutions to restore, maintain or improve the tissue function. [16]

To regenerate new tissue, three basic building blocks play together. These three are scaffolds, cells and (growth-) factors (Figure 3). [22] Living cells are manipulated to generate tissue substitutes. These substitutes can be implanted into the body to form new tissue. [23]

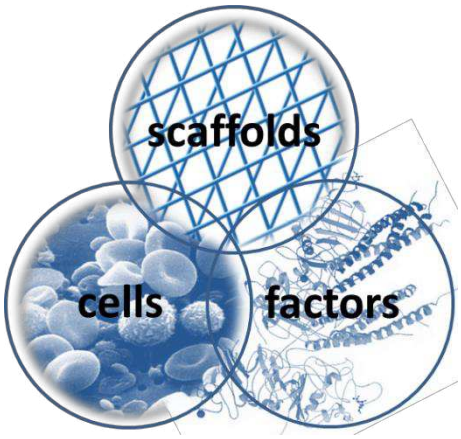

Figure 3: Three-pillar Model of Tissue Engineering

Materials are currently being designed with the aim of regulating tissue regeneration by various mechanisms, including control of specific cell-binding interactions, release of growth factors, controlled degradation and response to environmental influences. [24]

In vitro or *in vivo* seeding of cells on the scaffold is possible. In principle, *in vivo* seeding would be preferable, as this would mean that the scaffold only has to be implanted and the new tissue would grow automatically. However, this is a very rare case. For this reason, the scaffolds are seeded before implantation and the tissue can then grow under ideal conditions *in vitro*. Cell growth, cell adhesion and cell differentiation are influenced by signals and growth factors. They are also responsible for immune response. [16, 25, 26]

A bioactive scaffold consists of biomaterial that acts as a support template for the surrounding cells/tissues to improve growth and promote tissue regeneration in infected or damaged tissues. This tissue engineering system should meet the following important requirements: (1) The scaffold surface should allow both cell adhesion and growth. (2) The scaffold should have a reasonably porous structure, which in turn can improve cell seeding and diffusion of cells and nutrients throughout the structure. (3) The scaffold should provide appropriate mechanical support, i.e. it should serve as a shield for tissue to prevent damage by compressive or tensile forces. (4) The degradation product of the scaffold must not cause toxicity and should ideally be fully resorbed. (5) The degradation rate of the scaffold and the tissue regeneration process should be kept in a balanced state. The matrix should support the

construct as long as new tissue builds up and has fully compensated the defect. In the meantime, the matrix should slowly degrade (Figure 4). [5]

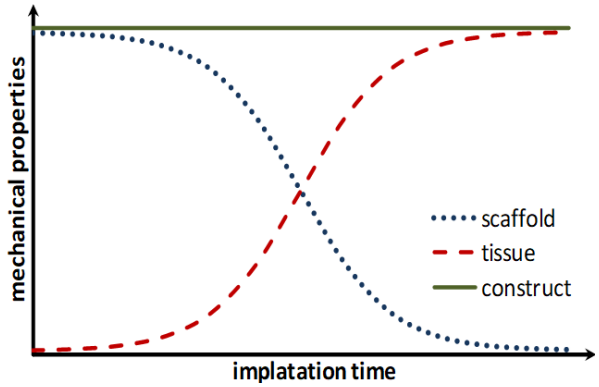

Figure 4: Degradation of a biodegradable scaffold (schematic and ideal) while tissue regeneration. [27]

The early stage of interaction between biomaterial and biological system was due to protein adsorption on the surface of the biomaterial. Although different biomaterials, such as polymers, ceramics and metallic components, have different surface properties, they have the same interaction mechanism with the protein adsorption of a biological system, but to different degrees. This initial stage has a significant influence on subsequent events in the material biological reactions. [28] In general, controlling the surface properties of the biomaterial and increasing and decreasing protein adsorption, respectively, is the key to improving the biocompatibility of a bioactive scaffold. [8]

Ceramic scaffold [29], bioactive glasses [30], metal-based materials [31], polymers [32] and composites [33] are examined as biomaterials. Polymeric fibers have been suggested to create the desired extracellular matrix (ECM)-like morphology. [31] These materials will be discussed in more detail in the following chapter of Biomaterials.

3. Biomaterials for Bone TE

In TE, a wide variety of biomaterials is currently used. Classical biomaterials are **ceramics**, **metals** and/or **polymers/composites**. [34]

As early as the 1960s, inorganic **bioglasses** appeared as biomaterials, which are a subclass of **ceramics**. Bioglasses have an amorphous structure and are the first materials with the ability to bind to bone tissue and promote cell growth, which means that they are bioactive. These include 45S5 Bioglass® and subsequently Novabone® and PerioGlas®. [35] These properties are ensured by the surface treatment with hydroxycarbonate apatite as coating material. [36, 37]

However, besides their positive properties they also have disadvantages. The mechanical properties, like fracture toughness and the flexural strength are poor. Ceramic implants are used due to their similarity to the natural apatite of human bone, hydroxyapatites, tricalcium phosphate or calcium phosphate are processed. [38, 39] Depending on the application, their properties range from inert, non-degradable and dense to degradable and porous materials. Ceramic implants made of β-tricalcium phosphates can be produced in porous and particulate form and are biodegradable under physiological conditions. All calcium phosphate-based materials show good biocompatibility due to their similarity to minerals in natural bone tissue. [40, 41] This favors their osteoconductivity and therefore a good ingrowth of the surrounding bone material into the scaffold. [42] However, the degradability rate is low and the mechanical properties are improper with their field of application.

Magnesium and its alloys are used as **metal implants**, if high fracture toughness and mechanical strength is needed. [43] Magnesium ions are involved in many essential metabolic processes in the human body. [35, 44] Furthermore, these implants underlie an *in vivo* corrosion and therefore degrade within 12-18 weeks. [45] Non-degradable metal implants are e.g. cobalt or titan. They can be found in orthopaedic applications, both as coating layers and as full volume implants. One disadvantage is that they can only be produced in limited geometries and complexity. Such metal implants are used for hips, knees or ankle replacements, but also as nails, plates or screws. [35] In order to ensure interaction between the surrounding tissue and the implant, these are usually coated with bioactive substances such as calcium phosphates. These layers additionally protect the implant against oxidation. [46]

Biodegradable **polymers** can be classified as natural or synthetic polymers depending on whether they originate from natural sources or if they are synthetically produced. Polysaccharides including hyaluronic acid, chitosan and alginate and proteins like collagen, gelatin and fibrin are examples of natural polymers. [47, 48] *Hyaluronic acid* is a polysaccharide, which occurs e.g. in large quantities in human tissue (skin, cartilage and vitreous humor) [49] and has been studied for biomaterials applications. [50, 51] This polymer is produced during early stage of wound healing by cells. For this reason, it is established for wound dressing applications. [52] In addition, *chitosan*, which originates from crustaceans exoskeletons and *alginate*, derived from brown algae are other prominent polysaccharides, which are used as wound dressing materials [53] and drug delivery devices. [54] Polymers derived from proteins and other amino acids are preferred biomaterials, as they are a major component of natural tissue.

Collagen is present in large quantities in the skin and muscle tissue and thus measures one of the largest protein proportions. For instance, Biobrane® and Alloderm® are established as wound-dressings, whereas Sulmycin® and Septocoll® are used for drug delivery for antibiotics. Collagen-based materials are used as biodegradable synthetic bone grafts (e.g. Collagraft®). [53] They have unique mechanical and biological properties and are enzymatically degradable. For collagen-based biomaterials, their mild immunogenicity is a disadvantage. [53] If collagen is denatured, *gelatin* is generated. Gelatin is also used in biomedical applications, for example for the preparation of biodegradable hydrogels [55, 56], microencapsulation of drugs [57] or as coating materials [58]. *Fibrin* sealant products are used for hemostasis and tissue sealing applications due to its great biocompatibility, biodegradability and injectability. Furthermore, several extracellular matrix proteins, such as fibronectin are present and affect cell adhesion and proliferation. [53]

Besides natural polymers, synthetic polymers are synthesized under controlled conditions and therefore, the mechanical and physical properties are reproducible. In addition, they have no immunogenicity and the risk for infections is low. In contrast to natural polymers, most of these polymers are degradable by hydrolytic cleavage of labile bonds in the backbone. Such labile bonds are e.g. ester, anhydride, carbonate bonds etc. Examples for synthetic polymers are poly(hydroxy acids) including poly(glycolic acid) (PGA), poly(lactic acid) (PLA) and poly(ε-caprolactone) (PCL), poly(carbonates) like poly(DTR carbonate) (DTR = desaminotyrosyl tyrosine alkyl ester) and poly(anhydrides) like poly(carboxyphenoxypropane) (PCCP). [59-61]

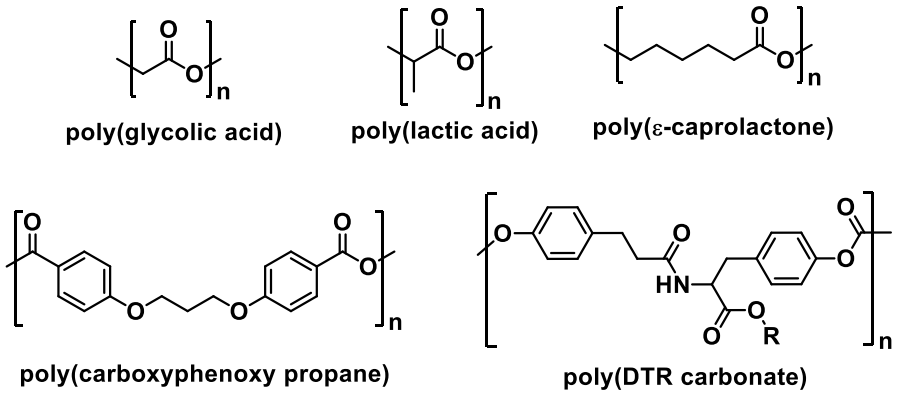

Figure 5: Chemical structures of selected biodegradable polymers.

The earliest and most extensively investigated class of synthetic biodegradable polymers are the poly(hydroxyl acids). A variety of monomers can be used and the polymers are synthesized via ring opening. PGA and PLA are well established and can be found in many medical

products. Besides polymers based on pure enantiomers (poly(D-lactic acid), poly(L-lactic acid)) also polymers from racemic mixture are available. Polymers containing only one enantiomer are crystalline and their elastic modulus is high. Therefore, they can be considered for load-bearing applications like orthopedic fixation devices. If a racemic mixture of monomer for polymerization is used, the material has amorphous character and therefore, the mechanical strength is lower, however the degradation rate is higher. Due to these characteristics, the polymer is rather used for drug delivery applications. Moreover, copolymers of PGA and PLA are used for surgical sutures with optimized mechanical properties and degradation rates. [53] The semicrystalline polyester PCL is also synthesized via ring opening polymerization, using ε-caprolactone as a quite cheap monomer. PCL is a suitable candidate for long-term drug delivery systems, due to its non-toxicity, high permeability for a large number of drugs and slow degradability. [62, 63] Moreover, polymer networks based on PCL have shape memory properties and are therefore reported for biomedical applications. [64] Above mentioned synthetic polymers degrade by a so-called bulk erosion. If acid-catalytic ester cleavage occurs in PCL, autocatalysis follows. The resulting carboxyl groups in turn catalyze the ester cleavage, resulting in an increase in the hydrolysis rate. [65]

The release of acidic degradation products cause a decrease of the pH value and this may lead to tissue necrosis. [66, 67] In contrast to bulk erosion mechanism, some polymers, e.g. poly(anhydrides) and poly(carbonates) in Figure 6 degrade via a surface erosion mechanism. There are some recent studies about the potential use of poly(carbonates) for bone tissue engineering[61, 68, 69] and furthermore for soft tissue applications. [70] Photocrosslinkable poly(anhydrides) are suitable for dentistry due to their high-strength and for orthopedic applications because of their tunable degradation behavior. [60, 71, 72]

poly(anhydrides) **poly(carbonates)**

Figure 6: Poly(anhydride) and poly(carbonates), which degrade via a surface erosion mechanism.

Other possible functionalities, which overcome the problem of acidic degradation products, are acetals. [73] In the simplest way, acetals are obtained by reaction of a carbonyl compound (aldehyde or ketone) with two hydroxyl groups, as seen in Scheme 2. The starting materials

are also the degradation products after hydrolysis. These primary degradation products of these biomaterials are expected to not affect local acidity. [73]

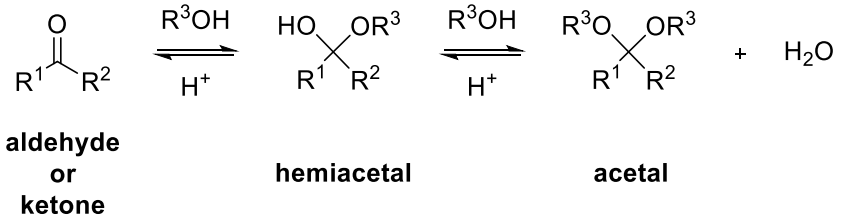

Scheme 1: Synthesis of an acetal by reaction of an aldehyde or ketone with an alcohol.

Since it is difficult to achieve the right properties with just one material, **composites** are also popular. Composites consist of at least two different materials. They are usually composed of a continuous phase (a synthetic or natural polymer) and a filler (often inorganic, particles, fibers, whiskers or lamellas). The aim is to combine stiffness and toughness. [37] They are categorized by their combination of materials (matrix/filler). [35]

- organic/organic (e.g. synthetic polymers reinforced with natural fibers)
- organic/inorganic (e.g. polymer matrix with inorganic fibers, particles, etc.)
- inorganic/inorganic (e.g. mixed inorganic minerals, although not a composite in closest sense)

The processing of the materials for the devices in TE can be done in many different ways, for example by milling. However, one focus of this work is on the Additive Manufacturing Technology.

4. Additive Manufacturing Technologies

Additive Manufacturing Technology (AMT), also known as Solid Freeform Fabrication (SFF) is a method to fabricate complex 3D structures with defined and interconnected pores without the use of molds. By selectively adding material, normally layer by layer as specified by a CAD (computer-aided design) file, objects can be build. The process of CAD model via computer processed slicing to the real model is shown in Figure 7.

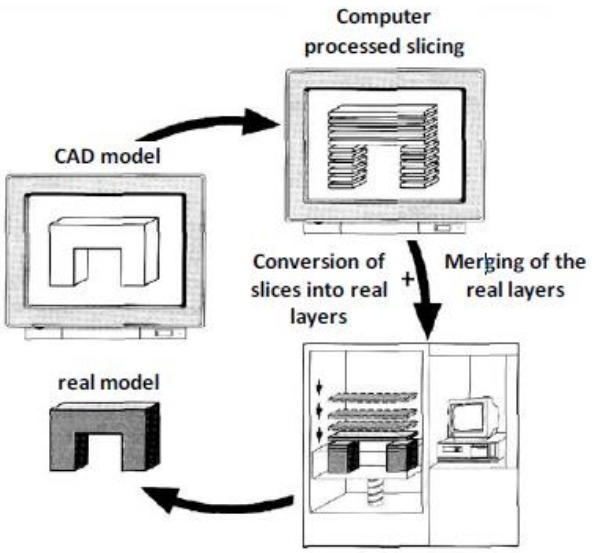

Figure 7: Principle of the layer-by-layer AMT techniques. [74]

There is no need for tools or masks for fabrication of parts, which are the key benefits compared to traditional manufacturing methods. Which means, that the shape complexity is unlimited.

Leong *et al.* [75] and Hutmacher *et al.* [76] give a good overview on additive manufacturing technologies used in TE.

AMT methods can be divided into three categories, depending on their solid material forming mechanism, either *melt and dissolution techniques, particle bonding techniques,* or *photopolymerization of photosensitive resins,* which are discussed in the next chapters.

4.1. Melt and dissolution deposition systems

While moving across the plane of the layer cross-section, each layer is created by extrusion and deposition of a strand material through an orifice. For the melt deposition method, the material solidifies and adheres to the previous layer by cooling down. A complex 3D-structure is obtained, if the process is repeated. By controlling the spacing between adjacent filaments, porosity in the horizontal xy-plane is created. The vertical z gap is formed by depositing the subsequent layer of filaments at an angle with respect to the previous layer. In this way, structures with defined porosity can be obtained. Another special mode is the Robocasting or direct ink writing (DIW). In this case, a ceramic slurry is extruded through a nozzle. The sheer thinning behaviour is used to keep the shape of the material. An advantage is that heating or time to cooling down is not necessary for solidification. [77]

4.2. Particle bonding techniques

The particle bonding method is based on inkjet printing of a binder compound. Ceramic powders or particles are sticked together by this binder. Afterwards, they are sintered, which yields in dense ceramic parts. There, the particles are selectively bonded in thin layers of powder material. During fabrication, the unprocessed powder acts as a support for the structured object, which allows for shaping complex and overhanging features. The structure is removed from the bed of unbonded powder after all layers are completed. Generally, the structuring of every powder material is possible, no matter if it is a single compound powder or a blend of materials. The size of the droplets and particles define the resolution. In addition, the latter also limits the size of macropores that can be built. The space between the granules of powder define the rough surface and microporosity. These features favor cell adhesion and viability. [78]

4.3. Light based AMT

Beside the techniques mentioned above, a range of 3D printing methods is based on curing of liquid resins by photopolymerization (light-based AMTs). The mechanism of radical photopolymerization is described in detail in Chapter 5. Several advantages of photopolymerization, like spatiotemporal control of polymerization, fast curing rates at moderate temperatures and minimal heat production make photopolymerization very favourable for 3D printing applications. [79]

The light-based AMT works by either selective deposition or selective irradiation of the photo-curable resin as seen in Figure 8. [80]

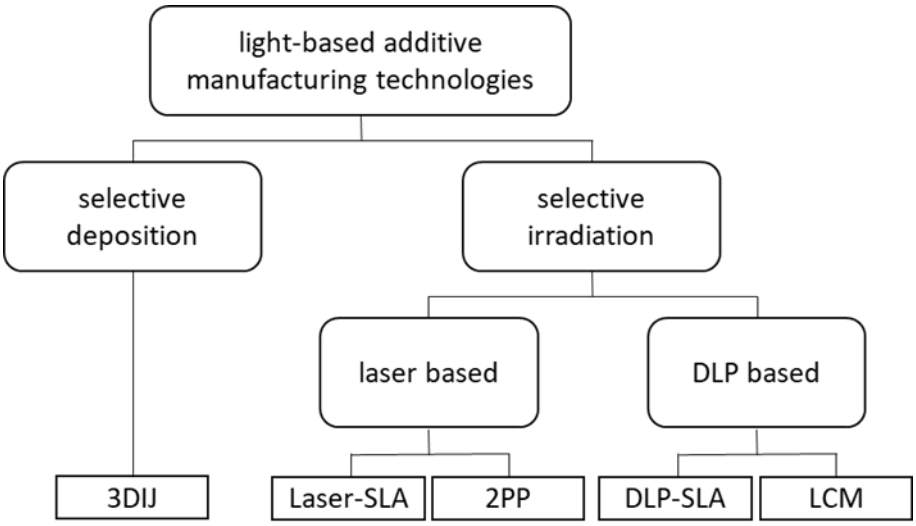

Figure 8: Light-based 3D printing technologies.

4.3.1. Selective Deposition

3D inkjet printing (3DIJ) is based on selective deposition. This process uses photosensitive resins, which are applied dropwise and are assembled by nozzles of a printer head. Instantly the layer is irradiated with UV light, crosslinking takes place and the resin is cured. The platform is lowered and the process is repeated. This method opens the possibility to generate multi-materials, but a huge disadvantage is the need of considerable amounts of support material for cavities and overhanging structures. Afterwards, the support material has to be removed mechanically. Moreover, the surface is of poor quality. In literature, the application of this method for orthopaedic procedures is described, but not for tissue engineering in particular. [81, 82] A schematic illustration of this method is shown in Figure 9 A.

4.3.2. Selective Irradiation

Technologies, which are based on selective irradiation (**lithography-based techniques**), can be divided into three basic methods with different irradiation schemes: (1) The laser based stereolithography (**Laser-SLA**), (2) the digital light processing-based stereolithography (**DLP-SLA**) and (3) two-photon polymerization (**2PP**).

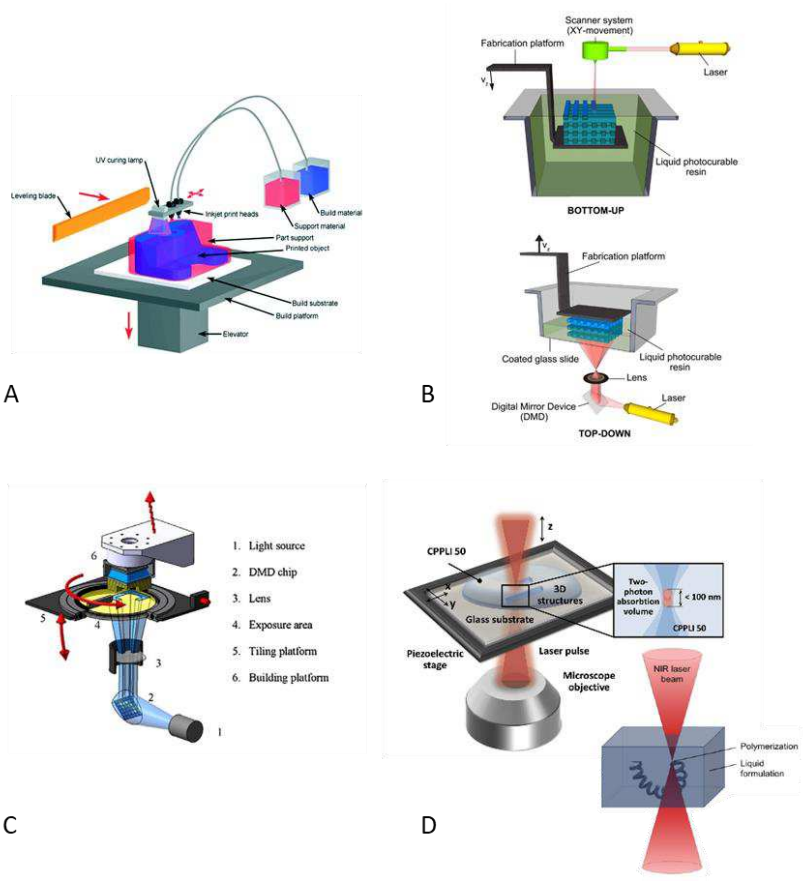

Figure 9: Schematic setup of a photopolymer based inkjet printer (Copyright © 2008 CustomPartNet) (A) [83], bottom-up and top-down SLA setups (B) [84], lithography-based ceramic manufacturing method (LCM) (C) [85], and 2PP setting (D). [86, 87]

4.3.2.1. Laser-SLA

Laser-SLA employs a UV laser beam to initiate photopolymerization. The beam scans over the surface - polymerization takes place, where the beam hits the photocurable resin. After the material is polymerized, the fabrication platform moves stepwise in z-direction. [84] For such systems, two different arrangements are possible, either bottom-up or conventional SLA setup (here, the light is applied on the surface of the photosensitive material), or the top-down or inverted SLA setup (the resin is irradiated through a transparent bottom plate) as seen in Figure 9 B. [84, 88] After irradiation, the platform is moved in z-direction (lowered or lifted, respectively) and a new layer of the liquid resin is formed. The process is repeated for all layers of the construct. Due to its special arrangement, the top-down setting avoids most of the inhibition of polymerization by ambient oxygen, moreover, this setting enables an economical material management as only low material amounts are needed for the process and not a full vat as it is the case for bottom-up methods. However, care has to be taken in

order to make sure that the constructs adheres to the base plate but not on the transparent bottom plate.

4.3.2.2. DLP-SLA

DLP-SLA, in contrast, employs a digital mirror device in a LED light engine for a pixel-wise simultaneous irradiation of the whole cross section. [85] While these system may speed up the process (esp. for large parts and cross sections, respectively), the laser-based process generally allows higher printing resolutions. A special DLP-SLA method is lithography-based ceramic manufacturing (LCM). A rotatable vat and a wiper blade are added to the arrangements (Figure 9 C), which enable processing of high-viscous slurries, which contain ceramic particles. [89] The photosensitive ceramic suspension solidifies during 3D printing and green parts are obtained. The organic matrix (binder) is removed thermally, before the parts are sintered. Thereby, the final dense ceramic parts are obtainable.

4.3.2.3. 2PP

All methods mentioned so far are so-called 2½D methods (indicating the layer-wise manufacturing mode); with 2PP, real 3D writing is realizable. [90-92] Here, polymerization is initiated by near-infrared (NIR) femtosecond laser pulses. A suitable photoinitiator absorbs two photons in the focal point of the laser. These two photons (each half of the energy, which corresponds to the mentioned NIR light) are absorbed simultaneously. [93] Polymerization takes place only in the focal area, but not along the path of the laser beam through the resin, where the photon density is too low for the two-photon process. [94]

5. Photopolymerization

As mentioned before, the above-described light-based AMT techniques are using the principle of photopolymerization. The mechanism of radical photopolymerization is divided in three distinct reaction steps as illustrated in Figure 10. During the initiation step, a photoinitiator (PI) forms free radicals (X·) due to excitation with photons from either the UV-, visible (VIS)- or near-infrared (NIR) range of the electromagnetic spectrum. Which light source is used, is depending on the initiator system. The formed radicals attach to a reactive, polymerizable monomer and the polymerization chain reaction starts. During propagation, monomer is

added repeatedly to the reactive chain end (XCHR·). During this step, the resin solidifies and a polymeric material is generated. Polymerization will end, when two radicals recombine, disproportionate *via* hydrogen abstraction or no more monomer is available.

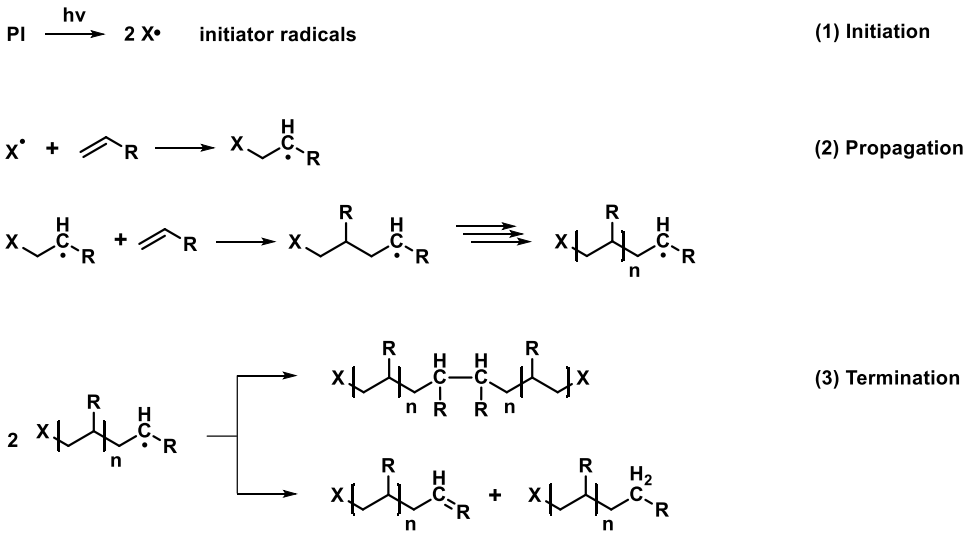

Figure 10: Steps of radical photopolymerization.

The photoinitiator is the key component for curing and influences the properties of the resulting polymer. It absorbs radiation energy from the used light source and converts it into chemical energy, which leads to a cleavage of the molecule and formation of radicals. Depending on the desired wavelength, different photoinitiators can be used. There are two types of photoinitiators, depending on their initiation mechanisms. The so called Type I PI forms active radicals by α-cleavage. The described α-cleavage of the Type I initiator usually occurs next to a α-carbonyl group and is depicted in Figure 11.

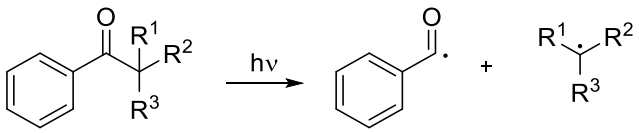

Figure 11: Cleavage of Type I photoinitiator.

The two resulting radicals can initiate the polymerization. Figure 12 shows two different Type I PIs, Irgacure 819® and Ivocerin®.

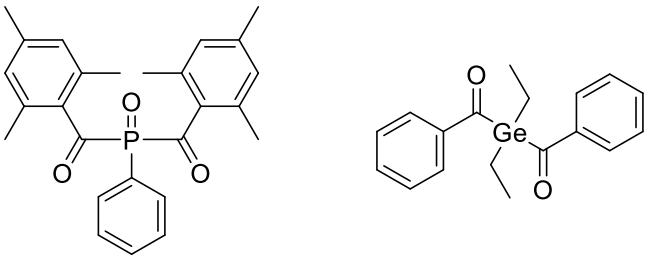

Figure 12: Type I photoinitiator Irgacure 819® (left) and Ivocerin® (right).

Type II PIs are bimolecular systems, consisting of an initiator and a co-initiator. Here, hydrogen abstraction or electron/proton transfer lead to the formation of radicals. [95] Benzophenone, camphor quinones or thioxanthones are typical examples for Type II PIs. Suitable co-initiators are, for instance amines, which transfer an electron to the initiator, in the first step. Thereby, a radical ion pair is formed. In the second step, the reactive radical is generated *via* proton transfer. In dental applications, the typically bimolecular system of camphor quinone (CQ) and 4-*N*,*N*-dimethylaminobenzoate (DMAB), is used. The according mechanism of this Type II PI system is shown in Figure 13. [96]

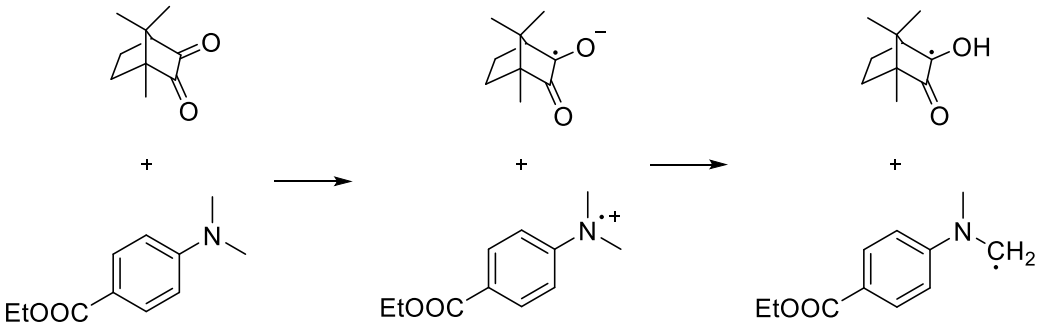

Figure 13: Mechanism of radical generation in Type II photoinitiators.

Atmospheric oxygen can cause inhibition of any radical polymerization. Oxygen can attach to the reactive ends or a hydrogen abstraction is induced. This leads to the termination of the propagation reaction, which causes a lower double bond conversion. This effect may be crucial in biomedical applications, as the unreacted monomer can leach out of the polymer and results in undesired toxic effects.

Often, high molecular weight photopolymer resins are used for technical applications. These contain a range of functional groups in order to adjust the properties of the material. For instance, unsaturated polyesters, (meth)acrylated polyesters, polyethers, epoxy resins and polyurethanes are commonly used photopolymer precursors (Figure 14).

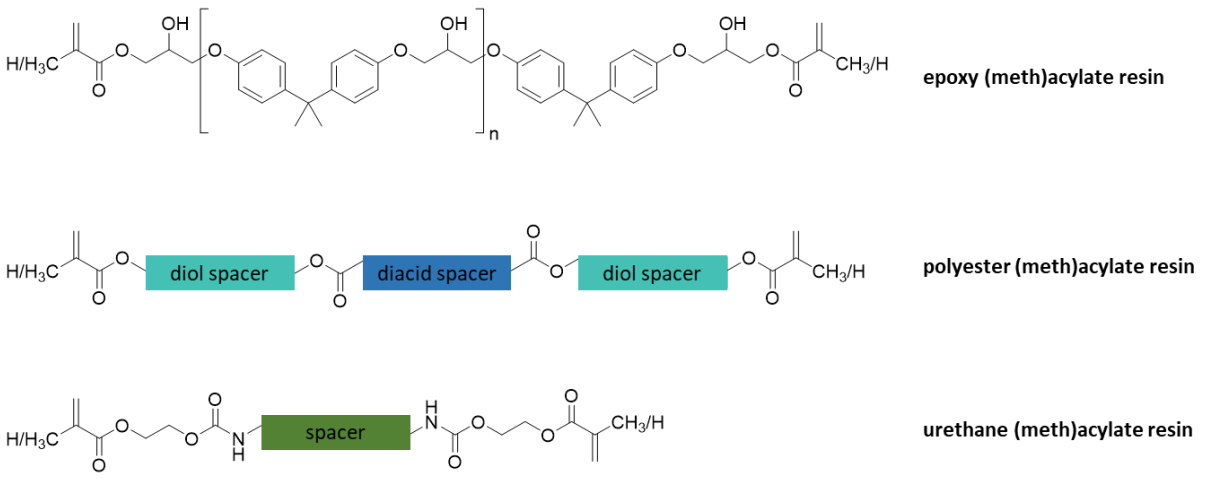

Figure 14: Examples for photopolymer resins with functional groups.

Bisphenol A is the most commonly used basis for *epoxy (meth)acrylate* resins. Due to its aromatic ring structure and the additional π/π-stacking, very hard but brittle materials are obtained. Resins with a wide spectrum from soft to hard, can be obtained with different spacers of *polyester (meth)acrylates* and *urethane (meth)acrylates*. In the case of urethanes, this group can form strong (intermolecular) hydrogen bonds, which lead to (micro)phase separation and thus have an additional effect on the mechanical properties of the material. Most commonly, (meth)acrylates are used as reactive groups for photopolymerization. Acrylates have a higher reactivity; however, methacrylates show a better biocompatibility according their lower cytotoxicity. [97]

Due to their high molecular weight and the functional groups, these monomers often show high viscosities. For this reason, low molecular weight monomers are added to the formulations to decrease the viscosity and to make the resin processable. They are also being referred as reactive diluents. Those influence the flexibility and elasticity of the cured material, but also the final crosslink-density and therefore the rigidity of the material. Examples for such diluents (Figure 15) are 1,4-butanediol diacrylate (BDDA), 1,6-hexandiol diacrylate (HDDA) or trimethylolpropane triacylate (TTA). [98]

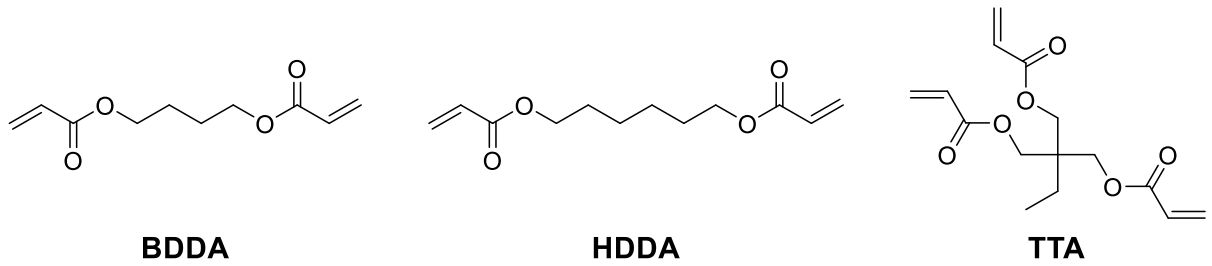

Figure 15: Common reactive diluents for photopolymerization.

OBJECTIVE

In modern times, medical care has significantly improved providing us with continuously increasing life expectancy. However, this results also in more age-related diseases, for example of joints and bones. The treatment of those diseases and the assistance of the healing process is done with suitable temporary substitutes. One important scope of recent research in the field is the development of new materials for bone scaffolds in tissue engineering (TE). The ideal bone substitute is biomimetic and could be designed patient specific. Essential properties of those materials are for instance biocompatibility and degradability. For bone replacement materials, the degradation behavior under acidic conditions (pH of about 4.5, adapted to the acidic environment of osteoclasts in bone) is preferable. However, polyesters, commonly used as biomaterials for TE only cleave very slowly under these conditions. Another huge disadvantage are the acidic degradation products, which lead to bulk erosion and can harm the surrounding tissue. Therefore, new cleavable moieties have to be considered, which can overcome these problems. Acetals are known to be stable under neutral and basic environment, but degrade hydrolytically under acidic conditions. Furthermore, primary degradation products of these biomaterials are expected to not affect local acidity.

The aim of this work is to consider hydroxyl terminated acetal-based building blocks for further monomer and polymer syntheses and for subsequent application in bone TE *via* structuring by light based additive manufacturing technology (AMT) methods. As starting point, spiroacetals (Figure 16), with terminal hydroxyl functionality and different aromatic substituents should be examined. Spiroacetals are chosen for the first studies, as they are known to be quite stable also under acidic conditions and therefore synthesis and purification should not lead to many difficulties. [99]

Figure 16: General structure of a spiroacetal unit, highlighted in red.

With a small spiroacetal model molecule, optimal reaction conditions for further synthesis should be studied. Moreover, this molecule should be used for the first degradation studies of spiroacetal-based compounds in comparison to ester based reference material. Based on these findings, oligomeric spiroacetals based on polyesters and polyacetals should be synthesized as precursor for photopolymerizable monomers.

In addition to the spiroacetals, linear and cyclic acetals (Figure 17) should be considered as they are expected to undergo faster degradation. [100, 101]

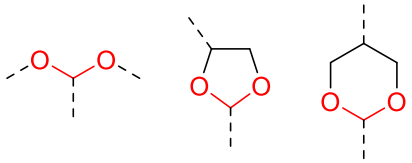

Figure 17: General structure of a linear acetal unit and cyclic acetal units (five- and six membered ring structure), highlighted in red.

The degradability of these acetals should be studied by ^{1}H-NMR spectroscopy and compared to the spiroacetal model molecule and polyester references. Furthermore, polymerizable functionalities can be attached to get suitable monomers for photopolymerization based AMT. The reactivity of these building blocks in photopolymerizable formulations with varying network densities should be studied *via* RT-FTIR-Photorheology. In addition to the synthesis and reactivity studies, the behavior of these polymer networks in aqueous environment can be examined *via* swelling tests.

STATE OF THE ART

Due to the increasing demands in healthcare, biomaterials have gained increasing interest in the last decade. Biodegradable polymeric materials are preferred as therapeutic devices, drug delivery vehicles or as scaffolds for Tissue engineering (TE) (3D porous structures). Biodegradable devices are believed to support selfrepair and regeneration of damaged tissue, organs or functions of the human body. [53] Important properties of biodegradable biomaterials are e.g. the non-toxic response upon implantation in the body and the mechanical properties that have to meet the requirements of the fief of application. Moreover, the degradation time of the device has to match the healing or regeneration process. It is important to note that the degradation products must not be toxic and have to be metabolized and cleared from the body.

Biodegradable polymers are divided according their degradation mode of sensitive bonds in the polymer. [60] They can degrade enzymatically or hydrolytically. Natural polymers mostly undergo an enzymatically degradation. Such biomaterials based on enzymatically degradable polymers include proteins, such as collagen and fibrin, and polysaccharides, like hyaluronic acid, chitosan and alginate. [53] Beside the enzymatically degradable polymers, there are the hydrolytically cleaved ones used as biomaterials. These have hydrolytically labile chemical bonds in their polymer back bone. For instance, esters, anhydrides, carbonates and to a less extent, amides and urethanes can be considered as labile functional groups, which are susceptible for hydrolysis. [102] Biomaterials, which are hydrolytically degradable, are of great interest to this work, due to their applicability as bone replacement material. The degradability under acidic conditions is necessary, because different cell types play an important role to restore damaged bone. There are the osteoblasts, which are bone-forming cells and responsible for the construction and remodeling of the bone matrix. Cells, which lost their cell division ability and are now mature bone cells, are called osteocytes. The reason for the demand of biomaterials, which are degradable under acidic environment are the osteoclasts. [2, 6] There, preosteoclasts form sealing zones by binding to the bone matrix beneath cells. They interact with RGD (arginine, glycine and asparagine)- containing peptides in matrix proteins *via* their receptors in their cell membrane. [1] *Via* H^+-ATPase proton pumps and chloride channels in their cell membrane, osteoclasts can secrete hydrogen ions, thereby lowering the pH to approximately 4.5 (Figure 18). This acidic environment helps to mobilize

the bone mineral. [9] While resorbing, the osteoclasts release tartrate-resistant acid phosphatase, matrix metalloproteinase 9, gelatinase and cathepsin K. [103] These results in the digesting of the organic matrix. [1] Erosive pits on the bone surface, known as "Howship's lacuna", are created. [2, 4, 10-12]

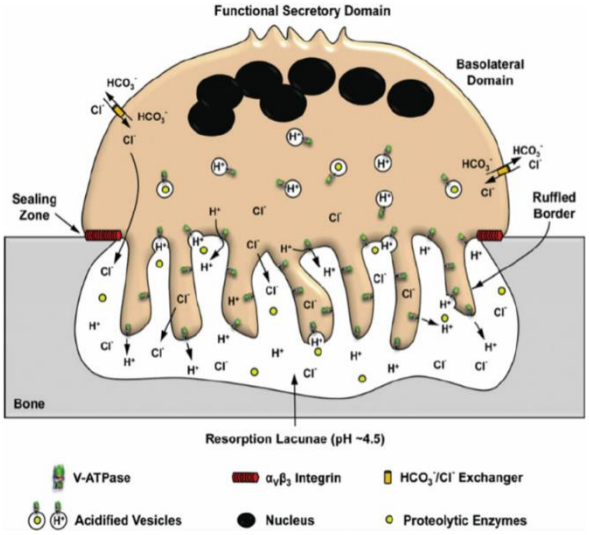

Figure 18: Illustration of the structure and function of active osteoclast. [104]

A number of functional groups, which cleave under acidic environment, have already been mentioned above. Unfortunately, some of them, e.g. polyester, degrade rather slowly and form acidic products, which may harm the surrounding tissue. This is followed by an accelerated degradation of the polymers and fast loss of mechanical properties. Therefore, biomaterials based on acetal moieties have been considered to overcome this disadvantage. [73] Primary degradation products of these biomaterials are expected to not affect local acidity. [73] The term acetal include all diethers of geminal diols and does not distinguish between acetals derived from aldehydes or from ketones. [105, 106] In the simplest way, acetals are obtained by reaction of a carbonyl compound (aldehyde or ketone) with two hydroxyl groups, as seen in Scheme 2. Ketals are acetals, which are formed by reaction of ketones, but the term has been reinstated as a subclass of acetals. [106]

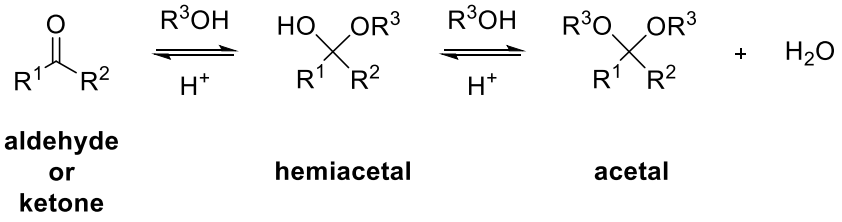

Scheme 2: Synthesis of an acetal by reaction of an aldehyde or ketone with an alcohol.

Well-known natural polymers such as cellulose or starch contain also acetal units (Figure 19). Therefore, it is one of the most common degradable bonds in biopolymers. [99]

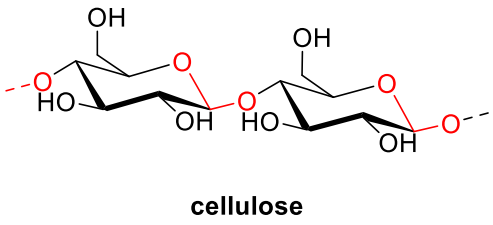

cellulose

Figure 19: Cellulose as example for biopolymers (polysaccharide), containing acetal units (highlighted in red).

In general, acetals are divided into categories based on their general structure (Figure 20): spiroacetals, cyclic acetals (different ring sizes) and linear acetals.

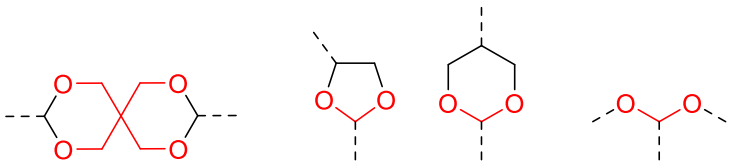

spiro **cyclic** **linear**

Figure 20: Differentiation of acetals due to their structure.

Acetals are usually prepared both with protic acids such as hydrochloric acid [107], sulfonic acid [108], acetic acid, oxalic acid, p-toluenesulfonic acid [107] and Lewis acids (e.g. zinc chloride). [109] However, these catalysts may have several drawbacks, such as secondary reactions (oxidation, etherification, and dehydration), corrosion of equipment, contamination of the environment, low reactivity or their non-recoverability. [109]

The first class, the **spiroacetals** can be synthesized with polyols, like pentaerythritol and two equivalents of an appropriate carbonyl compound (Scheme 3). [110]

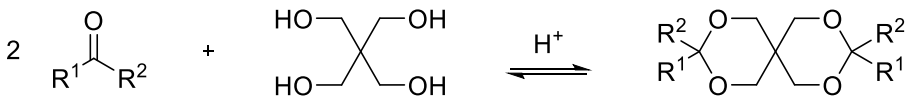

aldehyde or ketone **pentaerythritol** **spiroacetal unit**

Scheme 3: Synthesis of a spiroacetal by reaction of an aldehyde or ketone with pentaerythritol.

For such spiroacetals, different catalysts were especially designed to circumvent the above described problems in synthesis. One example is cellulose sulfuric acid, which can be easily prepared from cellulose with chlorosulfonic acid. [111] Both starting materials are inexpensive and excellent yields in the reaction of pentaerythritol with aldehydes and ketones under solvent-free conditions are reported. [112] Moreover, the work up is simple and the catalyst is biodegradable. [112] Then there are catalysts reported, which work solvent-free and are activated by microwave irradiation. Acid activated clay catalyst [113], tungstophosphoric acid (HPA, e.g. for 4-*tert*-butyl cyclohexanone) [114], silica sulfate (e.g. for 4-chlorobenzaldehyde) [109] or anhydrous ferrous sulfate [115] are examples for such catalysts. Advantages of these catalysts lie therein that under the before mentioned solvent-free conditions a significant decrease in reaction time can be achieved. In addition, the work-up is considerably simplified and costs are reduced. [109, 113, 114, 115] Another catalyst is based on glycerol. It was used for the preparation of pentaerythritol diacetals by condensation of pentaerythritol with aromatic aldehydes in toluene at 80 °C in quantitative yields. [116]

Typical examples for spiroacetals from literature (Figure 21) are low molecular weight spiroacetals (top) or a wholly aromatic polyspiroacetal having flexible side chains [110] (bottom).

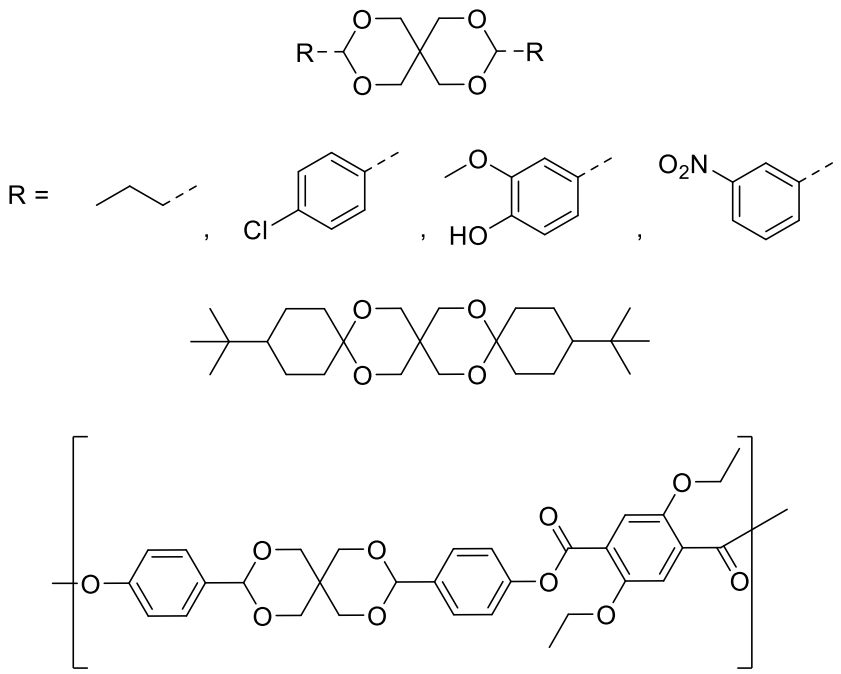

Figure 21: Examples for low molecular weight spiroacetals and a wholly aromatic polyspiroacetal having flexible side chains [110] (bottom).

Spiroacetals, generated with pentaerythritol are applied as plasticizers and vulcanizers [107, 112] and are also used for protection of aldehydes and ketones. [109] Moreover, they can be applied as physiologically active substance. [112] They show excellent mechanical strength, good hardness and water- and heat resistance. Furthermore, *polyspiroacetals* (Figure 21, bottom) were described. They have rod-like chain structures, which might be considered as high performance fibers. However, they are hardly processable. A phenylene group directly connected to a spiroacetal moiety results in insolubility and infusibility due to their polymer backbone stiffness. [110] Polymers containing these groups were investigated for their hydrolytic stability. These show no significant degradation under acidic conditions and elevated temperatures during the period of investigation. [117]

In case of certain 1,2- or 1,3- polyols as hydroxyl group containing building blocks combined with a carbonyl group, **cyclic acetals** (five-, six membered rings and all combinations) are usually formed. Scheme 4 shows a bonding of 5-fluorouridine (an anticancer compound), containing a syn-1,2 diol, to an aromatic aldehyde via formation of a cyclic acetal using pTsOH-catalyst. Both cis- and trans-diastereomers were produced in approximately a 1:1 ratio. [118] These pH sensitive molecules are used in drug carriers as they release their biologically active substance, due to pH change of diseased tissue. [119]

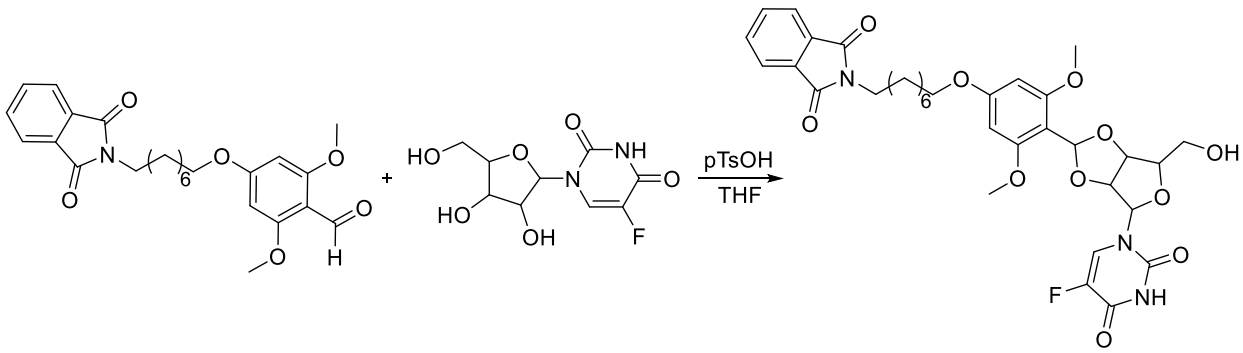

Scheme 4: Synthesis of a cyclic acetal conjugate based on a 2,6-dimethoxy-4-hydroxybenzaldehyde-derivate and 5-fluorouridine as starting material for a further activated polymer. [118]

Polyacetals are of great interest as they degrade under acidic conditions to generate non-toxic degradation products such as alcohols and aldehydes or ketones. [120] Figure 22 (left) depicts another example for a low molecular weight 5-membered acetal. It is used to create degradable hyperbranched polyglycerols (HPGs). Therefore, an anionic ring opening copolymerization of glycidol with the ketal-containing epoxide monomer is implemented.

These hyperbranched networks are important in numerous biomedical applications, like drug delivery, bio-conjugation and tissue engineering. [120]

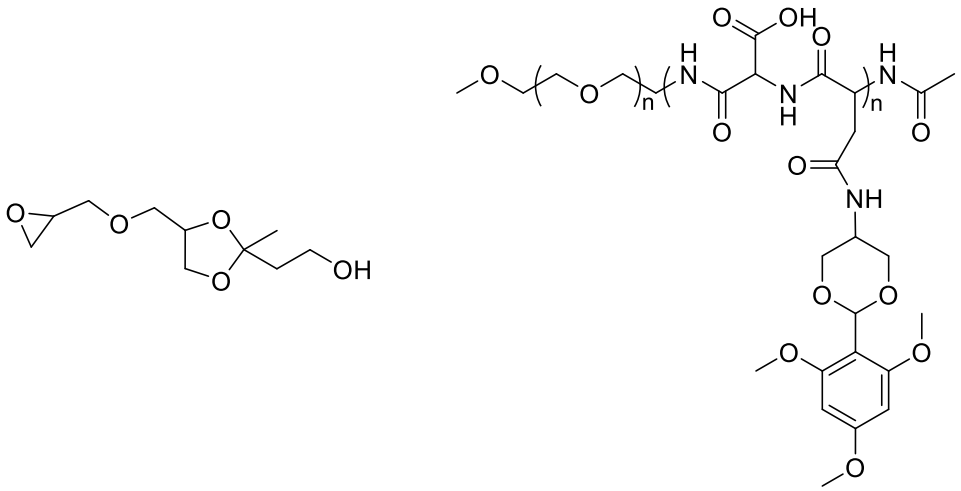

Figure 22: Examples of a low molecular weight 5-membered acetal (left) [120] and a polymer with a 6-membered acetal unit (right) [121].

On the right side of Figure 22, a cyclic benzylidene acetal is shown. This kind of acetal was chosen as it shows several favorable characteristics. First, the aromatic ring is hydrophobic and therefore it will contribute to micelle formation. [118, 121] Moreover, it can mask the polarity of a bonded copolymer and this leads to a better solubility change when the copolymer will later be hydrolyzed. [121] Such properties are used during the past decade in various biomedical applications such as drug delivery (therapeutic or other bioactive agents) [122] and tissue engineering. In detail, an endolysosomal release of therapeutic payloads such as proteins, nucleic acids and anti-inflammatory agents as well as targeting the acidic environment of the tumor cells. [120] It is important to control the drug release over the time or at a specific location. [123] Inflammatory and tumor tissue (pH of about 6.8) as well as in lysosomal and endosomal compartments of cells (pH of 5 to 6) provide a favorable environment for the release. [121] The polymer based delivery vehicles are triggered by the pH-change of the medium, the acetal cleaves and due to this, the polymers release the small bioactive molecules. Such an example of degradation for drug release of small bioactive molecules is shown in Figure 23. [122]

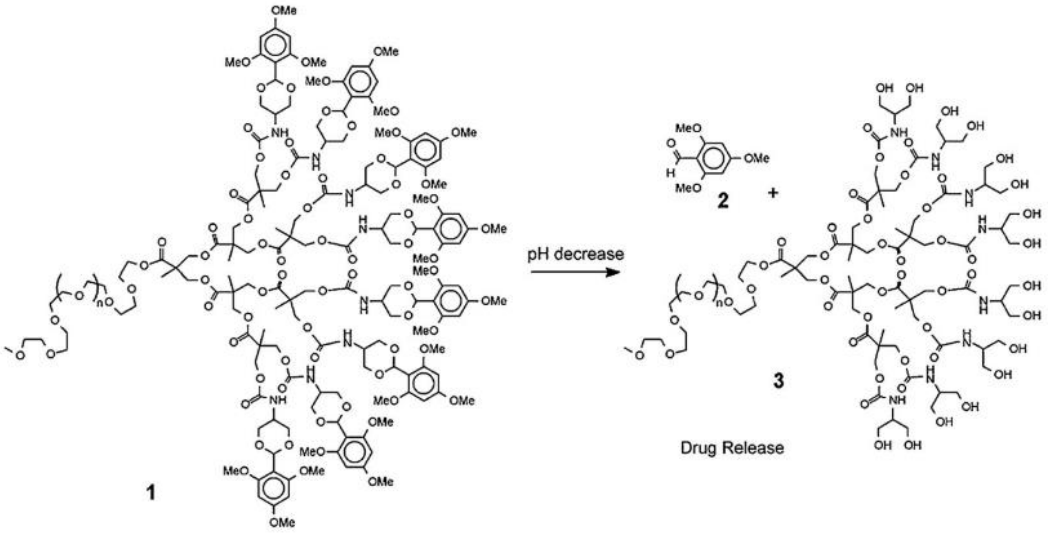

Figure 23: Drug delivery vehicle triggered by pH-change of the medium and release of small bioactive molecules. [123]

Beside spiro- and cyclic acetals, also **linear acetals** are presented in literature. [124, 125] Figure 24 shows some examples of linear acetals, which can be used as cross-linker for micelles stabilization.

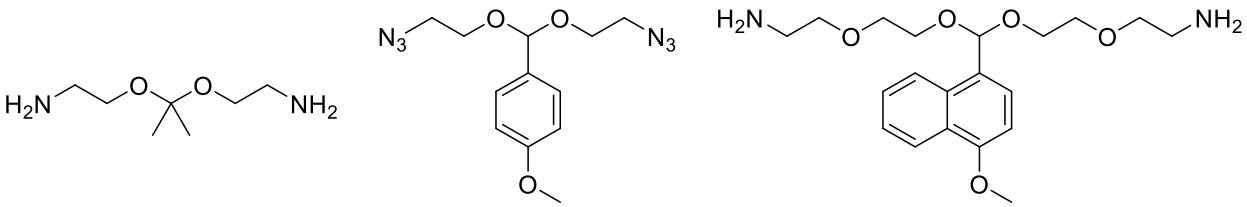

Figure 24: Linear acetal cross-linkers (general structure highlighted in red) used for micelles stabilization. [124]

Other examples in literature [125] are *linear polyacetals*. They can be formed by conversion of a linear diol, like PEG and an aldehyde as lilial (Scheme 5). The chain length of PEG prevents the formation of cyclic acetals. [125] This polymer is used as "profragrances" in food and cosmetic field.

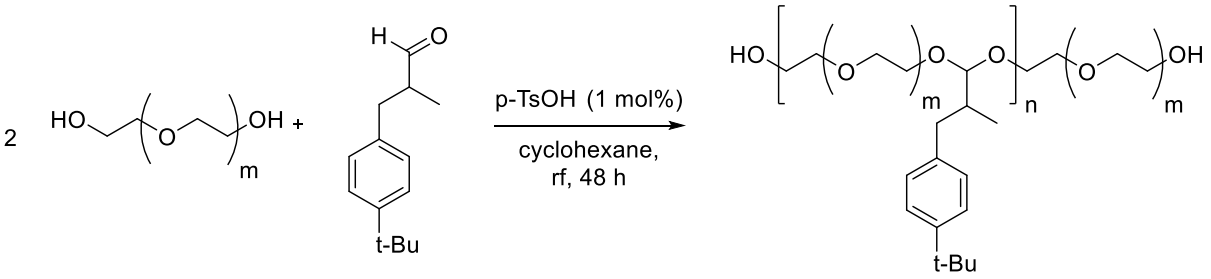

Scheme 5: Synthesis of polyacetal by polycondensation of PEG and lilial. [125]

Aldehydes and ketones are often used as ingredients for body care and household applications such as shampoos, laundry detergents and fabric softeners. In these applications, a long lasting of scent is preferable. Due to high volatility and aerobic oxidation, polyacetals, like the example in Scheme 5, are developed to solve this problem. [125]

Due to the fact, that the formation of the acetal is an equilibrium reaction, aqueous acidic conditions cause the cleavage of acetals. The structure of the acetal is here important. Linear acetals are less stable against hydrolysis, than their cyclic counterparts are. Hydrolytic degradation of linear acetals is more entropically favored. Moreover, acetals obtained from ketones are more sensitive to hydrolysis than one, which are derived from aldehydes. The reason is the stability of the carboxonium type intermediates existing during hydrolysis. The most stable intermediate is the carboxonium of ketones, then of aldehydes and then of formaldehyde. In conclusion, the more stable the intermediate of the carboxonium type, the less stable the acetal against hydrolysis. [99, 101] In addition, the substituents of the carbonyl compound effect the rate of hydrolysis. Substrates with electron withdrawing groups show resistance or lower reactivity to hydrolysis under acidic conditions. [109, 116, 126] The development of acetal moieties for degradable materials in tissue engineering applications is described in recent studies. [73, 127, 128]

Ancillary to the property of degradability, acetal-containing polymers are also of interest for devices in tissue engineering applications. Beside the fabrication of specifically shaped materials, a suitable pore morphology promotes tissue in-growth. [129, 130] The precise morphology and the patient specific shape can be realized by using additive manufacturing technologies (AMT). This technology uses either true 3D-methods or layer-by-layer techniques to build the desired shape. The light-based AMT works by selective deposition or selective irradiation of a photo-curable resin. [80]

In general, **polymerizable acetals** are already known e.g. as degradable polycyclic cross-linker for UV-curing nanoimprint lithography (Figure 25). Such monomers can be synthesized from 1,4-cyclohexanedione with glycerol, which is followed by an esterification with acryloyl chloride. The formed polymer network were used as positive, which can be etched in acidic media (e.g. *p*-toluenesulfonic acid solution) to generate nanostructures e.g. for optical filters. [131]

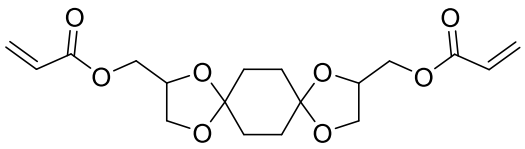

Figure 25: Structure of 2,10-diacryloyloxyl-1,4,9,12-tetraoxaspiro[4.2.4.2]tetradecane. [131]

Another example is the UV-curable pro-antimicrobial monomer p-anisaldehyde diallylacetal (pAA), which is synthesized with p-anisaldehyde (pA, antimicrobial) and allyloxytrimethylsilane (Scheme 6). Thiol-ene polymerization method is used to fabricate a fully degradable polymer network. Under hydrolytic conditions, pA is released and show effectiveness against bacterial and fungal pathogens. These properties have potential to be used in agriculture, pharmaceuticals, cosmetic, household/personal-care and food industries. [132]

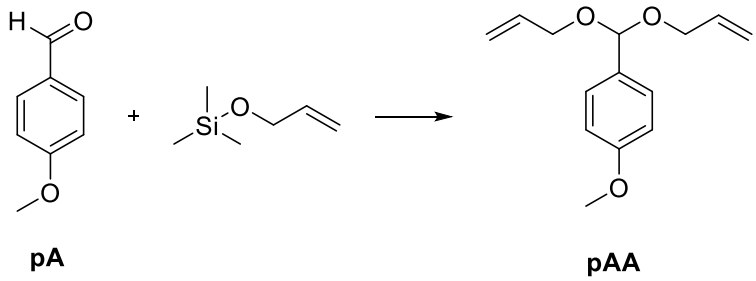

Scheme 6: Synthesis of the monomer for PANDA fabrication. [132]

However, there are also described polymerizable *polyether-acetals*, like diacrylated poly[poly(ethylene glycol)-co-cyclic acetal] (PECA-DA, Figure 26), as precursor for biomaterial hydrogels. This hydrogel contains a hydrophilic poly(ethylene glycol) (PEG) segment and a hydrolytically degradable cyclic acetal segment. PEG is used to produce a suitable matrix for cell encapsulation and in addition for formation of scaffolds. [133]

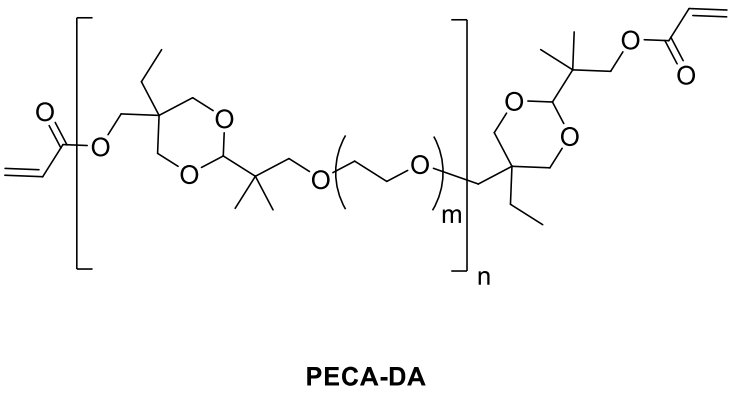

Figure 26: Example for polyacetal; diacrylated poly[poly(ethylene glycol)-co-cyclic acetal] (PECA-DA). [133]

One of the most present monomer in the research field of tissue engineering is 5-ethyl-5-(hydroxymethyl)-b,b-dimethyl-1,3-dioxane-2-ethanol diacrylate (EHD, Figure 27). It was commercially available (but may be easily synthesized) [130] and contains a cyclic acetal unit to be biodegradable. If the polymer degrade by hydrolysis, it will form diol and propanal degradation products, which are not acidic by-products. [134] Furthermore, it contains two terminal acrylat functionalities, which leads to the formation of EHD networks. Scaffolds based on EHD (Figure 28) are investigated to facilitate the skeletal muscle regeneration and therefore abdominal wall hernia repair. [128] Similar molecles have been utilized as a tissue glue. [127]

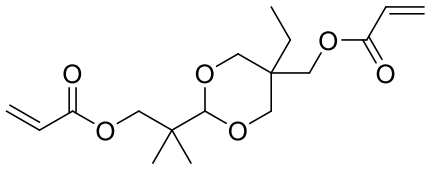

EHD

Figure 27: Structure of the monomer 5-ethyl-5-(hydroxymethyl)-b,b-dimethyl-1,3-dioxane-2-ethanol diacrylate (EHD). [127]

Cyclic acetal nanocomposites were also synthesized for craniofacial tissue engineering applications. Hydroxyapatite (HA) was incorporated within a hydrogel generated from poly(ethylene glycol) diacrylate (PEGDA, Figure 28) and EHD (Figure 27).

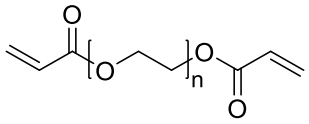

PEGDA

Figure 28: Structure of the monomer poly(ethylene glycol) diacrylate (PEGDA) to form cyclic acetal hydrogels with EHD. [134]

The formed hydrogel can support the surface adhesion of bone marrow stromal cells [73] and a recent study demonstrated the utility of EH-PEG hydrogels to repair craniofacial defects. [130]
In this work, the focus is on the development of photopolymerizable resin formulations that form degradable polymer networks. Spatiotemporal control of polymerization, fast curing rates at moderate temperatures and minimal heat production during the curing procedure, are some advantages of photopolymerization. [79] With light-based AMTs, liquid resins can be cured to generate the desired scaffold. This resin system must have certain properties. Both, the photoinitiator and the monomer itself, must be considered in terms of cytotoxicity. Bryant *et al.* [135] have shown that the concentration and hydrophobicity of the photoinitiator

plays an important role with regard to toxicity. [135] However, this molecule is only used in very small amounts in such formulations. Monomers are much more abundant. State-of-the-art monomers for photopolymerization are acrylates. For radical photopolymerization, they show a high reactivity and are available in various variations of molecular weight, viscosity, or spacer in the molecular backbone. However, there are also disadvantages with respect to TE. A severe problem is that acrylates are very cytotoxic. With NH- and SH- groups of proteins, they can undergo a so-called Michael addition reaction. This leads to non-reversible aliphatic adducts and this in turn to irritations and toxic effects. Despite the fact that the polymer can be considered as non-toxic this effect occurs with residual free monomers but also with non-polymerized groups within the network, since the DBC of the highly cross-linked polymer networks is usually only between 60 and 90%. [136] However, the degradation products of the polymer also lead to problems. During hydrolytic degradation poly(acrylic acid) is formed. This high molecular weight polymer cannot be transported within the human body. The formation of acids in turn leads to a decrease in the pH value and inflammation of the tissue, which causes an accelerated decay of the scaffold. [137] Furthermore, polyacids (like polyacrylic acids) can be cross-linked by multivalent ions, e.g. Ca^{2+}, which are present in bone in a high concentration, thus avoiding the polymer to be transported within the human body. In comparison, methacrylates are less toxic, though they polymerize rather slowly, there are prominent examples for materials, used in treatment of bone defects, e.g. as bone cement. [59] Therefore, they were also used in this work as ready-available photopolymerizable building blocks containing acetal moieties. Generally, sufficient toughness is an issue in case of photopolymers [138] and therefore, oligomeric monomers are investigated.

RESULTS AND DISCUSSION

1. Oligomeric Spiroacetals

Up to now, degradable biomaterials are predominantly based on polyesters. They cleave fast under basic conditions, but for application, where an acidic degradation is necessary (e.g. for bone regeneration due to the acidic environment produced by osteoclasts), they may not be suitable, due to their slow cleavage. Therefore, the aim of the first chapter of this thesis is to improve the degradability of such biomaterials. For this reason, acetal moieties should be integrated into the polymer. A faster cleavage than the before mentioned polyesters under acidic conditions is expected. Furthermore, the mechanical properties of such polymeric scaffolds are controlled via the molecular weight of the polymer. It is well accepted that high molecular weight leads to tougher materials. Hence, hydroxyl functional oligomers that exhibit an acetal moiety should be synthesized as suitable building blocks. Terminal hydroxyl groups are necessary, since these end groups can be readily reacted with other functional groups, for example with acid chlorides to form polyesters. In addition, the hydroxyl groups can also be used to install photopolymerizable functionalities onto the molecule. The concept for such oligomeric building blocks and formation of subsequent reactive polymers is shown in Figure 29.

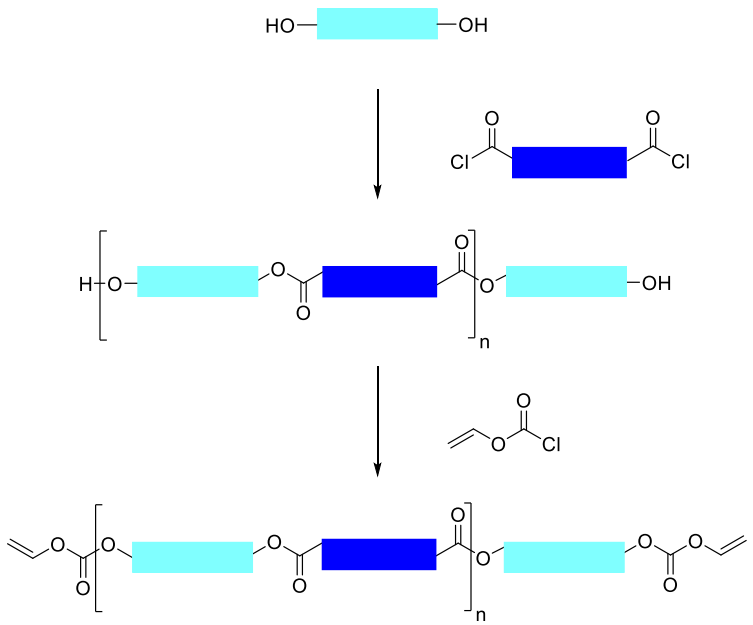

Figure 29: Schematic illustration of the work concept. The light blue squares represent the acetal moiety and the dark blue squares arbitrary spacers for control of the properties of the material.

1.1. Synthesis of Spiroacetals

In the first chapter of this thesis, different dihydroxy spiroacetals building blocks were synthesized. Spiroacetals were the first choice, as there are commercially available compounds and they are easy to handle, as they are quite stable also under acidic conditions. [99] Different aromatic systems, containing an aldehyde, should be converted with pentaerythritol as a tetrafunctional alcohol, to form the spiroacetal moiety. Aromatic aldehydes were chosen, as they are known to be less toxic than aliphatic aldehydes. [139] Furthermore, two terminal hydroxyl groups or groups, which can be converted into this one, must exist for the above-described oligomeric system. Thus, vanillin and 4-hydoxybenzaldehyde were chosen, as hydroxyl groups already exist. 4-Formylbenzoic acid has a carboxy group as functional group, which can be reduced to the desired hydroxyl substituent. Terephthalaldehyde was also chosen as starting material, because polyacetals can already be synthesized here. The selected aldehydes and the envisioned reaction are shown in Scheme 7.

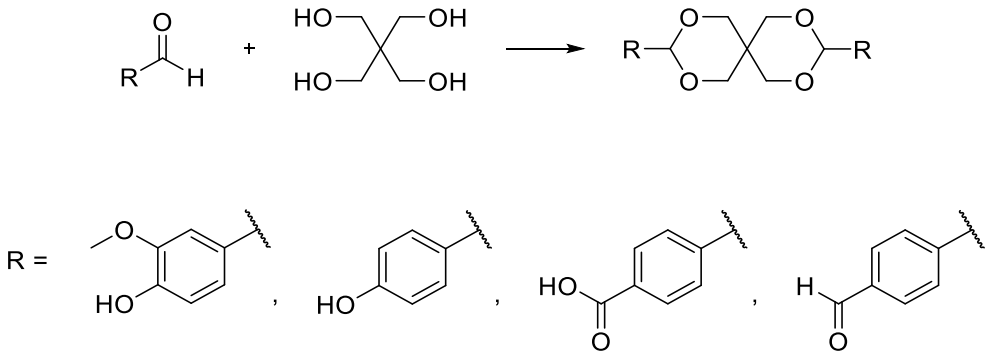

Scheme 7: Synthesis of spiroacetals and selection of appropriate aromatic aldehydes.

Generally, the conversion of carbonyl compounds with pentaerythritol is described in several publications. [99, 140] Under neutral and basic conditions, acetals are rather stable and therefore frequently used as protecting group. Acidic conditions cause the cleavage of acetals or ketals because of the acid-catalyzed hydrolysis. Such acetals and ketals are usually prepared using protic acids such as hydrochloric acid, [107] sulfonic acid [108], acetic acid, oxalic acid, p-toluenesulfonic acid [107] or Lewis acids (e.g. zinc chloride) as catalysts. [109]

1.1.1. Spiroacetal based on Vanillin (VanSPG)

In a first attempt, vanillin was the preferred aldehyde because it is a renewable resource and additionally, Ummadisetti *et al.* [116] already reported the reaction of vanillin with pentaerythritol with a yield of 95%. A glycerol-based catalyst [116] (Scheme 8) was chosen there due to the simple preparation procedure.

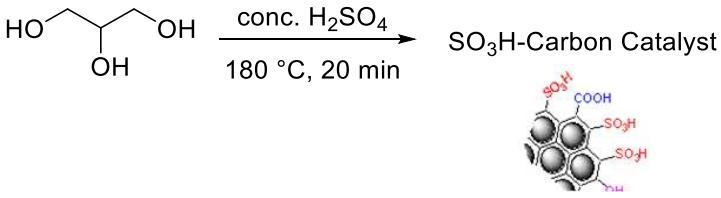

Scheme 8: Synthesis of the glycerol-based catalyst.

For the preparation of the catalyst, glycerol was mixed with conc. H_2SO_4 in a ratio of 1:3 and the reaction mixture was heated to 180 °C until foaming had ceased.

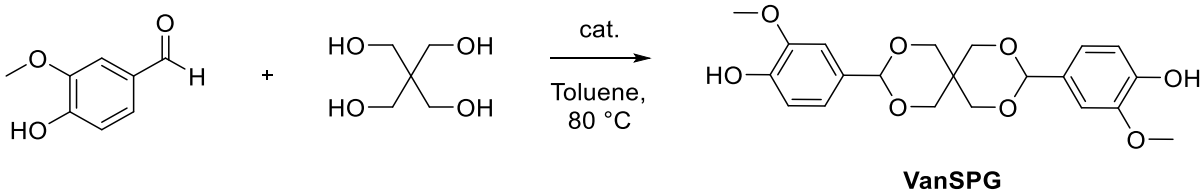

Scheme 9: Synthesis of spiroacetal based on vanillin (VanSPG).

For the preparation of the desired spiroacetal 4,4'-(2,4,8,10-tetraoxaspiro[5.5]undecane-3,9-diyl)bis[2-methoxy-phenol] (**VanSPG**, Scheme 9), the precursor vanillin (2 eq.) was first dissolved in dry toluene. Pentaerythritol (1 eq.) and the freshly prepared glycerol-based catalyst were added and the reaction mixture was heated up to 85 °C for 48 h. TLC indicated no conversion. Therefore, the reaction was continued for 48 h, however, still only sparse conversion was observable. The catalyst was filtrated off, the reaction mixture was dried *in vacuo* and the generated precipitate was recrystallized from EtOH. The desired product **VanSPG** was obtained in 9% of theoretical yield. Due to the low yield, the synthesis route was changed to conventionally used catalysts like pTsOH. [107] Therefore, vanillin (2 eq.) and pentaerythritol (1 eq.) were dissolved in dry toluene and pTsOH-monohydrate was added. Moreover, a Dean-Stark apparatus was used to remove the formed water during the reaction. During the different washing steps of the reaction mixture, precipitates of the product with varying purity grades are obtained. Recrystallization experiments proofed that ethyl acetate

is the best solvent to purify the product. The final purity was checked with HPLC (only one signal) and NMR and was approved as sufficiently pure.

In comparison to the first **VanSPG** synthesis (SO_3H-carbon catalyst) mentioned above, the yield could be increased through this approach up to 36%.

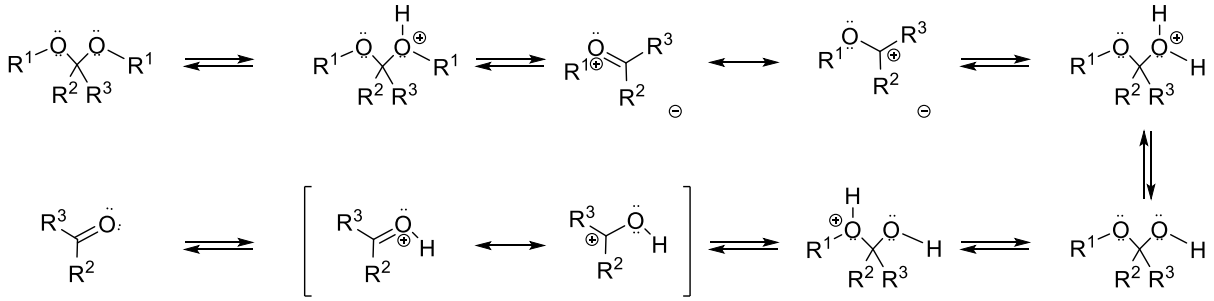

Figure 30: Well-established mechanism of the hydrolysis of acetals and ketals. Formation of the resonance-stabilized carboxonium ion intermediate, shown within the square bracket in the top, is considered to be the rate-determining step of this cleavage reaction. [101]

The substituents of aldehydes or ketones play an important role in the synthesis of acetals. Electron donating groups stabilize the carboxonium ion intermediate and its cationic character (Figure 30). The substituents R^2 and R^3 have contributions from inductive and resonance effects, whereas R^1 has greater contributions based on inductive effects. [101] Since the formation of acetals is an equilibrium reaction, the equilibrium is in the case of strong electron donating substituents, on the side of the educts, which reduces the yield of the desired product.

The hydrolysis of different benzaldehyde derivatives is described in the literature and shows that the methoxy-group has less influence in meta- than in para-position. However, if hydroxyl and methoxy groups in para position are compared, it was found that the latter one has a greater influence. This again means that in a reaction with methoxy substituents in para-position ,but also to a less extent with hydroxyl groups, the equilibrium is shifted to the side of the starting materials.[141]

1.1.2. Spiroacetal based on 4-Hydroxybenzaldehyde (4HBSPG)

Based on previous experiments the decision was made to create aromatic systems with less electron donating substituents compared to vanillin. Thus, 4-hydroxybenzaldehyde was

selected as a starting material as it has no additional electron-donating methoxy group. Again, the hydroxyl group is an interesting moiety for further functionalization or for follow up reactions e.g. esterification. In literature, the desired product is synthesized with different catalysts, such as the before mentioned glycerol-based in toluene or methanol. [116]

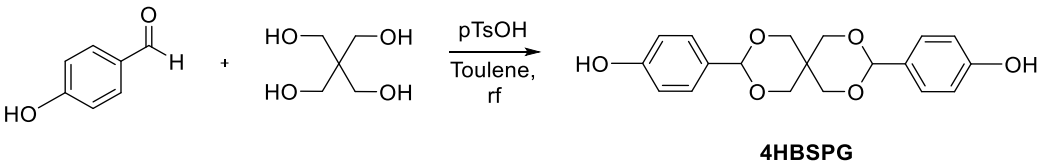

4HBSPG

Scheme 10: Synthesis of spiroacetal based on 4-hydroxybenzaldehyde (4HBSPG).

For the synthesis of 4,4'-(2,4,8,10-tetraoxaspiro[5.5]undecane-3,9-diyl)bis-phenol (**4HBSPG**) according to Hirose *et al.* [142], 4-hydroxybenzaldehyde (2 eq.), pentaerythritol (1 eq.) and pTsOH-monohydrate were dissolved in dry toluene and the flask was equipped with a Dean-Stark apparatus to remove the formed water. The product precipitated during washing as reddish solid. **4HBSPG** could be isolated pure in 70% of theoretical yield. The purity was checked with HPLC (only one signal) and NMR and was approved as sufficiently pure.

As electron-donating substituents hinder the synthesis of such spiroacetals, another route was aimed at.

1.1.3. Spiroacetal based on 4-Formylbenzoic acid (4FBASPG)

To improve the yield, the hydroxyl group in the para position of the aromatic aldehydes is substituted to a more electron withdrawing carboxylic acid to further accelerate the acetal formation. Afterwards, this carboxylic acid can be reduced to the corresponding alcohol functionality. This reduction step leads to a primary alcohol, which shows higher reactivity for further reactions. Furthermore, this new formed $–CH_2OH$ group makes the product more flexible and could therefore improve the solubility. In literature, the desired product is synthesized from 4-formylbenzoic acid, pentaerythritol in excess and $InBr_3$ as catalyst. All starting materials are grinded and the product was formed. [143] However, due to the good yield of the acetal based on 4-hydroxybenzaldehyde, the synthesis of 4,4'-(2,4,8,10-tetraoxaspiro[5.5]undecane-3,9-diyl)bis-benzoic acid (**4FBASPG**) was carried out as before.

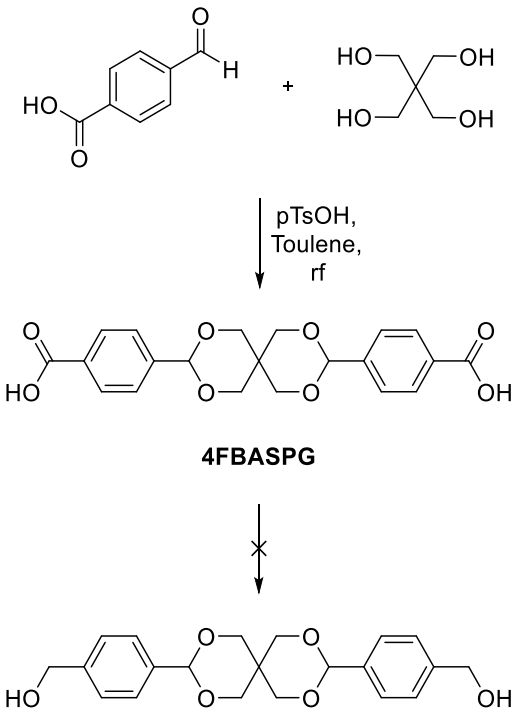

Scheme 11: Synthesis of spiroacetal based on 4-formybenzoic acid (4FBASPG).

For the synthesis of **4FBASPG** (Scheme 11) according to Hirose *et al.* [142], 4-formylbenzoic acid (2 eq.), pTsOH monohydrate and pentaerythritol (1 eq.) were dissolved in dry toluene and stirred at reflux for 48 h. A Dean-Stark apparatus was used to remove the formed water. A white precipitate was formed during the reaction and was separated from the solution by filtration. The precipitate was analyzed by ^{1}H-NMR (impurity aldehyde, ≤ 4%) and HPLC (two signals found: 4FBASPG, 4-formylbenzoic acid) and confirmed to be the desired **4FBASPG**. The yield of the reaction was 84%. The product was not soluble in chloroform, ethyl acetate, toluene or water. Due to the poor solubility, the product was excluded for further syntheses.

In conclusion, the formation of spiroacetals was possible. Vanillin as starting material was not as successful as 4-hydroxybenzaldehyde and 4-formylbenzoic acid due to the electron donation methoxy group. Unfortunately, the solubility of spiroacetals with aromatic substituents is quite low in typically used organic solvents. This is explainable by the very stiff structure as a consequence of the combination of the spiro-structure and the aromatic moieties.

1.2. Optimization of Esterification of Spiroacetals

Dihydroxy spiroacetals building blocks were synthesized before to generate in further reactions suitable polyesters, as typically degradable polymers. [144] For the synthesis of high molecular weight polymers, a near to quantitative conversion is needed, with regard to the Carothers equation. Due to that, the optimal reaction conditions have to be found. Polyesters can be synthesized by different methods. In general, polyesters are generated via condensation reactions. For esterifications, e.g. carboxylic acids and an alcohol are converted under acid catalysis. [145] Unfortunately this is not compatible with acetals as they are known to be acid-sensitive. Therefore, acid chlorides should be converted with an alcohol as an alternative approach to form the desired ester. As a catalyst, a base is used, for instance sodium hydroxide (Schotten-Baumann reaction). [146] A disadvantage of this method is the possible saponification of the formed ester. Due to that, a special form, the Einhorn-Acylation is used for the formation of the ester. There, a catalyst (4-dimethylaminopyridine (DMAP), trimethylamine (Et_3N) or pyridine) at the same time acting as an acid scavenger is used. [147]
A small test molecule was designed to study optimal reaction conditions for further esterifications. In addition to the optimization of the reaction conditions, the degradation time of acetals compared to esters should be examined by using this model compound (see Chapter 1.4). Therefore, the above mentioned test molecule should contain both moieties. The model compound was prepared from an aliphatic diol (**IBSPG**), which is commercially available and contains the spiroacetal moiety, and a propionic acid chloride (Scheme 12).

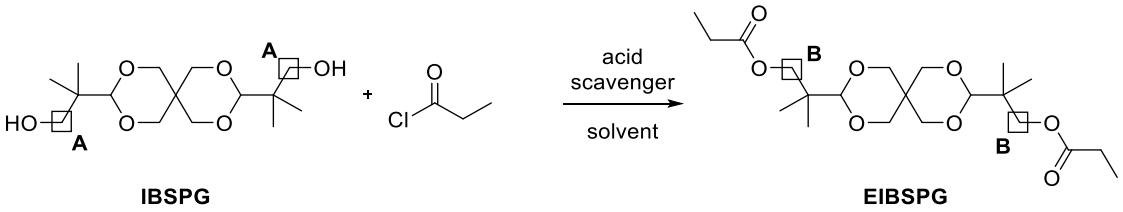

IBSPG EIBSPG

Scheme 12: Esterification reaction of the aliphatic spiroacetal IBSPG to form EIBSPG; A and B are CH_2-groups for the calculation of the conversion.

For the reaction optimization, different solvents (toluene and THF) and different acid scavengers (DMAP, Et_3N, and pyridine) were tested (Table 1). For all attempts, **IBSPG** and the acid scavenger (2.1 eq.) were dissolved. The vials were purged with argon and the acid chloride (2 eq.) was added dropwise at room temperature. After addition, the reaction mixture was stirred for 18 h. For the calculation of the conversion, a small equivalent of the

reaction mixture was taken and quenched with saturated NH_4Cl solution. Afterwards, the organic phase was dried *in vacuo* and the residue was dissolved in d_6-DMSO.

Table 1: Optimization study of the esterification. The conversion was determined by ^{1}H- NMR. *in catalytic amounts

No.:	solvent	acid scavenger	conversion
1	THF	Et_3N	74%
2	Toluene	Et_3N	69%
3	THF	Pyridine	43%
4	THF	DMAP	74%
5	THF	-	53%
6	THF	Et_3N/DMAP*	69%

Conversions were calculated from ^{1}H-NMR experiments. As internal standard, the signal of the CH_2-group (**A**, Scheme 12) was chosen. If the esterification was successful, the NMR signal of the CH_2-group of **IBSPG** (A) was shifted downfield from 3.41 ppm to 3.91 ppm (**B, EIBSPG**). As it can be seen in Table 1, reaction no. 1 with Et_3N and reaction no. 4 with DMAP as acid scavengers have the highest conversions. For the up-scaling of the esterification to get enough model molecule for degradation studies, the reaction conditions of attempt no. 4 were used, because in comparison to Et_3N as acid scavenger, less byproducts are generated. Therefore, IBSPG were used in combination with 2.4 eq. propionyl chloride and 2.5 eq. DMAP. This way, the theoretical yield was increased up to 82%. The purity was checked with HPLC and NMR. The increased ratio acid chloride to diol was only made to achieve a higher yield of the product **EIBSPG**. For further polyester reactions, the functional group ratio must be exact 1:1 to receive high molecular weights.

1.3. Synthesis of Oligomeric Spiroacetals

An alternative concept would be the direct synthesis of oligomeric aromatic spiroacetal (Scheme 13), e.g. with terephthalaldehyde and pentaerythritol as starting materials to implement the spiromoiety into the polymer backbone. However, in literature [148] polyacetals with similar structures are known to be stable and insoluble in common organic solvents.

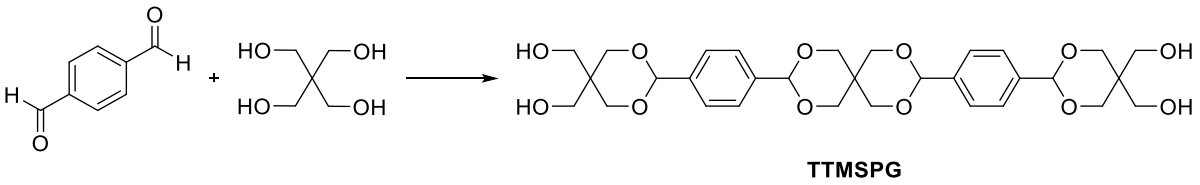

Scheme 13: Synthesis of spiroacetal based on terephthalaldehyde (TTMSPG).

For this reason and due to the good conversion of the esterification of the optimization reaction, which is described in Chapter 1.2, an initial attempt to synthesize a polyester with hydroxyl end groups (Scheme 14) was made. Thus, a difunctional acid chloride was converted with the commercially available spiroacetal based diol.

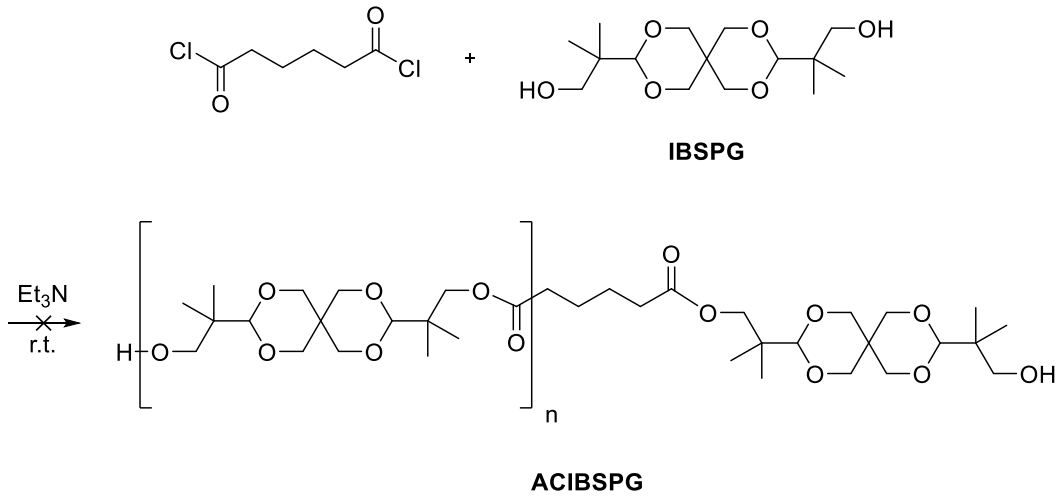

Scheme 14: Polyester synthesis to synthesize ACIBSPG with commercially available IBSPG.

The conversion of the reaction was assumed to be about 74% as found in model reaction (Chapter 1.2). In accordance to Carothers equation, this expected conversion theoretically leads to a polymerization degree of 2.7, in case a ratio of diacid chloride to diol of 3:4 is chosen and corresponds to a molecular weight of approximately 720 g/mol.

$$r = \frac{N_A}{N_B} < 1$$

Carothers equation:

$$\overline{X_n} = \frac{1 + r}{1 + r - 2pr}$$

r = ratio of monomers

$N_{A \text{ or } B}$ = molecules of monomer A or B

X_n = degree of polymerization

p= conversion

Due to the insolubility of **IBSPG** in dichloromethane, the reaction was performed in suspension, however no successful conversion was observed. For this reason, the solvent was changed to dry THF and the diol was first dissolved completely. Upon addition of the adipoyl dichloride (1 eq.) to **IBSPG** (1.33 eq.) and trimethylamine (2.2 eq.) at room temperature, a white solid (presumably $NHEt_3^+Cl^-$) precipitated. In order to monitor the reaction process, ^{1}H-NMR spectra were made. Here, after 43 h, the precipitate was filtrated off. The solvent was evaporated and the residue solid and the precipitate were analyzed. However, in the ^{1}H-NMR the CH_2-groups of the acid dichloride were not observable anymore, due to possible evaporation. Moreover, no signals, which would support an esterification, were found. Only signals of the starting material **IBSPG** were detectable. In addition, a ^{13}C-NMR was measured, but no quaternary C atoms of the ester-groups could be found. The reaction mixture was heated to reflux for about 36 h, but again, no signals of the preferred product was observable in the NMR. Therefore, this strategy was not further considered.

1.4. Degradation Model Study of Spiroacetal Derivatives

For application as bone replacement material, degradable moieties should cleave at a pH of about 4.5. Up to now used ester-based polymers were substituted with spiroacetals in this chapter. Therefore, the degradation of the acetal moiety and the ester group of the synthesized aliphatic spiroacetal (**EIBSPG**) was studied by ^{1}H-NMR spectroscopy over a few weeks to compare these two functional groups. The studies are conducted in CD_3CN/D_2O (1:1). Altogether three different pH-equivalents were measured. One of the NMR tube contained NaOD, which is equivalent to a pH of 12.0, one contained DCl, a pH-equivalent of 2.1, and the last tube was measured in the plain NMR solvent. The ^{1}H-NMR spectra are always standardized to the signal of the CH_2-group of **EIBSPG** at 4.41 ppm, which is labeled as **A** in the according Figures and Schemes. The other signals are referenced to **A** and are described in the following discussion concerning the degradability. With the signal **A**, the amounts of the degraded product can be determined. This reference signal was chosen, as the acetal signal -$CH(O)_2$- (4.85 ppm) is overlapping with some signals of the pentaerythritol-unit (4.98 - 4.86 ppm). Moreover, the signal of the acetal was not shifted during the ester cleavage.

Scheme 15 shows the reaction scheme expected for basic conditions. The signal of the CH_2-group of the formed **IBSPG** is labeled as **B**. As found in the NMR experiments (Figure 31 and Figure 32), at basic pH, only a cleavage of the ester takes place but no formation of an aldehyde. The ester undergoes a fast cleavage; already 83 mol% are cleaved during the first 24 hours and then it stays quite constant for the remaining period of measurement.

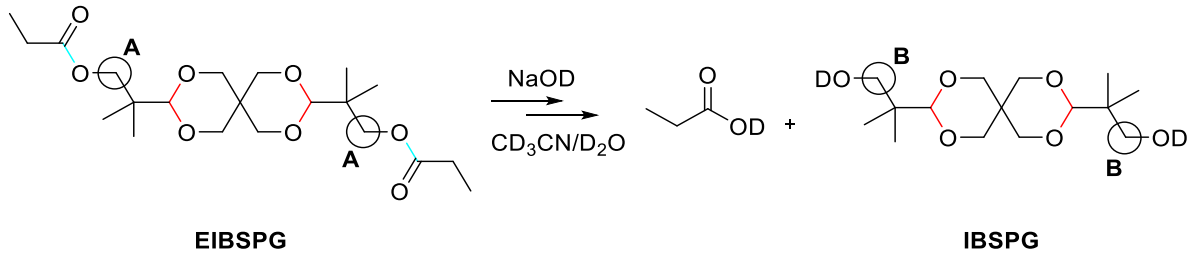

Scheme 15: Degradation of EIBSPG under basic conditions.

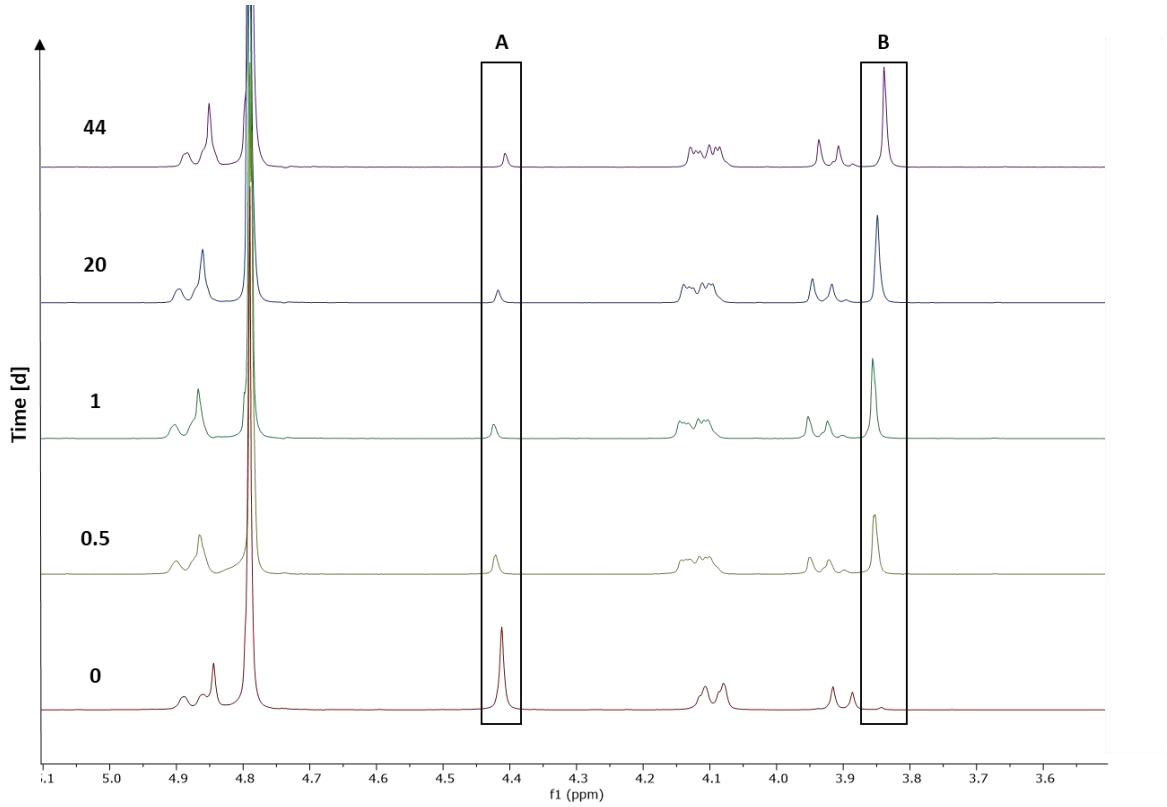

Figure 31: ^{1}H-NMR spectrum (CD_3CN:D_2O (1:1) + 0.5 µl NaOD (40 wt% NaOD in D_2O), pH-equivalent of 12.0) of EIBSPG under basic conditions during a period of 44 days; Time t_0 (0 d, bottom) and t_4 (44 d, top); A: standardized CH_2-signal of EIBSPG; B: referenced CH_2-signal of IBSPG.

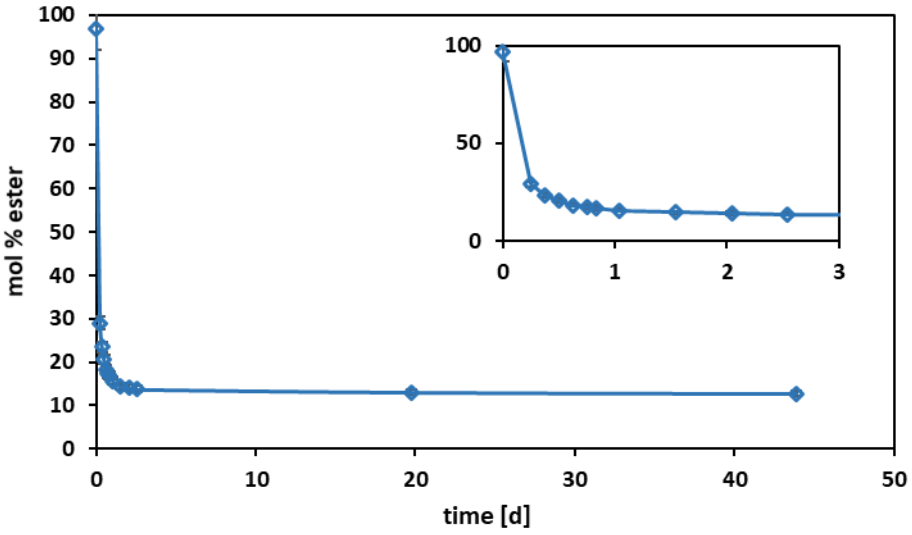

Figure 32: Degradation process of EIBSPG under basic conditions (pH-equivalent of 12.0) during a period of 44 days.

Scheme 16 shows the expected reaction for the acidic degradation of **EIBSPG**.

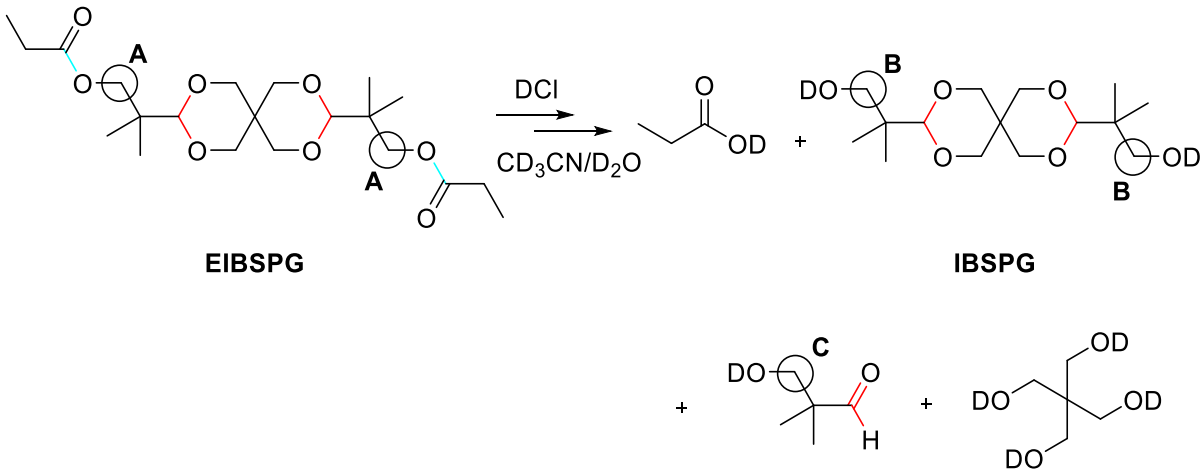

Scheme 16: Degradation of EIBSPG under acidic conditions.

Under acidic conditions, the ester as well as the acetal are cleaved. Figure 33 displays the NMR data of the degradation under acidic environment during a period of 0 h and 44 days. The diagram (Figure 34) shows the progress of the degradation. Already in the first 24 h, a cleavage of the ester can be noted due to the ratios of the CH_2-group-signals. After 44 days, approximately 45 mol% are cleaved. For the calculation of the formed aldehyde, also the CH_2-group **C** was chosen because the aldehyde's proton is only visible in the noise after 21 days. However, signal **C** already shows an earlier cleavage. Due to the rather stable spiroacetal,

the corresponding aldehyde 3-hydroxy-2,2-dimethylpropanal is formed slowly and so, after 20 days only 0.7 mol% aldehyde and after 44 days 6.4 mol% are generated.

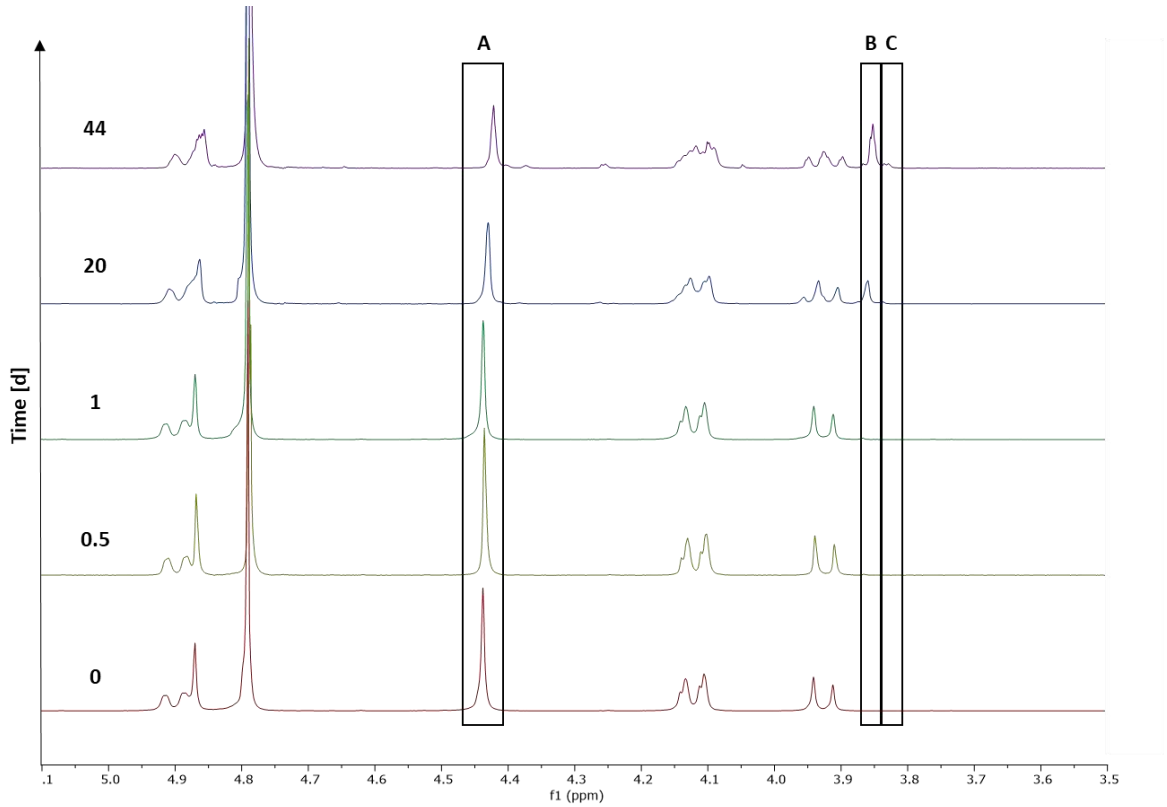

Figure 33: ^{1}H-NMR spectrum ($CD_3CN:D_2O$ (1:1) + 0.5 µl DCl (38 wt% DCl in D_2O), pH-equivalent of 2.1) of EIBSPG under acidic conditions during a period of 44 days; Time t_0 (0 d) bottom spectrum and t_4 (44 d) top spectrum

A: standardized CH_2-signal of EIBSPG; B: referenced CH_2-signal of IBSPG; C: referenced CH_2-signal of 3-hydroxy-2,2-dimethylpropanal.

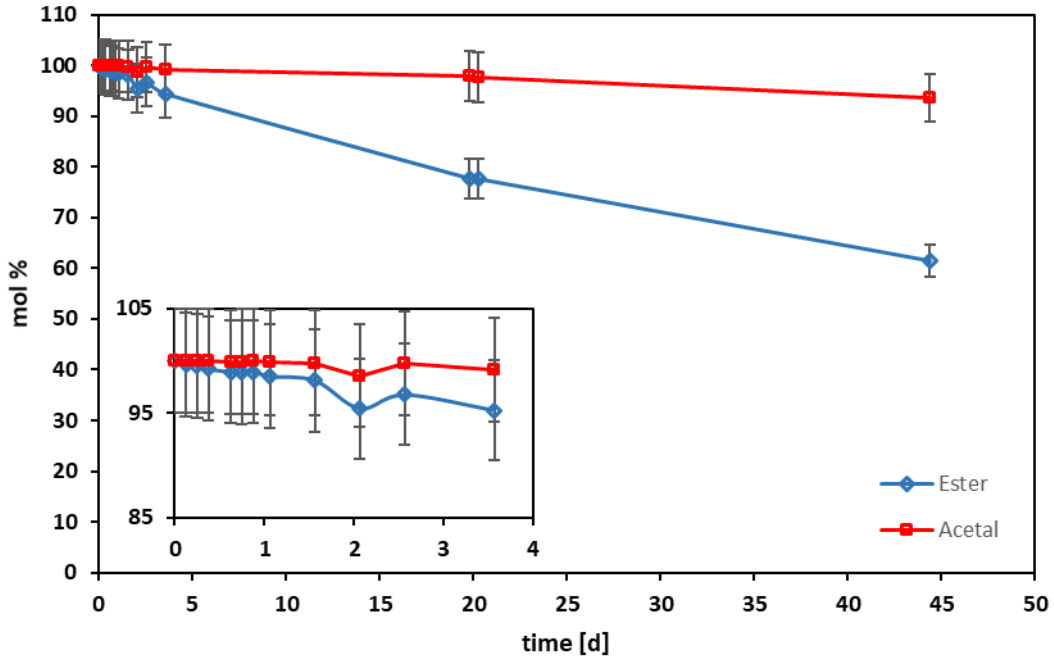

Figure 34: Degradation process of EIBSPG under acidic conditions during a period of 44 days.

Additionally, the degradation behavior was determined under neutral conditions. In the whole period of the measurement, no cleavage of the ester and the spiroacetal was observable and thus no NMR spectrum and degradation process is shown.

In conclusion, the spiroacetal is stable under neutral and basic and only degrades slowly at acidic conditions. In comparison, the ester cleaves very fast at basic environment and faster than the acetal under acidic conditions. The high stability of spiroacetals [117] was confirmed with these experiments and therefore, spiroacetals as cleavable moiety are not appropriate for the designated application.

2. Low Molecular Weight Linear and Cyclic Acetals

Due to the slow degradability of the spiroacetals (see Chapter 1.4), other types of acetals should be considered. These acetals are expected to be less stable than the spiro-compounds. [99, 110, 117, 140]

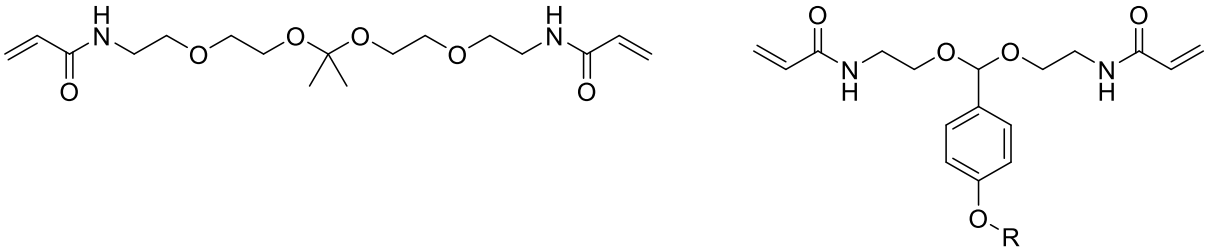

Figure 35: Linear acetal monomers for vaccine carriers. [149, 150]

If, for example, one compares the two monomers for vaccine carriers (Figure 35), the left acetal with an aliphatic substituent degrades three times faster than the liner acetal with aromatic substituent. [149, 150] The presence of a hydroxyl group as a p-substituent on a benzene ring compared to a methoxy group leads also to a faster hydrolysis. [100, 124] This effect is explainable by the electron withdrawing ability of the substituents. The hydroxyl group has a slightly less withdrawing effect than the methoxy group. This leads to an increased reactivity of the benzene ring, which causes the hydrolysis of the substituted acetal bond. [100, 109, 116, 126] These facts approved, that the substituents have an important effect on the hydrolysis. [151, 101] Moreover, the general structure of the acetal is important. Hydrolytic degradation of linear acetals is more entropically favored. [99] For this reason, linear acetals are less stable against hydrolysis, than their cyclic counterparts are. [99, 151, 126] In general, a higher degree of substitution at the central carbon increases the hydrolysis rate. Thus, the relative rate follows the order: formaldehyde (CH_2O) < aldehyde (RCHO) < ketone (RCOR). [152, 153, 101] In addition, the ring size plays a significant role in the hydrolysis rate for cyclic acetals. For example, 5-membered rings are more stable than 6-membered rings, if one compares two molecules with the same substituents. [153]

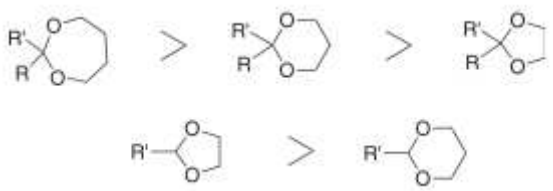

Figure 36: Relative rates of acid-catalyzed hydrolysis of some dioxolanes. [153]

To first evaluate the degradation behavior of the different acetal structures, low molecular weight test systems were planned, which are shown in Figure 37. Various starting materials were chosen to widen the substrate scope. Linear acetals with aromatic (**VanKMA**) as well as aliphatic substituents (**VKMA**) and additionally cyclic acetals (**T5MA**) should be studied. Based on the facts described in the literature, linear acetals are expected to be more stable than cyclic acetals. For the first two linear acetals (Figure 37) it is assumed that the aliphatic acetal (**VKMA**) is more stable against hydrolysis than the aromatic linear acetal (**VanKMA**). In addition, photopolymerizable functionalities are already added to the molecule to determine the degradation behavior in a polymer network. Methacrylates were chosen as they are common rather biocompatible functional groups for photopolymerization. The last molecule in Figure 37 (**MB5**), with terminal hydroxyl groups, was targeted, because this diol allows the functionalization of molecules with other photopolymerizable groups (e.g. vinyl carbonates). Moreover, it can be used as building block for oligomeric systems.

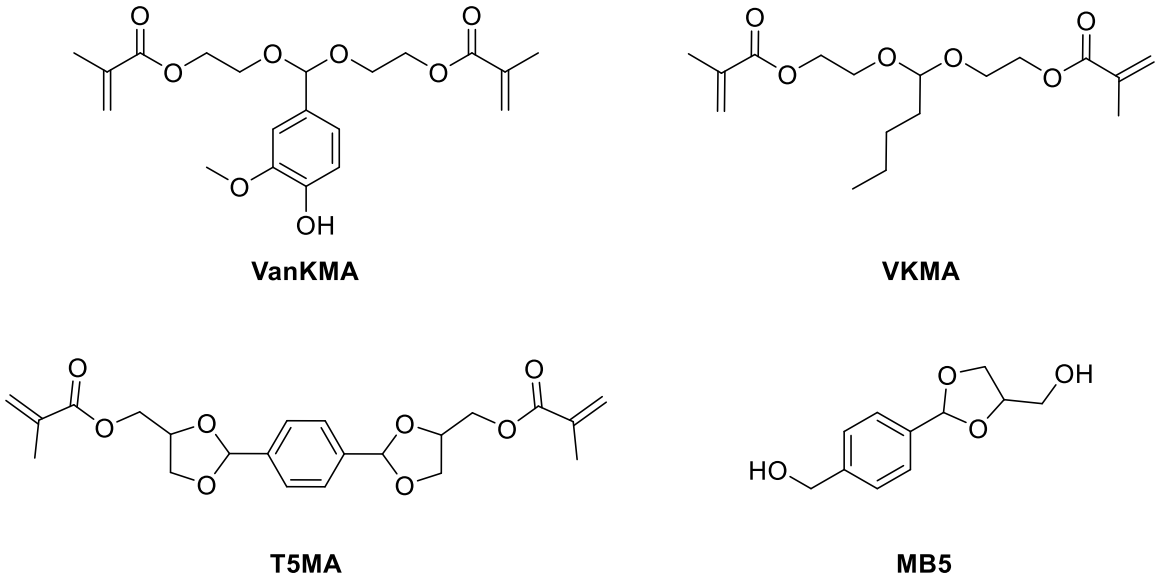

Figure 37: Planned alternative acetals.

After the synthesis (Chapter 2.1), the reactivity and degradability of the acetal containing systems are determined in the subsequent Chapters 2.2 and 2.3.

2.1. Synthesis

As the spiroacetals have shown extreme high hydrolytic stability, a series of less stable acetals have to be synthesized. These acetals are obtained by the reaction of the desired carbonyl compound with at least two hydroxyl groups that could be in one molecule (for cyclic acetals)

or in two molecules (for linear acetals). In general, they are prepared using protic acids as catalysts such as sulfonic acids [108] or p-toluenesulfonic acid [107]. The syntheses are described in detail in the following subchapters.

2.1.1. Linear acetal based on Vanillin and HEMA (VanKMA)

Vanillin was chosen as starting material, as it is a cheap and natural product. Therefore, the synthesis of a polymerizable acetal **VanKMA** was planned according to Scheme 17.

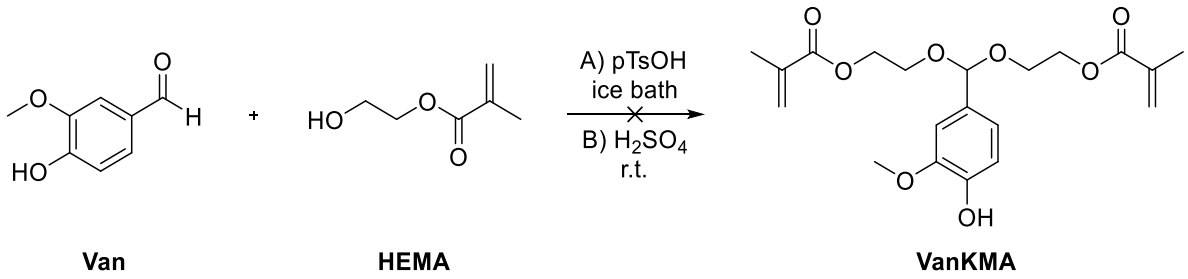

Scheme 17: Synthesis of acetal based on vanillin and HEMA (VanKMA).

For the preparation of 1,1'-[[(4-hydroxy-3-methoxyphenyl)methylene]bis(oxy-2,1-ethanediyl)]-2-propenoic acid ester (**VanKMA**), the aldehyde vanillin was converted with 5.17 eq. of HEMA in dry THF, using pTsOH-monohydrate as catalyst according to Bulmus *et al*. [100] (reaction conditions **A**, Scheme 17). A molecular sieve was applied to absorb the generated water. The solution was stirred with an ice bath overnight. The process of the reaction was followed by TLC (TLC-plate was first neutralized with PE:EA (1:1) + 1% Et_3N). Only the starting materials could be determined.

A second attempt was performed at room temperature according to Liu *et al*. [101] using again HEMA (3.17 eq.) in excess but conc. H_2SO_4 as catalyst (reaction conditions **B**, Scheme 17). Similar to the first experiment, no product formation was observed by TLC.

As described in Chapter 1.1.1, it is assumed that the functional groups in vanillin lead to a decrease in conversion, because the substituents of the carbonyl compound affect the equilibrium of the reaction to be on the side of the educts. Substrates with electron-withdrawing groups show lower reactivity to hydrolysis under acidic conditions. [109, 116, 126] Aromatic aldehydes with electron withdrawing groups, for example nitro- or halogen substituents react faster compared to aromatic aldehydes with strong electron-donating groups, e.g. methoxy-, hydroxyl- or methyl groups. Moreover, the

derivatives of benzaldehyde with electron poor substituents show a higher reaction rate for the acetal formation and higher yields are achieved. [116]

Therefore, the formation of the acetal is suppressed, respectively, the hydrolysis is promoted. Due to this reason, this target molecule was rejected.

2.1.2. Acetal based on Valeraldehyde and HEMA (VKMA)

As the aromatic acetals lead to problem in synthesis, also aliphatic acetals should be investigated. The structure of aliphatic aldehydes plays a major role in toxicity, for instance unsaturated aldehydes are more toxic than saturated ones. In addition, the toxicity decreases with increasing chain length. [154] For these reasons, valeraldehyde was selected as the starting material.

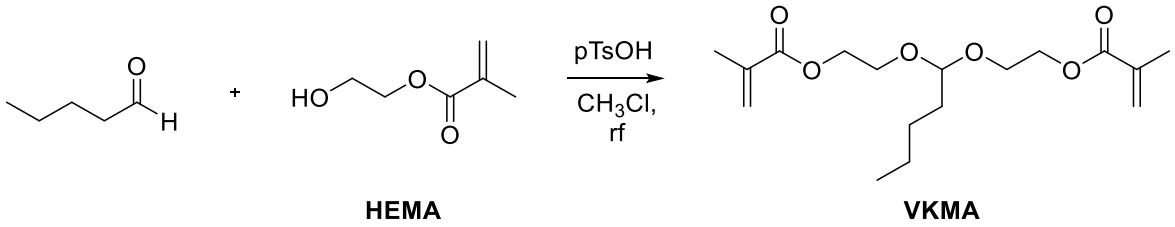

HEMA **VKMA**

Scheme 18: Synthesis of acetal based on valeraldehyde and HEMA (VKMA).

For the synthesis of 1,1'-[pentanebis(oxy-2,1-ethanediyl)]-2-methyl-2-propenoic acid, ester (**VKMA**) according to literature [142], an excess of HEMA (2.66 eq.) was dissolved first in chloroform. Subsequently valeraldehyde (1eq.) and pTsOH-monohydrate as catalyst were added to the stirred mixture. A Dean-Stark apparatus was used to remove the formed water. After 5 days, the reaction mixture was quenched, phenothiazine (125 ppm) and MEHQ (291 ppm) were added to the solution, extracted and the solvent was removed. At high vacuum ($1.7 \cdot 10^{-1}$ mbar, 40 °C), the excess of HEMA was evaporated. The purity was checked with HPLC (two signals: HEMA and **VKMA**) and NMR (impurity HEMA, ≤ 17 mol% (NMR)). The product was isolated as yellow oil in 85% yield.

2.1.3. Acetal based on Terephthalaldehyde and Glyceryl Methacrylate (T5MA)

The synthesis of an aromatic cyclic acetal required two steps. First, a diol (**GMA**) had to be prepared by ring opening of the epoxy group from glycidylmethacrylate, which can further react with terephthalaldehyde and thus forms the desired acetal **T5MA**.

The synthesis of 2,3-dihydroxypropyl-2-methyl-2-propenoic acid ester (**GMA**) was performed according to Ratcliffe *et al.* [155].

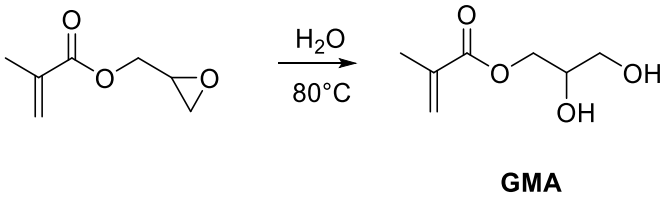

Scheme 19: Synthesis of glyceryl methacrylate (GMA).

Therefore, glycidyl methacrylate was stirred with an excess of deionized water (71 eq.) at 85 °C for 36 h. The now homogenized solution (due to the solubility of the product in water) was cooled and the product was isolated by vigorous extraction with ethyl acetate. 500 ppm phenothiazine were added and the solvent was removed *in vacuo*.

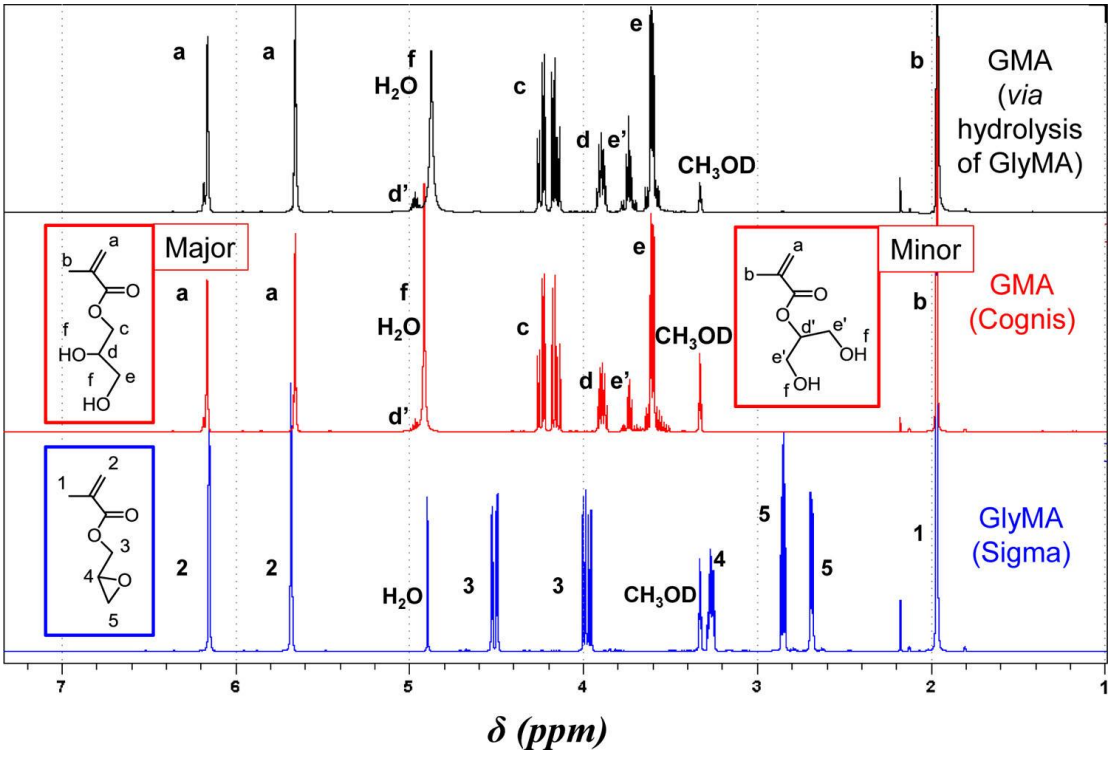

Figure 38: **^{1}H NMR spectra (CD_3OD) of glyceryl methacrylate (GMA) monomer prepared via hydrolysis of glycidyl methacrylate (GlyMA) at 10% w/w (top), commercial GMA monomer donated by Cognis (middle spectrum), and commercial glycidyl methacrylate monomer (bottom)** [155].

In addition to ring opening of the epoxy group, there is also a side reaction described in literature. [155] This side product (2-hydroxy-1-(hydroxymethyl)ethyl-2-methyl-2-propenoic acid ester), which is possibly formed due to intramolecular rearrangements, was also observable during the synthesis in this work but only in small amounts of less than 14%. In Figure 38 a ^{1}H-NMR spectrum of the commercial reference molecule from Cognis and the prepared

products **GMA** can be seen. [155] The side product will also react with terephthalaldehyde and will form a six-membered acetal. However, this product will not interfere, as it is also a cleavable acetal.

In the second step, the formation of the acetal **T5MA** with the generated **GMA** and terephthalaldehyde, which was recrystallized with toluene, was accomplished.

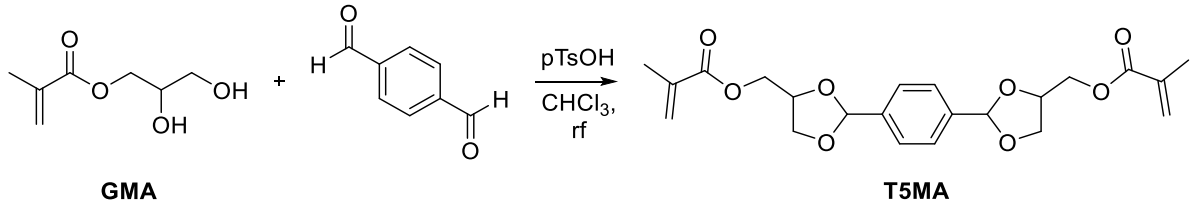

Scheme 20: Synthesis of acetal based on terephthalaldehyde and glyceryl methacrylate (T5MA).

For the synthesis of 1,1'-[1,4-phenylenebis(1,3-dioxolane-2,4-diylmethylene)]-2-methyl-2-propenoic acid ester (**T5MA**), **GMA** (2.66 eq.), terephthalaldehyde (1 eq.) and pTsOH-monohydrate were dissolved in EA and heated to reflux. Anhydrous Na_2SO_4 was used for removing the formed water according to Leibler *et al*. [156] The progress of the reaction was monitored by ^{1}H-NMR spectroscopy. After two days, no formation of a product could be detected. In the ^{1}H-NMR spectrum, the signal of the aldehyde at 10.14 ppm of the starting material disappeared and another proton signal at 10.04 ppm appeared. This signal is probably from the single substituted-product and because of this, the signal of the aldehydes' proton is shifted. Therefore, more Na_2SO_4 and catalyst were added and the solution was heated to reflux again. However, there was no change in the spectrum observable. For this, the reaction mixture was rejected.

In a second attempt, the solvent was changed to chloroform and an inverse Dean-Stark-Apparatus was used to remove the formed water. [115] The reaction mixture (terephthalaldehyde (1 eq.), 2.66 eq. of **GMA** and pTsOH-monohydrate) was heated to reflux and stirred for two days. The solution was allowed to cool down and was quenched with a solution of saturated $NaHCO_3$ to neutralize the catalyst. A high amount of water was necessary for extraction to remove the remaining excess of **GMA**. Phenothiazine (112 ppm) and MEHQ (324 ppm) were added for removal of small amounts of not converted terephthalaldehyde in high vacuum ($1.7 \cdot 10^{-1}$ mbar, 40 °C). Unfortunately, the product polymerized during distillation.

Therefore, the synthesis was repeated as before, but the evaporation step on high vacuum for purification was skipped. The purity was checked with HPLC (two signals: terephthalaldehyde and T5MA) and NMR (impurity terephthalaldehyde ≤ 10 mol%; mono-substituted ≤0.3%). The ratio of these products may be explained by the preferential formation of the disubstituted product, once a mono-substituted has been formed. **T5MA** could be isolated with 99% yield as pink and highly viscous oil.

2.1.4. Acetal linked Diol based on 4-Formylbenzoic acid and Glycerol (MB5)

For the synthesis of the diol (4-(4-(hydroxymethyl)-1,3-dioxolan-2-yl)phenyl)methanol (**MB5**), two reaction steps were necessary (Scheme 21). In the first step, an acetalization should be performed. In the second step, the carboxyl group can be reduced to the desired alcohol.

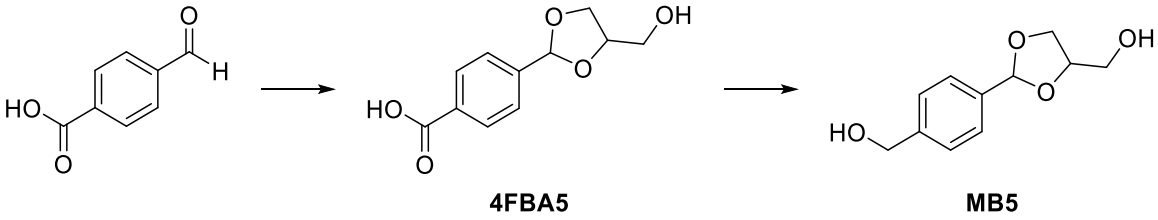

Scheme 21: Synthesis of acetal linked diol based on 4-formylbenzoic acid and glycerol (MB5).

It should be noted that this reaction results in two products. [157] In the reaction of an aldehyde with glycerol as polyhydric alcohol, both a 5-membered and a 6-membered ring are formed, as illustrated in Figure 39. The 5-membered ring is more stable and thus is formed in larger quantities. For this reason, only this product is shown in the further reaction steps.

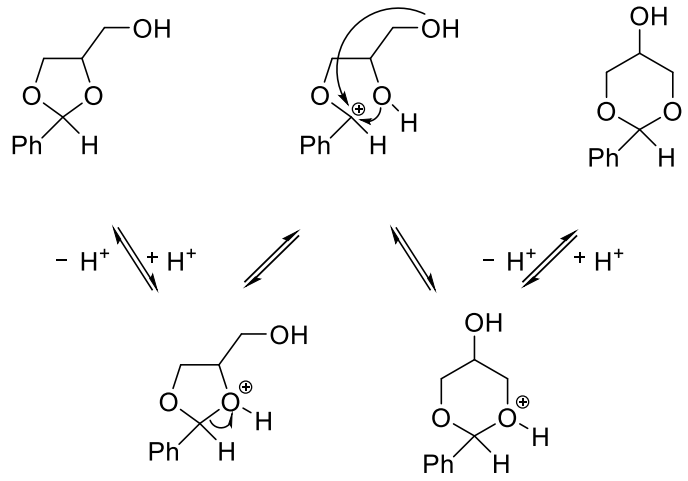

Figure 39: Acid-catalyzed equilibrium between 5- and 6- membered ring (ring transformation). [157]

2.1.4.1. Synthesis of Acetal based on 4-Formylbenzoic acid (4FBA5)

As mentioned before, the first step in the preparation of **MB5** is the formation of the acetal 4-(4-(hydroxymethyl)-1,3-dioxolan-2-yl)benzoic acid (**4FBA5**) by the reaction of 4-formylbenzoic acid with glycerol.

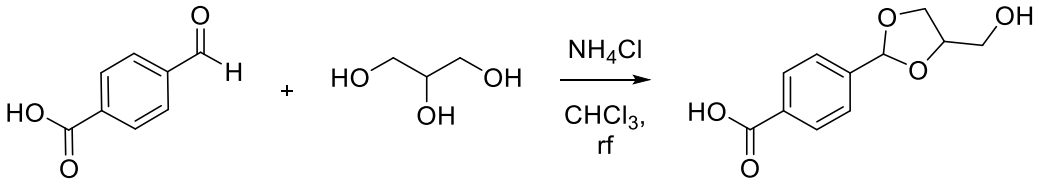

4FBA5

Scheme 22: Synthesis of acetal based on 4-formylbenzoic acid (4FBA5).

First, the purity of 4-formylbenzoic acid was checked with ^{1}H-NMR and proved as sufficiently pure. Glycerol was dried over a molecular sieve. The formation of the acetal 4-(4-(hydroxymethyl)-1,3-dioxolan-2-yl)benzoic acid (**4FBA5**) was inspired by Wildling *et al.* [158]. Therefore, 4-formylbenzoic acid (1 eq.), NH_4Cl (5.6 eq.) and glycerol (1.33 eq.) were dissolved in chloroform and refluxed for 24 h. An inverse Dean-Stark apparatus was used to remove the formed water. ^{1}H-NMR spectroscopy after one day showed still high amounts of aldehyde. Therefore, the reaction mixture was stirred for five more days. The solution was cooled down and the product precipitated to give the desired product **4FBA5** in 68% of the theoretical yield with small amounts of aldehyde (≤ 7% (NMR)). No further purification was made, due to the low stability on the acidic silica column. Furthermore, no suitable solvent was found for recrystallization.

Unfortunately, the scale-up of the synthesis was difficult. The starting materials have poor solubility in the solvent chloroform and the yield was quite low (18% yield).

2.1.4.2. Synthesis of MB5

The next step was to reduce the carboxyl group to the corresponding primary alcohol (Scheme 23).

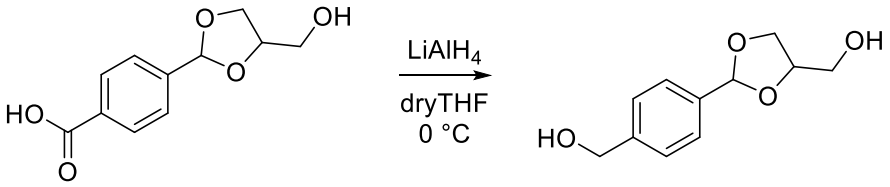

4FBA5 **MB5**

Scheme 23: Synthesis of acetal linked diol based on 4-formylbenzoic acid and glycerol (MB5).

(4-(4-(Hydroxymethyl)-1,3-dioxolan-2-yl)phenyl)methanol (**MB5**) according to Blake *et. al.* [159]. Therefore, lithium aluminum hydride ($LiAlH_4$, 2 eq.) was added to a flask with dry THF and stirred for ten minutes. **4FBA5** (1 eq.) dissolved in dry THF was added dropwise to the reaction mixture. The solution was stirred at r.t. overnight, quenched with aqueous KOH (2.5%) and extracted with EA. **MB5** was obtained as white powder with a yield of 67%. The purity was checked with HPLC (one clear signal, one minimal: 4-formylbenzoic acid and **MB5**) and NMR (≤ 4% of aldehyde).

2.2. Degradation Model Study of Low Molecular weight Acetals

The degradation of the linear and cyclic acetals had to be studied in order to assess their potential for biomaterials in tissue engineering. Important considerations were degradability characteristics in comparison with the already studied spiroacetals (Chapter 1.4) and ester groups commonly employed in degradable polymers. ^{1}H-NMR spectroscopy as method was chosen again. The studies are conducted in CD_3CN/D_2O (1:1). All samples were measured under acidic conditions. The NMR tube contained DCl, which would be a pH-equivalent of 2.1.

2.2.1. Degradation of VKMA

Scheme 24 shows the hydrolytic degradation scheme of the aliphatic acetal **VKMA** expected for acidic conditions.

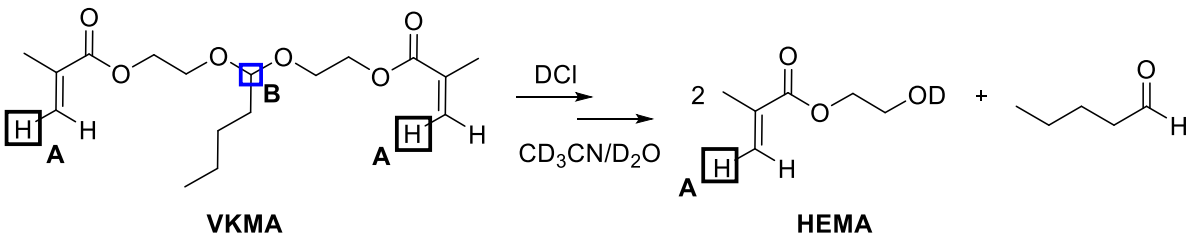

Scheme 24: Degradation of VKMA under acidic conditions.

In the ^{1}H-NMR spectra the CH_2-signals of the ethylene glycol units (4.75 and 4.25 - 4.43 ppm) of **VKMA** are overlapping with the signals of the solvent (D_2O, 4.79 ppm) and with the signal of the CH_2- group of HEMA (4.32 - 4.30 ppm). The CH_3-signals (2.49 ppm) are overlapping with the signals of CD_3CN (shifted from 1.94 ppm to 2.58 ppm due to the solvent-mixture and no clear phase). With a ^{1}H-NMR the amount of HEMA was calculated. Therefore, the integral of the proton's signal of the double bond at 6.67 ppm of **VKMA** was calibrated to two protons. The signal of HEMA at 6.73 ppm has an integral of 0.41, which represents 17 mol% HEMA. For this reason, the ^{1}H-NMR spectra are always standardized to the proton's signal of the double bond and the protons of HEMA, which are labeled as **A** in the degradation Scheme 24 and in Figure 40. For further calculations, the sum of the integrals of **A** were always set to 2.41 protons (calculated with 17 mol% HEMA). The signal of the acetal $-(O)_2CH-$ is referenced to this one and is labeled as **B**.

The studies showed that during the first 6 hours already 50 mol% of the acetals are cleaved and after about 4 days it can be considered as completely degraded (Figure 41).

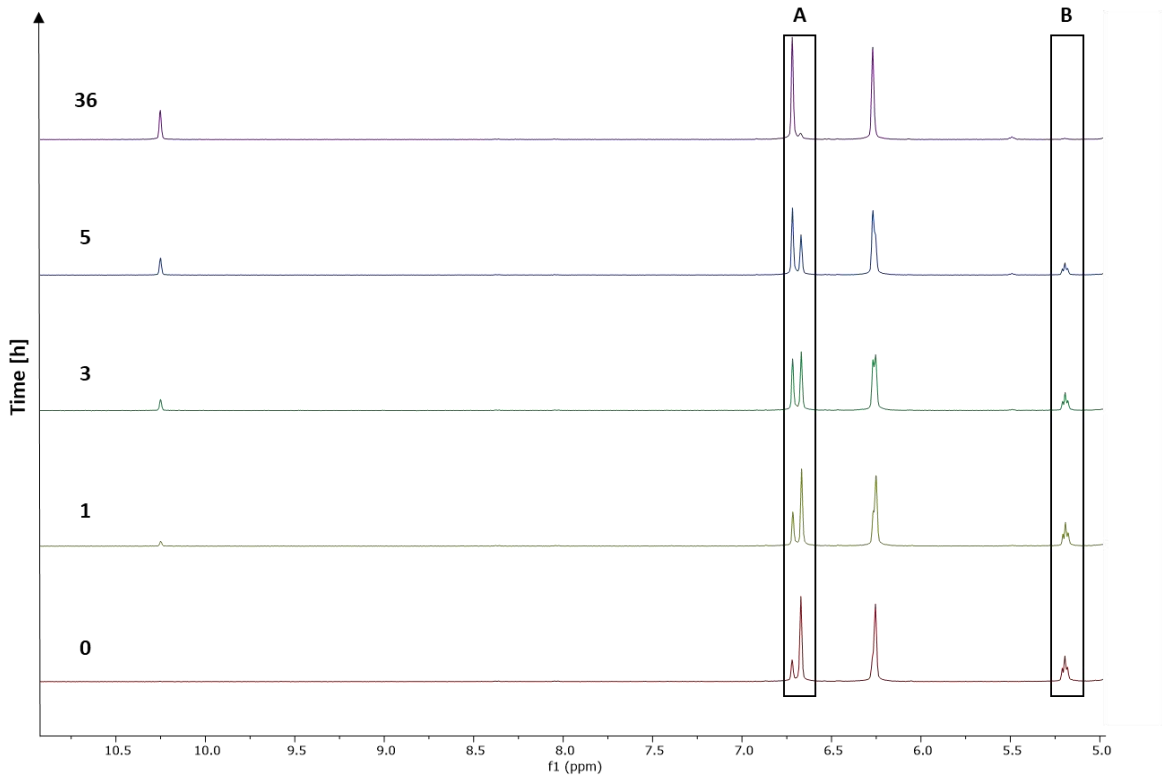

Figure 40: ^{1}H-NMR spectrum ($CD_3CN:D_2O$ (1:1) + 0.5 µl DCl (38 wt% DCl in D_2O), pH-equivalent of 2.1) of VKMA under acidic conditions during a period of 36 hours; Time t_0 (0 h, bottom) and t_5 (36 h, top).

A: standardized CH-H-signal of the double bond of VKMA; B: referenced CH-$(O)_2$-signal of VKMA.

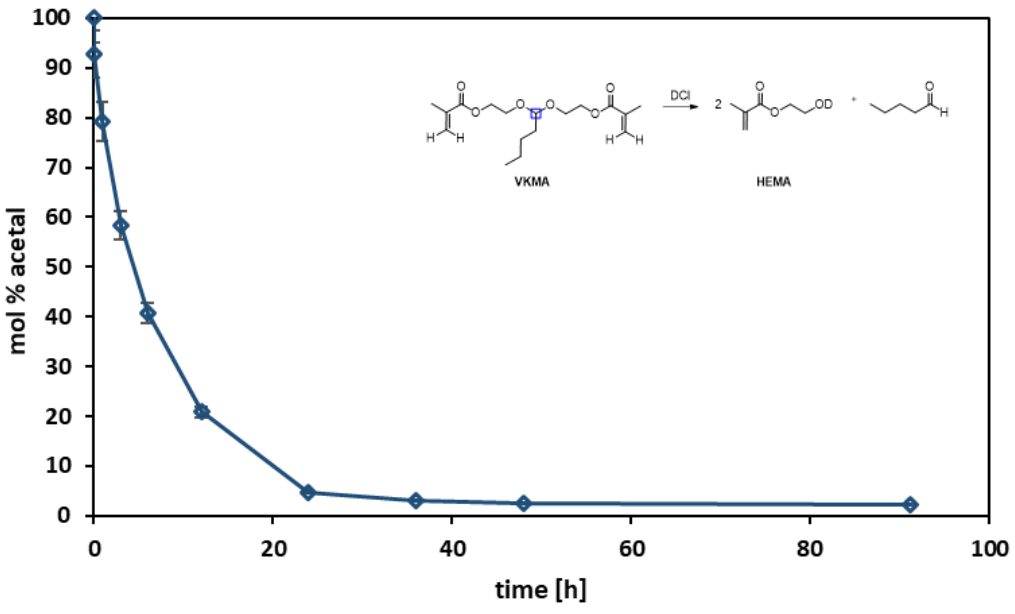

Figure 41: Degradation process of VKMA under acidic conditions (pH-equivalent of 2.1) during a period of 4 days. (For a better visibility, the symbols were connected with straight lines.)

2.2.2. Degradation of T5MA

For comparison, the aromatic acetal **T5MA** was also studied. Scheme 25 shows the resulting degradation products of **T5MA** under acidic conditions. In order to monitor the degradation, the signal of the aromatic protons of **T5MA** is subsequently labeled as **A** and is used as internal standard. This signal can be recognized at a chemical shift between 7.92 and 8.12 ppm and is standardized to four protons. Under acidic conditions, a stepwise degradation occurs. First, a one-side-cleavage was observable and this leads to a splitting of the aromatic signals into two multiplets and a shift downfield. These new signals are labeled as **B**. Afterwards, a cleavage of the second acetal is possible, which leads to terephthalaldehyde as degradation product. The signals of the aromatic protons of terephthalaldehyde can be found at even higher shifts. Here the signal again becomes a singlet and is marked as **C**.

For the degradation study, a pure product is to be assumed. As it is another batch as described in the synthesis, 14 mol% of the mono-substituted product (**B**) is present as well as T5MA (**A**) but no terephthalaldehyde (**C**). For this reason, the area of the integral of the mono-substituted molecule in the beginning of the measurement ($\mathbf{B}_{t=0}$) was subtracted for further calculations of $\mathbf{B}_t$.

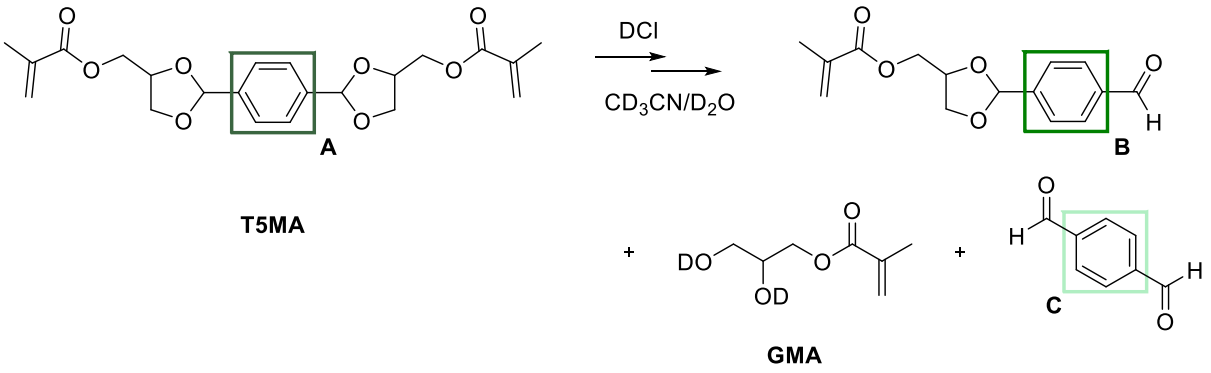

Scheme 25: Degradation of T5MA under acidic conditions.

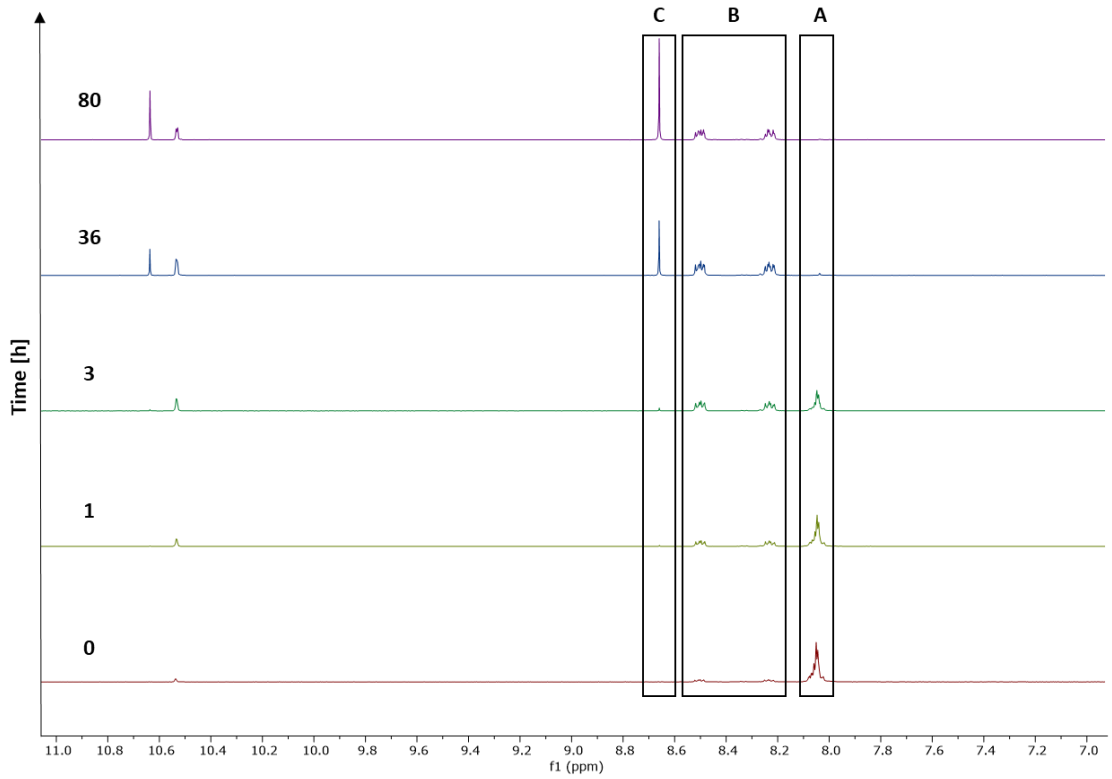

Figure 42: ^{1}H-NMR spectrum ($CD_3CN:D_2O$ (1:1) + 0.5 µl DCl (38 wt% DCl in D_2O), pH-equivalent of 2.1) of T5MA under acidic conditions during a period of 80 hours; Time t_0 (0 h, bottom) and t_5 (80 h, top).
A: standardized Ar-H-signals T5MA; B: referenced Ar-H-signals of the one-side-degraded molecule; C: referenced Ar-H of the two-side-degraded terephthalaldehyde.

The signals at 10.5 - 10.7 ppm in Figure 42 represent the protons of the formed aldehydes. First, only one singlet is observable at 10.5 ppm, which confirms the single-side-cleaved product. Already after three hours, a second signal of another aldehyde appears at 10.7 ppm. This one is shifted downfield and indicates the formed terephthalaldehyde. It can also be clearly seen that this signal increases over time and in comparison, the signal of the single-side-product decreases again. The progress of the reaction is also well illustrated in Figure 43. There, the round labels represent the starting material **T5MA**. The degradation curve is steep and after one day, the molecule could be considered as degraded. The other two curves represent the formation of the two aldehydes. The diamonds show the one-side-cleaved acetal. Within ten hours about 80 mol% of the single-side-cleaved product is formed. Afterwards, the amount of this product decreased, due to the cleavage of the second acetal. The squares represent terephthalaldehyde. The curve of the formation of terephthalaldehyde is ascending steadily.

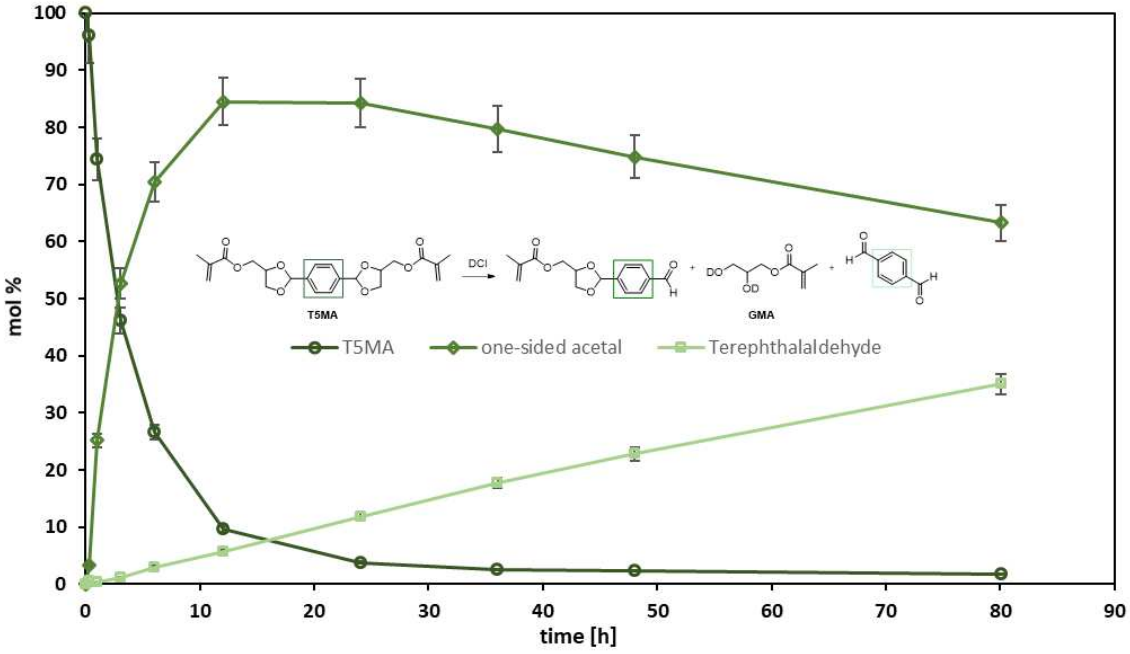

Figure 43: Degradation process of T5MA under acidic conditions (pH-equivalent of 2.1) during a period of 80 hours. (For a better visibility, the symbols were connected with straight lines.)

2.2.3. Degradation of MB5

Additionally, the degradation of **MB5** was studied. Once again, it should be noted, that the synthesis produced both 5- and 6-membered rings. Since only the signals of the aromatic protons do not overlap with other signals, these were standardized (8.07 - 7.90 ppm) to four protons and labeled as **A**. With this internal standard, it can be calculated that the acetals (5- to 6-membered ring) in a ratio of 60 mol% to 40 mol% were present. The more stable 5-membered ring was formed in larger amounts and the signal of the acetal is at 6.17 ppm, labeled as **B**. The signal of the other acetal is shifted slightly upfield (6.04 ppm) and marked as **C**.

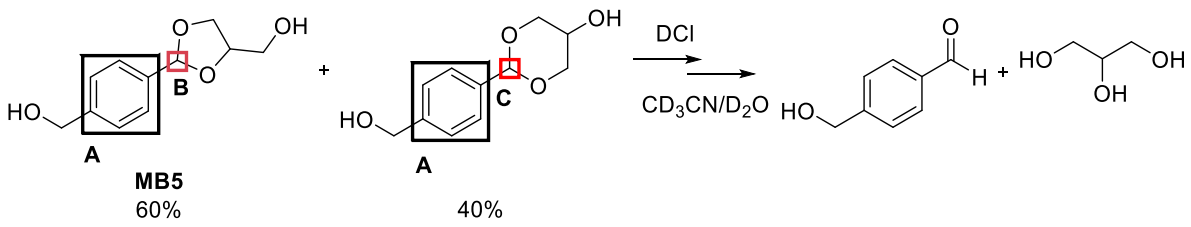

Scheme 26: Degradation of the diol under acidic conditions (some of the protons are exchanged with deuterium).

In the following Figure 44 it can be seen, that both acetals are nearly degraded completely within six hours and in Figure 45 completely within twelve hours. As expected, the 6-membered acetal degrades faster than the 5-membered ring (Figure 45).

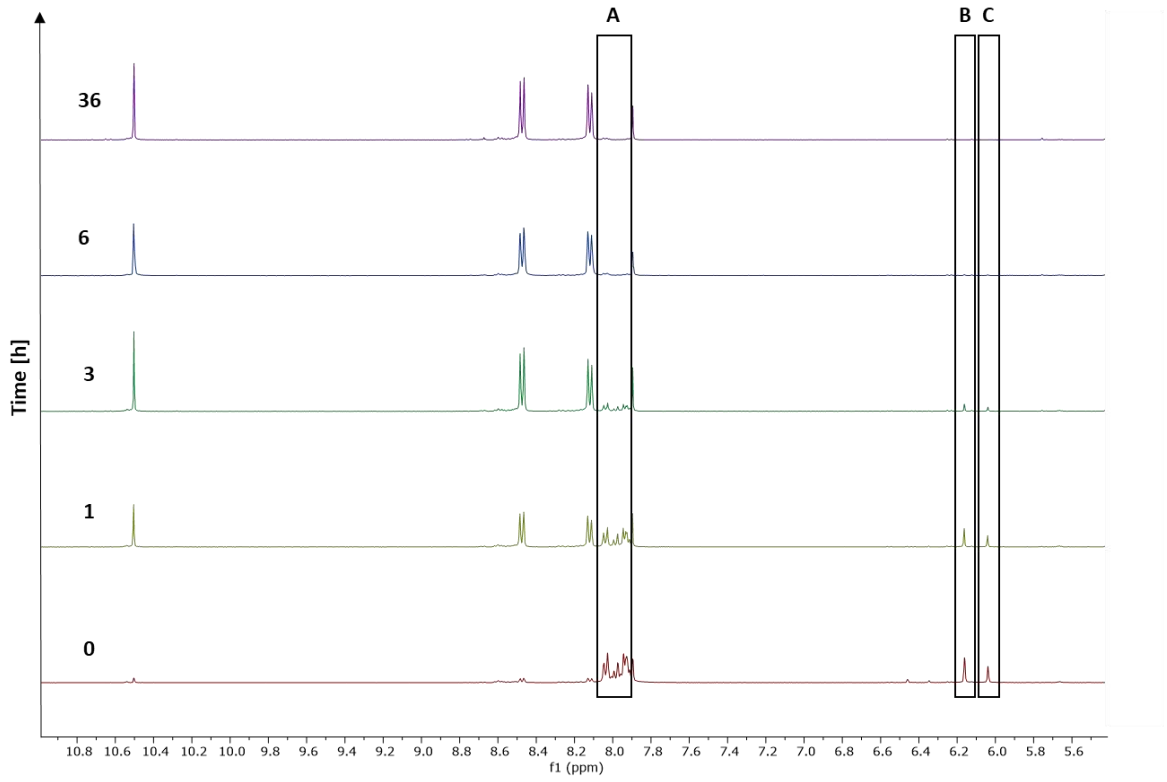

Figure 44: ^{1}H-NMR spectrum (CD_3CN:D_2O (1:1) + 0.5 µl DCl (38 wt% DCl in D_2O), pH-equivalent of 2.1) of the diol under acidic conditions during a period of 36 hours; Time t_0 (0 h, bottom) and t_5 (36 h, top) A: standardized Ar-H-signals of the diols; B: referenced to -CH-(O)-signals of the 5-membered ring; C: referenced -CH-(O)-signals of the 6-membered ring.

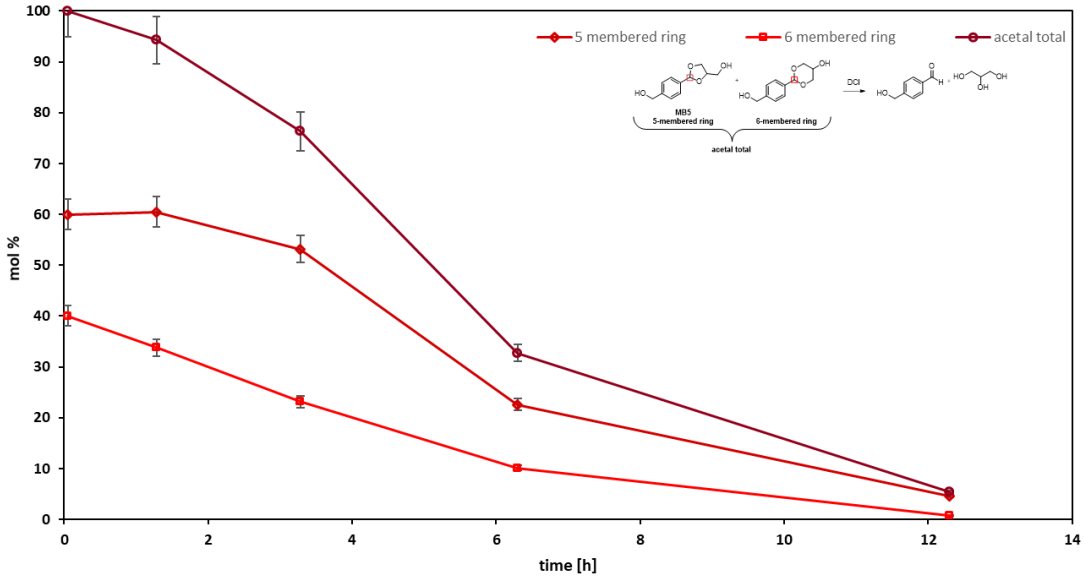

Figure 45: Degradation process of the diol under acidic conditions (pH-equivalent of 2.1) during a period of 14 hours. (For a better visibility, the symbols were connected with straight lines.)

In order to compare the degradation of the three different acetals, the first three hours were observed in detail. In this period the degradation can be linear approximated and the parameter mol% degradation per hour [mol%/h] was calculated and listed in Table 1.

Table 2: Degradation velocity (linear approximated with [mol%/h]) of EIBSPG and the alternative acetals (VKMA, T5MA and MB5) under acidic environment (pH-equivalent of 2.1), determined in the first three hours by ^{1}H-NMR spectroscopy.

compound	degradation [mol%/h]
EIBSPG	0.0 (spiroacetal)
	0.1 (ester)
VKMA	13
T5MA	18
MB5	8

Overall, it can be concluded that the polymerizable cyclic acetal **T5MA** degrades faster than the other two molecules. One acetal of **T5MA** cleaves first, and afterwards, the second one cleaves. **T5MA** degrades with 18 mol% per hour. The degradation of the aliphatic **VKMA** is progressing more slowly than the aromatic **T5MA**. The polymerizable linear acetal **VKMA** degrades with about 13 mol%/h. The most stable acetal (apart from the spiroacetals) is **MB5**, with 8 mol%/h in total. Taking a closer look, the 6-membered ring (40 mol% of total acetal)

degrades with 12.5 mol%/h and the 5-membered one (60 mol% of total acetal) with about 5 mol%/h.

In comparison to the esterified spiroacetal (**EIBSPG**), all alternative acetals degrade very fast. The ester of **EIBSPG** cleaves only with 0.1 mol/h in the first three hours and the acetal does not cleave at all in this time period.

2.3. Photopolymers

After synthesis and general degradation analysis of the monomers, characterization of the polymerization process and degradation behavior of fabricated polymers is necessary. These properties were investigated in the following two chapters via RT-FTIR-Photorheology and swelling tests, respectively.

Since the previously synthesized acetals **VKMA** and **T5MA** already have polymerizable functional groups, first degradation studies of polymer networks should be performed. Tightly crosslinked networks with rather slow degradation speed are expected to be formed.

Wichterle and Lim [160] were the first to show that a hydrogel based on hydroxyethyl methacrylate (HEMA) could be suitable as a biocompatible material. Since this pioneering work, hydrogels have been developed for a variety of medical applications, e.g. as wound covering materials [161] or for fixing a prosthesis in the intramedullary cavity due to the forces of the swollen hydrogel around the bone. [162] Therefore, HEMA should be used to adjust the network density and degradation behavior of the two base monomers **VKMA** and **T5MA**.

2.3.1. RT-FTIR-Photorheology

To study the photoreactivity and double bond conversions of the selected monomer formulations real-time-NIR-photorheology has been applied. Therefore, a conventional rheometer is combined with the feature to irradiate the sample with a UV or LED light source and a RT-NIR spectrometer to measure chemical information simultaneously. This setup is presented in Figure 46 and described in more detail in literature. [163]

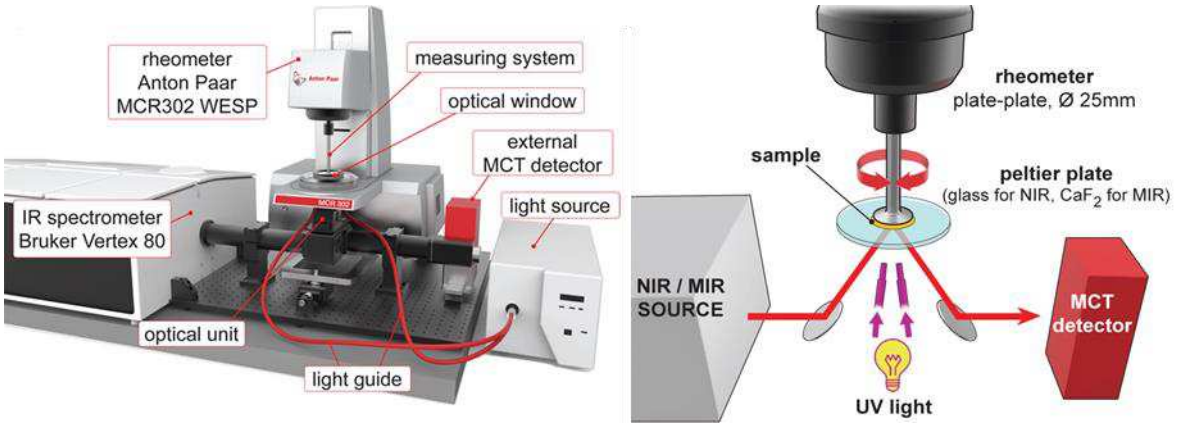

Figure 46: RT-FTIR-Photorheology setup (left) and illustration of the IR beam path and the irradiation (right). [163]

By this special method, important chemical and mechanical information can be determined during curing process of the photosensitive resin. During the whole measurement, the measuring system oscillates with a predefined frequency. Data of shear storage- and shear loss-modulus is provided by the rheometer during the curing process. The point, in which the two moduli curves intersect, is defined as gel point (t_g). Due to the simultaneously measured NIR spectra, the double bond conversions (DBC) can be calculated with the reduction of the peak area of the double bonds of e.g. methacrylates at ~ 6170 cm^{-1}. Therefore, the IR-bands were integrated before and after curing of the resin, using the Bruker OPUS software. Due to the real time infrared measurement, the DBC at the gel point (DBC_g) as well as the final DBC can be calculated. In addition, the shrinkage stress can be obtained by means of normal force measurements (F_N). A fixed gap size was set and a defined amount of sample was pipetted onto the glass plate of the rheometer making sure the whole gap is filled. Polymerization takes place during irradiation from below through the glass plate. Due to the gelation and shrinkage of the formed polymer network, the measuring plate will be pulled downwards. Therefore, the normal force will increase to keep the predefined gap constant. [163] The preparation of formulations was performed in the orange light lab to avoid an unintended polymerization. The initiator Ivocerin® (1 mol%) is used in this work due to its good compatibility with the LED light source of 460 nm, which is often used in AMT techniques. [164, 165] The initiator, the monomer and if necessary, also the reactive diluent HEMA were mixed. The samples were applied on a glass disk (+ PE tape) and a gap of 200 µm between the measuring system (PP25) and the disk was set. A broadband Hg-lamp was used with a 400-500 nm filter to irradiate the samples. All measurements were performed in triplicates at room temperature (25 °C) with 1 W cm^{-2} light intensity at the end of the light

guide. In order to determine the double bond conversion over the measuring period, the signal at ~ 6170 cm^{-1} was recorded and integrated over the measuring period related to the integral at t_0.

Photorheology experiments were performed to receive both rheological and kinetic data simultaneously. Therefore, measurements with both synthesized monomers, the aliphatic **VKMA** and the aromatic **T5MA** methacrylates were conducted. In addition, different dilutions with the reactive diluent HEMA were prepared. The addition of HEMA should adjust the mechanical properties and widen the polymer network. Due to the fact, that HEMA is a monofunctional methacrylate, twice the molar amount was necessary to provide double bond specific ratios of the dilutions. Three different formulations were prepared for each monomer. The basic formulation consisted of the photoinitiator with the pure monomer. Furthermore, two different dilutions with HEMA, a 1:1 and 1:4 molar mixtures were desired in each case. The formulations were prepared, but the impurities of the monomer were not included into the calculations. After including, a 1:1 and a 1:5 ratio of double bonds (DB-ratio) for **VKMA** resp. a 1:4 ratio for **T5MA** with the mono-functional reactive diluent HEMA were obtained.
First, the formulations of the pure monomers are examined in detail (Figure 47, left column in the diagrams for each monomer).

If one considers the process of polymerization, the time until gelation (t_g) is the first characteristic point, where storage- and loss modulus are equal. With NIR spectroscopy, the double bond conversion DBC_g can also be determined for both monomers at this point. **T5MA** reaches t_g with 1.4 s approximately four times faster than **VKMA** with 5.4 s. It can be also seen that the DBC_g for **T5MA** is significantly higher. A shorter time until gelation (t_g) for the aromatic cyclic acetal **T5MA** is well explainable, due to the rigid structure of the monomer **T5MA** compared to the linear aliphatic **VKMA**. The significantly higher DBC at the gel point could be not explained, especially it one considers that **VKMA** has a significant amount of HEMA as impurity.
After reaching the gel point, a tightly crosslinked network is formed during further conversion. For further characterizations, the time to reach 95% of the overall DBC (t_{95}) and the overall DBC itself are determined. The aliphatic **VKMA** already reaches 95% of the DBC after about 70 s and thus, it is twice faster than its aromatic counterpart. In addition, the overall DBC is clearly higher with 88% for the linear aliphatic monomer than for the cyclic aromatic **T5MA** with 78%. This trend can be well explained by the chemical structure and its influence on the

network formation. Due to its aromatic and cyclic structure of **T5MA**, a more rigid polymer network is formed. For this reason, remaining monomer diffusion is hindered, therefore leading to higher t_{95} and limiting the final DBC compared to **VKMA**.

So far, only the formulations of the pure monomer systems were considered. Now, the formulations of the monomers with different amount of reactive diluent are examined in detail (Figure 47). The second column for each methacrylate is a formulation with a DB-ratio of 1:1 (monomer:HEMA). The right column is for **VKMA** a 1:5 and for **T5MA** a 1:4 molar mixture with the reactive diluent HEMA.

First, the gelation behavior will be considered again. A similar trend for t_g was observed for both monomers. As expected, with increasing amount of reactive diluent t_g increased due to the lower content of crosslinking monomer. Due to the rigidity of the system, formulations with **T5MA** as monomer gel significantly faster. Also due to the lower network density, the DBC_g increases with increasing amount of HEMA. However, for **T5MA** an unusual trend was observed. The DBC at the gel point with 24% for the pure monomer is higher, compared to the dilutions. Based on the fact that the high DBC_g for pure **T5MA** could also be not explained in the previous section of the pure crosslinkers, there seems to be a systematic error for this value.

In terms of the overall network formation, a decrease of t_{95} and an increase of the overall DBC is observable for both monomers, with increasing of HEMA concentration. This effect can be easily attributed to the crosslink-density. In general, HEMA is a monofunctional methacrylate compared to the used monomers **VKMA** and **T5MA**, which are bifunctional. If the concentration of HEMA increases, the network density decreases. Furthermore, increasing content of HEMA decreases the viscosity of the formulation, which in turn contributes to the promotion of the diffusion of the monomers. This leads again to lower t_{95} and higher overall DBC.

As expected, these effects are more distinctive for the cyclic acetal, as the pure monomer **T5MA** is highly viscous. Furthermore, the effect of highly rigid networks is also diminished by using HEMA.

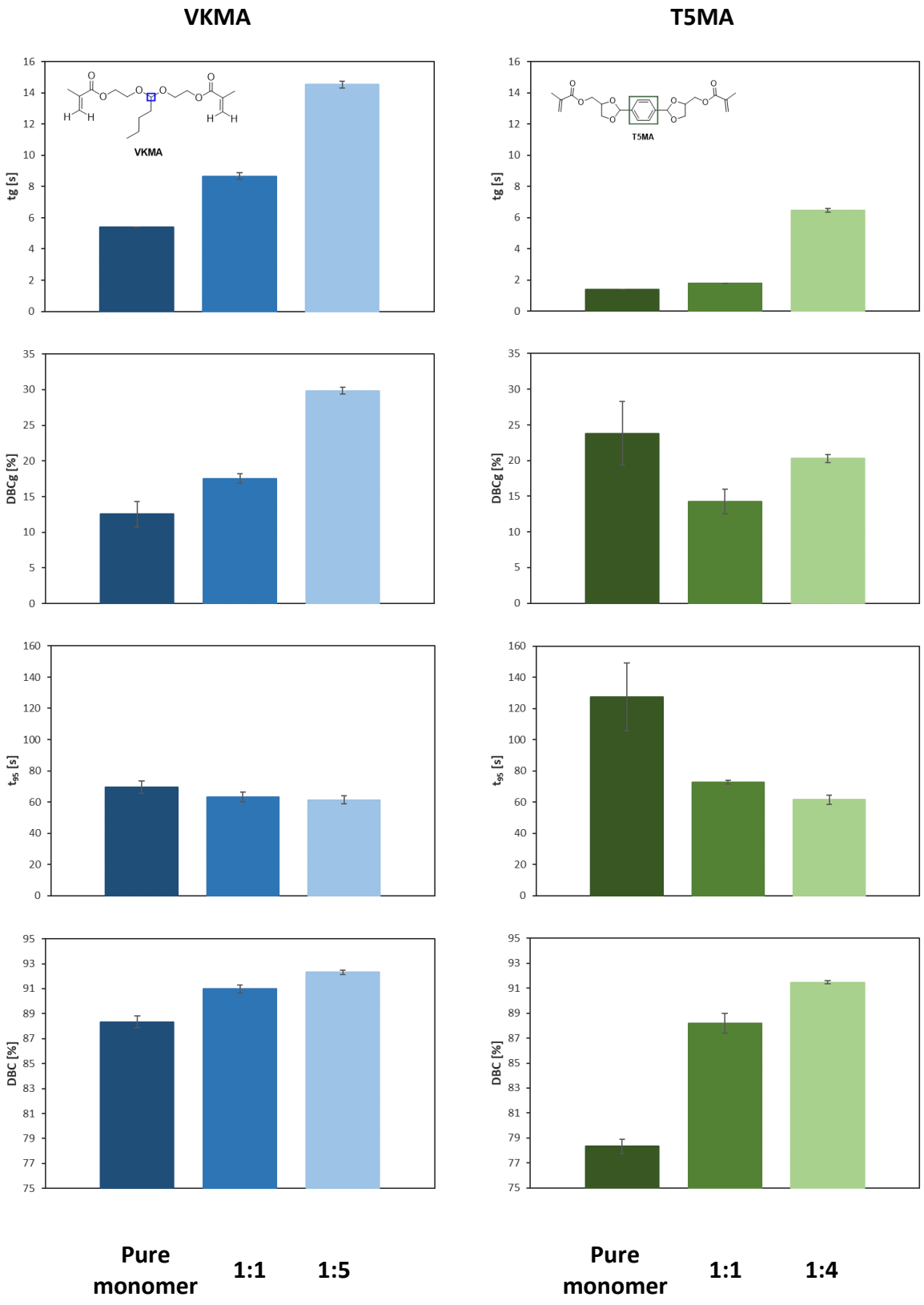

Figure 47: Results of RT-NIR-photorheology measurements of VKMA and T5MA. The left bar always show the formulation of pure monomer, the middle one the formulation in a ratio of 1:1 with the reactive diluent HEMA and the right bar the dilutions with a ratio of 1:5 (for T5MA 1:4). Presented is the time to gelation t_g (top), the DBC at the gel point DBC_g, time to reach 95% overall conversion t_{95} and the final DBC (bottom).

In conclusion, the highly rigid **T5MA** reaches the gel point at shorter time than the flexible **VKMA**. However, **VKMA** has shorter t_{95} and higher final DBC due to its flexible nature.

2.3.2. Swelling and Degradation Behavior

The degradation of the polymer networks had to be studied in order to assess their potential for the aimed application as bone replacement material. Degradation is a process where polymer chains are cleaved and form oligomers and in the end small molecules. Erosion describes the loss of material due to washing-out of oligomers and monomers from the polymer network. All degradable polymers share the property of eroding upon degradation at varying rates. [166, 167] These are observed in this chapter.

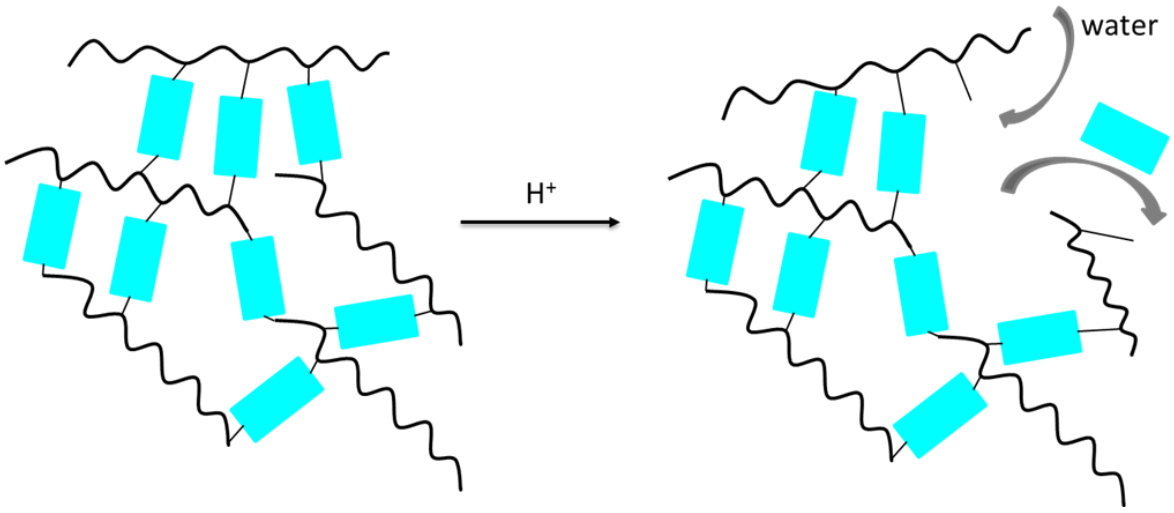

Figure 48: Pictorial representation of swelling and degradation of a polymer network in an acidic environment.

Figure 48 illustrates a schematic network and its swelling under hydrolytic conditions. The wavy black lines represent the polymer backbone and the blue squares the spacer between the acetal moieties.

During degradation, different processes are assumed. First, a spontaneous swelling, with increase of the mass, is expected. Due to network degradation, a higher water uptake is possible due to the wider network meshes and therefore, the mass will further increase. After cleavage of the labile bonds, oligomers and monomers can elute and mass-erosion can be observed.

The mass changes of the samples were determined according to the following equation.

$$Mass\ change\ [\%] = \frac{m_t - m_0}{m_0} \cdot 100$$

m_0 and m_t represent the initial weight and the weight at t (swollen) of the samples.

For a better observation of the process over time, the mass is plotted versus the measuring period in days. During swelling, the mass is increasing, which is expressed *via* a positive mass change. Mass erosion itself gives a negative mass change. However, it may happen that the swelling overcompensates the mass erosion and only a positive mass change is observable.

2.3.2.1. Narrow meshed polymer networks (undiluted)

First, narrow meshed polymer networks from the base monomers **VKMA** and **T5MA** should be studied. Thereby, the degradability of the different acetal moieties (linear and cyclic), the effect of the network density and the structure of the monomers on the swelling behavior, can be directly compared. For the swelling tests, an aqueous HCl solution was prepared. The pH was adjusted to 4.4 with a pH electrode at 22.5 °C. Photopolymerized samples with a defined thickness of 200 µm (from photorheology experiments) were used in triplicates. The samples were placed into tissue culture dishes and immersed into the acidic solution. After defined time ranges, samples were taken from the medium, wiped with tissue paper, weighed and placed into the medium again.

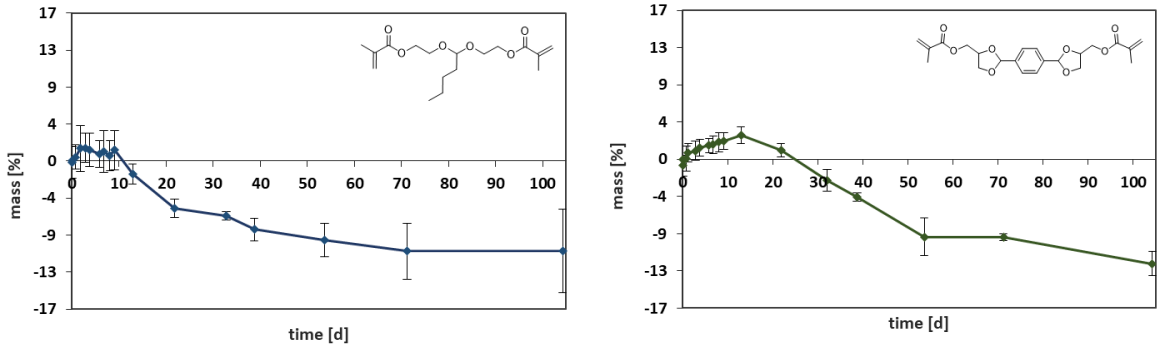

Figure 49: Swelling tests for crosslinked VKMA (left) and T5MA (right) in acidic environment at room temperature (HCl: pH = 4.4 adjusted at 22.5 °C).

Figure 49 shows the swelling of the narrow meshed **VKMA** polymer network on the left. For this aliphatic system with a linear acetal, there is swelling observed in the first two days. After that, the mass decreases, so the mass erosion over-compensated the swelling. After

approximately 10 days, the residual mass is below the initial mass. The mass erosion is steep in the beginning and after about 20 days, the curve flattens. Over the measuring period, the shapes of the samples are stable, however a softening effect was observed.
The right side of Figure 49 shows the swelling of the aromatic system with cyclic acetals **T5MA**. There, an increase of the mass is observed until day 13. After that day, a mass erosion can be detected. After approximately 32 days, the residual mass is below the initial mass. Here, the mass erosion has more effect on the system, than the swelling. After the beginning of mass erosion, the decrease is quite steep until 53 days. Afterwards, the curve flattens. Until these days, the shape of the samples is also preserved.

Compared to the aliphatic system, the network for the aromatic one is much more rigid. Thus, the water-uptake and therefore swelling takes much more time. If sufficient water is present, degradation can start. Considering the degradation model study of the two monomers (Chapter 2.2), it was found that the aromatic systems is cleaved faster, which could also explain the faster degradation of **T5MA** after the initial swelling process.

2.3.2.2. Wide meshed polymer networks (diluted)

After the investigation of the narrow meshed polymer networks, now also wide meshed networks will be investigated. HEMA was used because it is already known as comonomer photopolymerizable bone implants. [162] The behavior under aqueous acidic conditions of the wide meshed polymer networks were investigated as described before. The diluted networks were treated equally to the undiluted networks. However, for some formulations (DB-ratio of 1:5 for **VKMA** and 1:4 for **T5MA**), it was not possible to remove the disks from the disposable plates. Therefore, the disposable plates were weighed, then the rheology measurements were realized and the disposable plates with the adherent samples were placed into the acidic solution. Overnight the samples separated from the disposable plates. Afterwards, those were removed and the samples were immersed again into the solution. First, the aliphatic acetal in its dilutions will be discussed and afterwards the aromatic one.

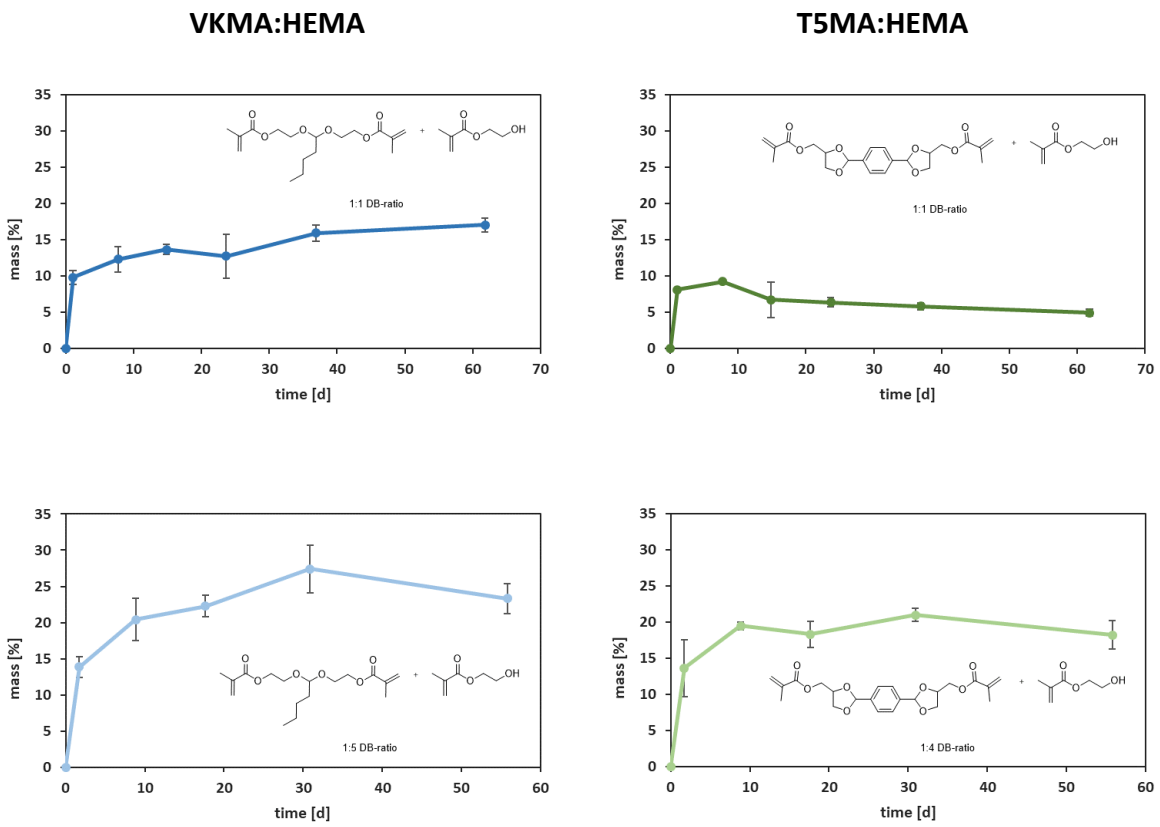

Figure 50: Swelling test for the formulations of the crosslinked VKMA:HEMA (left, in a DB-ratio of 1:1 (top) and 1:5 (bottom)) and T5MA:HEMA (right, in a DB-ratio of 1:1 (top) and 1:4 (bottom)) in acidic environment at room temperature (HCl: pH = 4.4 adjusted at 22.0 °C).

Figure 50 shows on the left column the results of the swelling tests of the different diluted networks of **VKMA** at pH 4.4 at room temperature. For the formulation with a DB-ratio of 1:1, the mass increases over the complete measuring period of about two months. The formulation with higher amount of reactive diluent has a higher water uptake compared to the other one in a ratio 1:1. After four weeks, a slow decrease of the mass is observable. The higher water-uptake can be explained by the presence of HEMA, which is well known to form hydrogels due to the polarity of the building block.

The right column displays the swellability of networks with varying dilutions of the aromatic monomer **T5MA**. The formulation with a DB-ratio of 1:1 shows an initial increase of about 9% of the mass for the first 8 days. After that time, a decrease of mass is already observable. The formulation of a DB-ratio of 1:4 shows in this period an increasing of about 20% of the mass. After four weeks, the curve decreases a little bit to 18%. The higher amount of the reactive diluent increase the possibility to swell, due to the wider network.

To summarize, in the presence of HEMA the mass loss is not directly visible, as the water-uptake by the polar HEMA moieties overcompensate this effect.

In further degradation studies, the swellability and the mass erosion will be considered separately.

EXPERIMENTAL

1. Oligomeric Spiroacetals

1.1. Synthesis of Spiroacetals

1.1.1. Spiroacetal based on Vanillin (VanSPG)

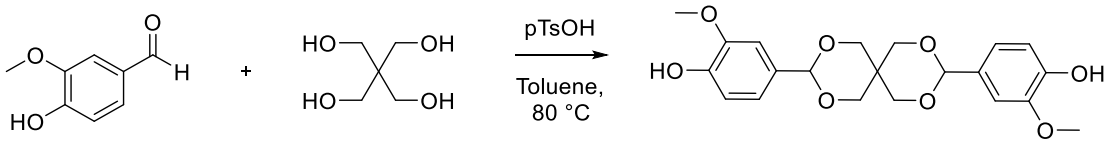

Van VanSPG

Reagents

	M [g/mol]	eq. [/]	n [mmol]	m [g]
Pentaerythritol	136.15	1.0	55.2	7.52
Vanillin	152.15	2.0	110.4	16.80
pTsOH-monohydrate	190.22	1 mol%	0.6	0.114

Procedure

4,4'-(2,4,8,10-Tetraoxaspiro[5.5]undecane-3,9-diyl)bis[2-methoxy-phenol] (**VanSPG**) was synthesized according to Hirose *et al.* [142]. Therefore, Vanillin, pentaerythritol and pTsOH-monohydrate were dissolved in 300 mL dry toluene in a round-bottomed flask. The flask was attached to a Dean-Stark apparatus and a reflux condenser. The apparatus was purged with argon and the reaction mixture was heated to reflux. After 36 h no more water was generated and therefore, the reaction mixture was allowed to cool down. The solution was washed with saturated Na_2CO_3 solution. While extraction some beige/white precipitate was formed (1.89 g) and filtrated through a sintered glass funnel. The filtrate was washed with deionized water and dried over anhydrous Na_2SO_4. The solution was concentrated *in vacuo* and a beige solid was obtained (15.64 g). All solids were recrystallized with ethyl acetate. The purified product was obtained in 7.96 g (36% theoretical yield) as white/beige powder. The purity was proved with HPLC (only one signal), NMR and m.p. and is approved as sufficiently pure.

^{1}H-NMR (400 MHz, $CDCl_3$): δ (ppm) = 7.03 (s, 2H, ArH), 6.98-6.89 (m, 4H, ArH), 5.65 (s, 2H, OH), 5.39 (s, 2H, ArCH), 4.86 (d, *J* = 11.2 Hz, 2H, OCH_2-H_{ax}), 3.92 (s, 6H, OCH_3), 3.85-3.80 (m, 4H, OCH_2-H_{eq}), 3.64 (d, 2H, *J* = 11.2 Hz, OCH_2-H_{ax}).

^{13}C-NMR (400 MHz, $CDCl_3$): δ (ppm) = 146.56, 146.43, 130.28, 119.63, 114.18, 108.37, 102.42, 71.21, 70.72, 56.06, 32.58.

m.p.: 169.8-170.9 °C (Lit.: 171 °C) [168]

1.1.2. Spiroacetal based on 4-Hydroxybenzaldehyde (4HBSPG)

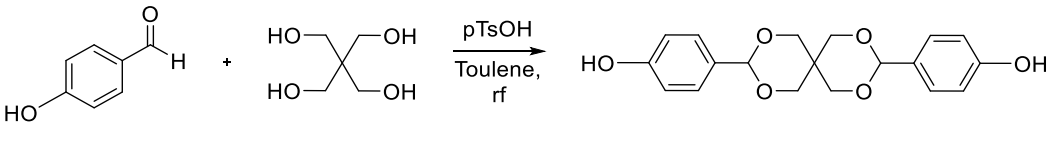

4HBSPG

Reagents

	M [g/mol]	eq. [/]	n [mmol]	m [g]
Pentaerythritol	136.15	1.0	20.5	2.787
4-Hydroxybenzaldehyde	122.12	2.0	41.0	5.007
pTsOH-monohydrate	190.22	1 mol%	0.2	0.039

Procedure

4,4'-(2,4,8,10-Tetraoxaspiro[5.5]undecane-3,9-diyl)bis-phenol (**4HBSPG**) was synthesized according to Hirose *et al.* [142]. Therefore, 4-hydroxybenzaldehyde, pentaerythritol and pTsOH-monohydrate were dissolved in 200 mL dry toluene in a round-bottomed flask. The flask was attached to a Dean-Stark apparatus and a reflux condenser. The apparatus purged with Ar and the reaction mixture was stirred at reflux for 18 h. A white precipitate was formed. Due to this, the reaction mixture was transferred to a bigger flask and 200 mL dry toluene were added. The reaction mixture was heated to reflux again but the solid did not dissolved. During the reaction time of 3 h, water was generated and therefore, the reaction mixture was extracted with saturated $NaHCO_3$ solution. During extraction, a reddish-brown precipitate occurred and was filtered. The organic phase was dried over anhydrous Na_2SO_4 and the solvent was evaporated *in vacuo.* No more product was isolated. The precipitate was dried

in vacuo and was isolated in 4.91 g (70 % theoretical yield) as reddish-brown powder. The purity was proved with HPLC (one signal), NMR and m.p. and was approved as pure.

^{1}H NMR (400 MHz, DMSO-d_6): δ (ppm) = 9.59 (s, 2H, OH), 7.27 – 7.12 (d, *J* = 4.71 Hz, 4H, ArH), 6.76 – 6.69 (d, *J* = 4.71 Hz, 4H, ArH), 5.36 (s, 2H, OCHO), 4.52 (d, *J* = 11.97, 2H, OCH_2C), 3.83 (d, *J* = 11.97 Hz, 2H, OCH_2C), 3.73 (dd, *J* = 11.5, 2.4 Hz, 2H, OCH_2C), 3.61 (d, *J* = 11.97 Hz, 2H, OCH_2C).

^{13}C-NMR (400 MHz, DMSO-d_6): δ (ppm) = 157.74, 129.15, 127.47, 114.65, 101.48, 69.93, 69.44, 31.82.

m.p.: 169.6-171.4 °C (Lit.: 170-171 °C) [109]

1.1.3. Spiroacetal based on 4-Formylbenzoic acid (4FBASPG)

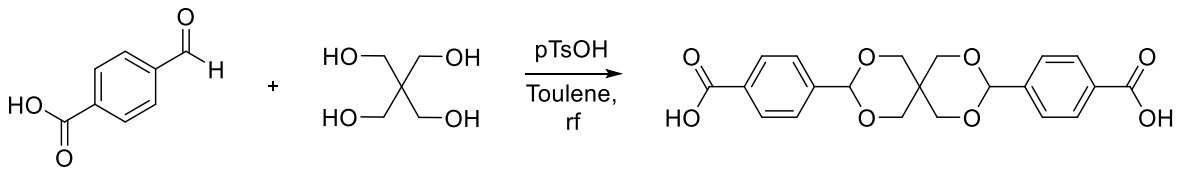

4FBASPG

Reagents

	M [g/mol]	eq. [/]	n [mmol]	m [g]
Pentaerythritol	136.15	1.0	16.7	2.267
4-Formylbenzoic acid	150.13	2.0	33.3	5.002
pTsOH-monohydrate	190.22	1 mol%	0.2	0.033

Procedure

4,4'-(2,4,8,10-Tetraoxaspiro[5.5]undecane-3,9-diyl)bis-benzoic acid (**4FBASPG**) was synthesized according to Hirose *et al.* [142] Therefore, pentaerythritol, 4-formylbenzoic acid and pTsOH-monohydrate were dissolved in 900 mL dry toluene in a three-necked round-bottomed. The flask was equipped with a reflux condenser and a Dean-Stark apparatus. The reaction mixture was stirred at reflux for 36 h. Some white precipitate was formed. The precipitate was separated from the solution and ^{1}H-NMR were measured in d_6-DMSO. The precipitate was identified as product and some traces of the aldehyde, but no pentaerythritol

was observed. Therefore, 45.38 mg (0.3 mmol) pentaerythritol were added and the solution was allowed to stir again at reflux for 18 h. No more water was formed, so the reaction was terminated. The precipitate was filtrated. The product could be isolated in 5.63 g (84% theoretical yield) as white powder. The product was analyzed by ^{1}H-NMR (impurity aldehyde, ≤ 4%) and HPLC (two signals found: 4-formylbenzoic acid: $t_{R(B)}$ = 2.4 min, **4FBASPG**: $t_{R(B)}$ = 1.5 min) and m.p..

^{1}H-NMR (400 MHz, DMSO-d_6): δ (ppm) = 13.02 (s, 2H, -COOH), 7.95 (d, *J* = 8.1 Hz, 4H, Ar-H), 7.57 (d, *J* = 8.2 Hz, 4H, Ar-H), 5.59 (s, 2H, Ar-CH), 4.58 (dd, *J* = 11.3, 2.3 Hz, 2H, OCH_2C), 3.94 (d, *J* = 11.2 Hz, 2H, OCH_2C), 3.83 (dd, *J* = 11.6, 2.3 Hz, 2H, OCH_2C), 3.71 (d, *J* = 11.5 Hz, 2H, OCH_2C).

^{13}C-NMR (400 MHz, DMSO-d_6): δ (ppm) = 166.99, 142.52, 131.14, 129.19, 126.40, 100.51, 69.93, 69.43, 32.14.

m.p.:291.4-293.8 °C (Lit.: 295-298 °C) [143]

1.2. Optimization of Esterification of Spiroacetals

1.2.1. Synthesis of Esterified Isobutyral-SPG (EIBSPG)

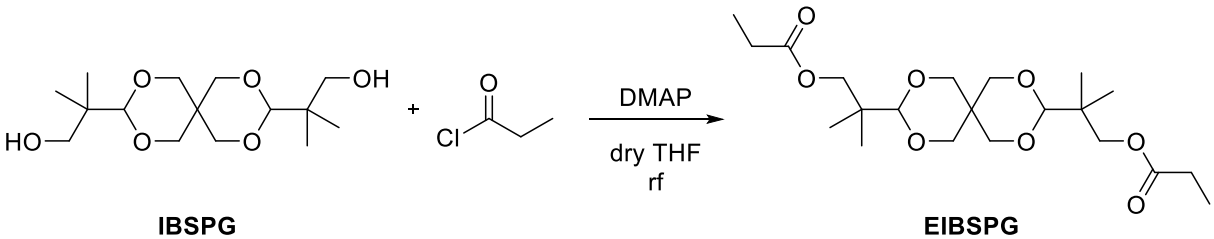

IBSPG **EIBSPG**

Reagents

	M [g/mol]	eq. [/]	n [mmol]	m [g]
Isobutyral-SPG	304.38	1.0	16.4	5.003
Propionyl chloride	92.52	2.4	39.5	3.650
DMAP	122.17	2.5	41.1	5.017

Procedure

During the attempts to optimize the esterification of IBSPG for polyester synthesis, which are described in the Chapter Results and Discussion (Subchapter 1.2), it was found that DMAP as

acid scavenger leads to the best results. For this reason, the following procedure was chosen, with the difference that the acid chloride was used in excess to further increase of the yield. Therefore, $\beta^3,\beta^3,\beta^9,\beta^9$-tetramethyl-2,4,8,10-tetraoxaspiro[5.5]undecane-3,9-diethanol (Isobutyral-SPG, **IBSPG**) and 4-dimethylaminopyridine (DMAP) were dissolved in 260 mL dry THF in a three-necked round-bottomed flask and the apparatus was flushed with argon. Propionyl chloride was added dropwise and a white precipitate (4-(dimethylamino)-pyridinium chloride) had formed. The reaction mixture was stirred at room temperature for 18 hours. The conversion was monitored by ^{1}H-NMR spectroscopy. The salt was removed by filtration and the reaction mixture was washed with saturated NH_4Cl solution (2 times) and brine (2 times). Then the organic layer was dried over anhydrous Na_2SO_4. Afterwards the solvent was evaporated and a light-pink solid (6.495 g) was obtained. The resulting powder was recrystallized in PE to isolate the product as light-pink powder in 5.61 g (82% theoretical yield). The purity was proved with HPLC and NMR.

^{1}H-NMR (400 MHz, $CDCl_3$): δ (ppm) = 4.50 (dd, *J* = 11.4, 2.5 Hz, 2H, OCH_2C), 4.24 (s, 2H, OCHO), 3.92 (s, 4H, $CH_2OC{=}O$), 3.56 (dd, *J* = 11.5, 2.6 Hz, 2H, OCH_2C), 3.50 – 3.42 (m, 2H, OCH_2C), 3.30 (d, 2H, *J* = 11.4 Hz, OCH_2C), 2.34 (q, 4H, *J* = 7.6 Hz, $C\underline{H_2}$-CH_3), 1.15 (t, 6H, *J* = 7.6 Hz,CH_2-$C\underline{H_3}$), 0.95 (d, 12H, *J* = 4.6 Hz, $C(CH_3)_2$).

^{13}C-NMR (400 MHz, $CDCl_3$): δ (ppm) = 174.49, 105.12, 70.74, 70.28, 69.32, 38.72, 32.65, 19.57, 19.39, 9.38.

HR-MS: calc. EM + Na: 439.23 g/mol; found: 439.23 g/mol

mp.: 86.2-87.2 °C

1.4. Degradation Model Study of Spiroacetal Derivatives

The degradation of the acetal moiety and the ester group of the synthesized aliphatic spiroacetal (**EIBSPG**) was studied by ^{1}H-NMR spectroscopy over a few weeks at room temperature. The studies were conducted in CD_3CN/D_2O (1:1). The signal of the solvent was locked to D_2O at 4.79 ppm. Altogether three different pH-equivalents were measured. One of the NMR tube contained 0.5 µl NaOD (40 wt% NaOD in deuterium oxide), which would be a pH-equivalent of 12.0, one contained 0.5 µl DCl (38 wt% DCl in deuterium oxide), with a pH-equivalent of 2.1 and the last tube was measured in the plain NMR solvent. First, the substance

was dissolved in 0.35 mL CD_3CN and afterwards 0.35 mL D_2O were added. The mass should not exceed much more than 5 mg as otherwise the substance precipitated again by addition of D_2O. The mass of the single experiments are shown in Table 3. Table 4 depicts the values of the ^{1}H-NMR degradation study under basic and Table 5 the values under acidic conditions. Additionally, the degradation behavior was determined under neutral conditions. In the whole period of the measurement, no cleavage of the ester and the spiroacetal was observable and thus no values are listed in a table.

Table 3: Mass for the NMR-degradation model study of the spiroacetal.

Conditions	m [mg]
Acidic	4.51
Neutral	4.51
Basic	5.11

Table 4: Values for the ^{1}H-NMR degradation study of EIBSPG under basic conditions (pH-equivalent of 12.0).

Time [d]	Remaining ester [%]
0.00	96.75
0.25	29.03
0.38	23.45
0.50	20.51
0.63	18.41
0.75	17.29
0.83	16.95
1.04	15.75
1.54	14.47
2.04	14.10
2.54	13.78
19.75	13.09
43.88	12.79

Table 5: Values for the ^{1}H-NMR degradation study of EIBSPG under acidic conditions (pH-equivalent of 2.1).

Time [d]	Remaining ester [%]	Remaining acetal [%]
0.00	100.00	100.00
0.13	99.58	100.00
0.25	99.54	100.00
0.38	99.20	100.00
0.63	98.93	99.86
0.75	98.89	99.92
0.88	98.93	99.95
1.06	98.51	99.83
1.56	98.10	99.79
2.06	95.43	98.56
2.56	96.75	99.72
3.56	94.44	99.16
19.81	77.75	97.87
20.27	77.65	97.61
44.39	61.49	93.59

2. Low Molecular Weight Linear and Cyclic Acetals

2.1. Synthesis

2.1.2. Acetal based on Valeraldehyde and HEMA (VKMA)

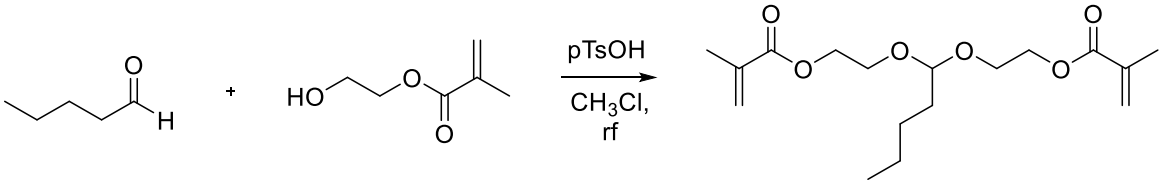

HEMA **VKMA**

Reagents

	M [g/mol]	eq. [/]	n [mmol]	m [g]
Valeraldehyde	86.13	1.0	35.2	3.03
HEMA	130.14	2.66	93.2	12.13
pTsOH-monohydrate	190.22	1 mol%	0.4	0.069

Procedure

First, the purity of HEMA and valeraldehyde has been proved by ^{1}H-NMR spectroscopy. Afterwards, 1,1'-[pentanebis(oxy-2,1-ethanediyl)]-2-methyl-2-propenoic acid ester (**VKMA**) was synthesized according to Hirose *et.al.* [142] Therefore, a 500 mL three-necked round-bottomed flask with an inversed Dean-Stark apparatus and a reflux condenser was evacuated and purged with argon (three times). Afterwards dry chloroform (200 mL), HEMA and pTsOH-monohydrate were added with countercurrent flow. Valeraldehyde was then added with a syringe to the reaction mixture within 2 minutes. Afterwards, the solution was heated to reflux and stirred for 36 h. The reaction progress was followed by ^{1}H-NMR spectroscopy. After 5 days the reaction mixture was quenched with saturated $NaHCO_3$, washed with brine and deionized water. The organic layers were dried over anhydrous Na_2SO_4, filtrated, phenothiazine (125 ppm) and MEHQ (291 ppm) were added and the solvent was removed *in vacuo*. With high vacuum ($1.7 \cdot 10^{-1}$ mbar, 40 °C), the excess of HEMA was distilled off. A further evaporation step did not change the content of HEMA (checked by weighing). The final purity was checked with HPLC and NMR. The product was isolated as yellow oil in

85% yield (**VKMA**: $t_{R(A)}$ = 4.7 min (HPLC); impurity HEMA: ≤ 17 mol% (NMR), $t_{R(A)}$ = 2.3 min (HPLC)).

^{1}H-NMR (400 MHz, DMSO-d_6): δ (ppm) = 6.02 (d, *J* = 1.6 Hz, 2H, C=C<u>H</u>-H), 5.68 (dh, *J* = 3.2, 1.6 Hz, 2H, C=CH-<u>H</u>), 4.61 – 4.52 (m, 1H, C<u>H</u>-(O-)$_2$), 4.21 (dd, *J* = 5.5, 4.0 Hz, 4H, OC<u>H$_2$</u>CH$_2$O), 3.74 (ddd, *J* = 9.3, 6.5, 4.0 Hz, 2H, OCH$_2$C<u>H$_2$</u>O), 3.69 – 3.62 (m, 2H, OCH$_2$C<u>H$_2$</u>O), 1.88 (dd, *J* = 3.3, 2.0 Hz, 6H, C-C<u>H$_3$</u>), 1.57 – 1.48 (m, 2H, (-O)$_2$-CH-C<u>H$_2$</u>-), 1.26 (dt, *J* = 8.3, 3.9 Hz, 4H, -CH-C<u>H$_2$</u>-C<u>H$_2$</u>-), 0.88 – 0.80 (m, 3H, -CH-CH$_2$-CH$_2$-C<u>H$_3$</u>).

^{13}C-NMR (400 MHz, DMSO-d_6): δ (ppm) = 166.39, 135.78, 125.65, 102.25, 63.66, 62.62, 32.36, 26.30, 21.78, 17.86, 13.83.

HR-MS: calc. EM + Na: 351.18 g/mol; found: 351.18 g/mol

n_D^{20} = 1.455

2.1.3. Acetal based on Terephthalaldehyde and Glyceryl Methacrylate (T5MA)

2.1.3.1. Glyceryl Methacrylate (GMA)

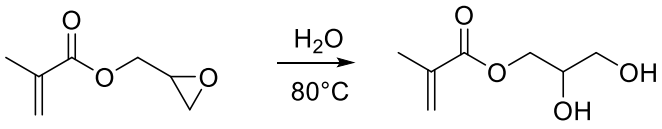

GMA

Reagents

	M [g/mol]	eq. [/]	n [mol]	m [g]
Glycidyl methacrylate	142.15	1.0	0.106	15.01
Deionized water	18.02	71	7.497	135.10

Procedure

2,3-Dihydroxypropyl-2-methyl-2-propenoic acid ester (**GMA**) was synthesized according to Ratcliffe *et al*.. [155] Therefore, glycidyl methacrylate and water were placed into a 250 mL three-necked round-bottomed flask, giving a two-phase reaction medium. The flask was equipped with a reflux condenser and the oil bath was heated to 85 °C. The reaction mixture was stirred for 36 h. Afterwards, the reaction mixture was single-phased (due to the solubility

of the product in water). First, the reaction mixture was allowed to cool down to room temperature and was then extracted with diethyl ether (4 times, 40 mL). The solvent was changed to ethyl acetate to enhance the solubility of the product in the organic phase. After 1½ L, no more product was in the aqueous phase (control of the organic phase with TLC). Phenothiazine (500 ppm) was added to the solution and the solvent was distilled *in vacuo*. The product **GMA** was isolated in 16.10 g (95% calculated yield) as colorless oil.

^{1}H-NMR (400 MHz, Methanol-d_4): δ (ppm) = 6.15 (dq, *J* = 8.5, 1.3 Hz, 1H, C=C<u>H</u>-H), 5.63 (p, *J* = 1.6 Hz, 1H, C=CH-<u>H</u>), 4.85 (s, 2H, -OH), 4.22 (ddd, *J* = 11.3, 4.4, 1.3 Hz, 1H, -O-C<u>H</u>-H-CH), 4.14 (ddd, *J* = 11.4, 6.1, 1.3 Hz, 1H, -O-CH-<u>H</u>-CH), 3.87 (qd, *J* = 5.8, 4.4 Hz, 1H,-C<u>H</u>-OH), 3.64 – 3.52 (m, 2H,-CH-C<u>H</u>$_2$-OH), 1.95 (dq, *J* = 2.6, 1.1 Hz, 3H, -CH$_3$).

n_D^{20} = 1.472 (Lit.: n_D^{20} = 1.470) [169]

2.1.3.2. Acetal T5MA

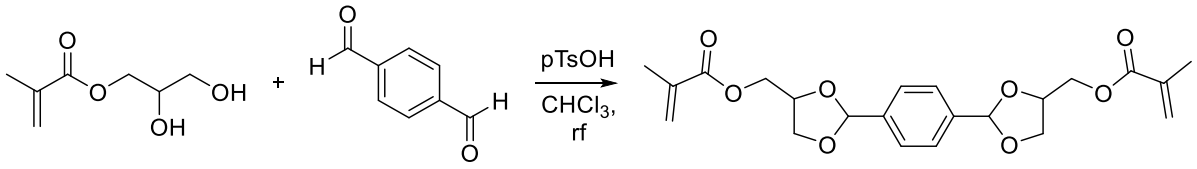

GMA **T5MA**

Reagents

	M [g/mol]	eq. [/]	n [mmol]	m [g]
Terephthalaldehyde	134.14	1.0	23.3	3.12
Glycerolmethacrylate	160.17	2.66	61.9	9.91
pTsOH-monohydrate	190.22	1 mol%	0.3	0.049

Procedure

1,1'-[1,4-Phenylenebis(1,3-dioxolane-2,4-diylmethylene)]-2-methyl-2-propenoic acid ester (**T5MA**) was synthesized according to Leibler *et al.* [156]. Terephthalaldehyde, which was recrystallized with toluene before, glycerolmethacrylate (GMA) and pTsOH-monohydrate were dissolved in 200 mL chloroform in a three-necked round-bottomed. A reflux condenser and a Dean-Stark apparatus were attached to the flask, the apparatus was purged with argon and the reaction mixture was heated to reflux and stirred for four days. The reaction mixture

was quenched and extracted with in sum 1.3 L saturated $NaHCO_3$. The combined organic layers were dried over anhydrous Na_2SO_4 and filtered. Phenothiazine (112 ppm) and MEHQ (324 ppm) were added and the solvent was evaporated. The purity was checked with HPLC (two signals, **T5MA**: $t_{R(A)}$ = 2.9 min; impurity terephthalaldehyde: $t_{R(A)}$ = 2.5 min) and NMR (impurity terephthalaldehyde: ≤10 mol%; mono-substituted, ≤0.3%). **T5MA** could be isolated with 99% yield as pink and highly viscous oil.

^{1}H-NMR (400 MHz, DMSO-d_6): δ (ppm) = 7.49 - 7.42 (m, 4H, Ar-H), 5.89 - 5.86 (m, 2H, C=CH-H), 5.78 - 5.86 (m, 4H, C=CH-H, -CH-(O-)$_2$), 4.55 - 3.93 (m, 10H, O=C-O-CH$_2$-, -O-CH$_2$-CH-O-, -O-CH$_2$-CH-O-), 1.93 – 1.88 (m, 6H, -CH$_3$).

^{13}C-NMR (400 MHz, DMSO-d_6): δ (ppm) = 166.36, 135.61, 126.73, 126.11, 103.18, 73.80, 68.18, 64.37, 17.98.

HR-MS: calc. EM + Na: 441.15 g/mol; found: 441.15 g/mol

n_D^{20} = 1.513

2.1.4. Acetal linked Diol based on 4-Formylbenzoic acid and Glycerol (MB5)

2.1.4.1. Acetal based on 4-Formylbenzoic acid (4FBA5)

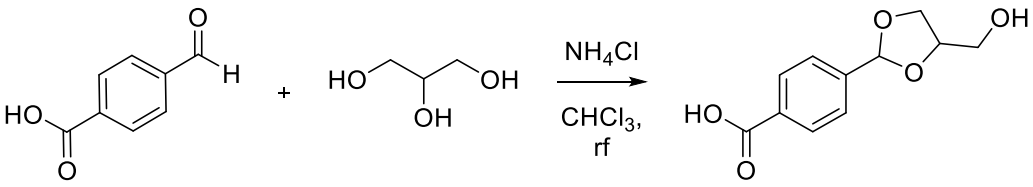

4FBA5

Reagents

	M [g/mol]	eq. [/]	n [mmol]	m [g]
4-Formylbenzoic acid	150.13	1	66.6	10.00
NH_4Cl	53.49	5.6	375.0	20.06
Glycerol	92.09	1.33	88.8	8.18

Procedure

First, glycerol was dried over a molecular sieve and the purity of 4-formylbenzoic acid was checked with ^{1}H-NMR and proved as pure. 4-(4-(Hydroxymethyl)-1,3-dioxolan-2-yl)benzoic acid (**4FBA5**) was synthesized according to Wildling *et al.* [158]. Therefore, 4-formylbenzoic acid, NH_4Cl and glycerol were dissolved in 200 mL chloroform in a three-necked round-bottomed flask. An inverse Dean-Stark apparatus and a reflux condenser were equipped onto the flask. The apparatus was purged with Ar and heated to reflux for 36 h. After that time, ^{1}H-NMR spectroscopy showed still a high amount of aldehyde. Therefore, the reaction mixture was stirred at reflux for five more days. The solution was cooled down and the white product precipitated. The purity was checked with HPLC (two signals, **4FBA5**: $t_{R(B)}$ = 2.1 min; impurity 4-formylbenzoic acid: $t_{R(B)}$ = 2.4 min) and NMR (<8% of aldehyde). After drying, the product was isolated in 68% theoretical yield.

^{1}H-NMR (400 MHz, DMSO-d_6): δ (ppm) = 13.03 (s, 1H, -COOH), 7.97 – 7.92 (m, 2H, Ar-H), 7.58 – 7.51 (m, 2H, Ar-H), 5.61 (s, 1H, -CH-$(O)_2$, 5-membered ring), 5.41 (s, 1H, -CH-$(O)_2$, 6-membered ring), 5.25 (d, *J* = 3.1, 1H, -OH (6-membered ring), 5.03 (d, *J* = 3.1, 1H, -OH (5-membered ring), 4.17 – 3.90 (m, 3H, (-O-C$\underline{H}_2$-CH-)$_2$, (-O-CH_2-C$\underline{H}$-) 6-membered ring; (-O-C$\underline{H}_2$-CH-) 5-membered ring), 3.79 – 3.68 (m, 1H, (-OH) (5-membered ring)), 3.56 – 3.50 (m, 2H, -C$\underline{H}_2$-OH). (mixture of 5- and 6-membered rings with a ratio of 60 mol% to 40 mol%, calculated with the signals of -CH-$(O)_2$ at 5.61 ppm and 5.41 ppm

^{13}C-NMR (400 MHz, DMSO-d_6): δ (ppm) = 167.08, 167.02, 143.13, 142.44, 130.99, 130.89, 129.96, 129.57, 126.42, 126.38, 99.48, 99.45, 71.67, 71.66, 71.47, 62.38, 60.21.

HR-MS: calc. EM + Na: 247.06 g/mol; found: 247.24 g/mol

mp.:169.2-172.1

2.1.4.2. MB5

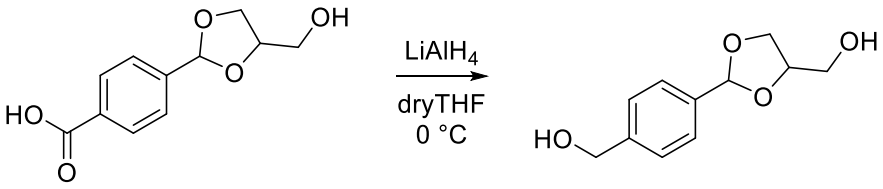

4FBA5 **MB5**

Reagents

	M [g/mol]	eq. [/]	n [mmol]	m [g]
4FBA5	224.21	1	11.6	2.61
LiAlH4	37.95	2	23.5	0.890

Procedure

(4-(4-(Hydroxymethyl)-1,3-dioxolan-2-yl)phenyl)methanol (**MB5**) was synthesized according to Blake *et al.* [159]. Therefore, dry THF (60 mL) was placed into a flask, cooled down with an ice bath and purged with argon. Afterwards, $LiAlH_4$ were added to the solvent and stirred for a few minutes. A solution of dry THF (100 mL) and **4FBA5** were placed into a dropping funnel and this solution was added dropwise about 90 minutes to the $LiAlH_4$ in THF. After finishing, the reaction mixture was stirred for 36 h at room temperature. A crude NMR was measured in DMSO-d6 and no acid-proton was detectable anymore. To quench the excess of the reduction agent, an aqueous KOH (12 mL) (2.5% solution) was added to the reaction mixture. The Li-salts precipitate as lubricious white solid. The precipitate was filtered off and the solution was extracted with ethyl acetate. The combined organic phases were dried over anhydrous Na_2SO_4 and filtered off. The solvent was concentrated *in vacuo* to obtain **MB5** in 1.63 g as white powder with a theoretical yield of 67%. The purity was checked with HPLC (one clear signal, one minimal; **MB5**: $t_{R(B)}$ = 2.8 min; impurity 4-formylbenzoic acid: $t_{R(B)}$ = 2.4 min) and NMR (≤ 4% of aldehyde).

^{1}H-NMR (400 MHz, DMSO-d_6): δ (ppm) = 7.40 – 7.27 (m, 4H, Ar-H), 5.51 (s, 1H, -CH-$(O)_2$, 5-membered ring), 5.39 (s, 1H, -CH-$(O)_2$, 6-membered ring), 4.49 – 4.48 (m, 2H, Ar-CH_2-OH), 4.13 – 4.10 (dd, *J* = 10.8, 5.3 Hz, 1H, -O-CH-CH_2-OH), 4.03 and 3.93 (d, *J* = 6.7 Hz, 4H, -O-CH_2-CH-CH_2-O-, -O-CH_2-CH-CH_2-OH), 3.74 – 3.66 (m, 1H, -O-CH_2-CH-CH_2-O), 3.50 – 3.26 (m, 2H, -O-CH-

$C\underline{H_2}$-OH). (mixture of 5- and 6-membered rings with a ratio of 60 mol% to 40 mol%, calculated with the signals of -CH-$(O)_2$ at 5.51 ppm and 5.38 ppm).

^{13}C-NMR (400 MHz, DMSO-d_6): δ (ppm) = 142.95, 142.83, 137.27, 136.54, 125.95, 125.89, 125.88, 125.82, 100.21, 100.19, 71.62, 71.35, 62.61, 62.57, 62.37, 60.22.

HR-MS: calc. EM + H: 211.10 g/mol; found: 211.10 g/mol

mp.: 76.2-79.2 °C

2.2. Degradation Model Study of Low Molecular weight Acetals

To estimate the degradation behavior of the linear and cyclic acetals ^{1}H-NMR spectroscopy as method was chosen again as for the esterified test compound **EIBSPG** (Chapter 1.3). The studies are conducted in CD_3CN/D_2O (1:1). First, the substance was dissolved in 0.35 mL CD_3CN and afterwards 0.35 mL D_2O were added. The mass of the test compounds are shown in Table 6. Due to the different states, there are slight differences between the masses. It is assumed that there will be no significantly difference for the highly diluted solutions for the NMR model studies. All samples were measured under acidic conditions at room temperature. The NMR tube contained 0.5 µl DCl (38 wt% DCl in deuterium oxide), which would be a pH-equivalent of 2.1. The signal of the solvent was locked to D_2O at 4.79 ppm.

Table 6: Mass for the NMR-degradation model study of the alternative acetals

Sample	m [mg]
VKMA	5.63
T5MA	6.93
Diol	4.17

Table 7: Values for the ^{1}H-NMR degradation study of VKMA under acidic conditions (pH-equivalent of 2.1).

Time [h]	Remaining amount VKMA [%]
0.0	100.00
0.05	92.83
0.97	79.28
2.98	58.37
5.98	40.65
12.00	20.87
23.98	4.79
36.00	2.99
47.98	2.59
91.20	2.35

Table 8: Values for the ^{1}H-NMR degradation study of T5MA under acidic conditions (pH-equivalent of 2.1).

Time [h]	Remaining amount T5MA [%]	Existing amount one-sided acetal [%]	Existing amount terephthalaldehyde [%]
0.00	100.00	0.00	0.00
0.30	96.09	3.24	0.67
1.05	74.39	25.15	0.46
3.05	46.15	52.68	1.16
6.06	26.58	70.43	2.99
12.05	9.66	84.55	5.79
24.07	3.77	84.33	11.91
36.05	2.56	79.74	17.70
48.05	2.38	74.82	22.80
80.08	1.69	63.26	35.05

Table 9: Values for the ^{1}H-NMR degradation study of MB5 under acidic conditions (pH-equivalent of 2.1).

Time [h]	Existing amount acetal total [%]	Existing amount 6-membered ring [%]	Existing amount 5-membered ring [%]
0.05	100.00	40.00	60.00
1.28	94.09	33.77	60.49
3.28	75.57	23.17	53.19
6.30	32.43	10.13	22.59
12.30	4.89	0.75	4.62

2.3. Photopolymers

2.3.1. RT-FTIR-Photorheology

The preparation of formulations was performed in the orange light lab to avoid an unintended polymerization. The initiator (1 mol%), the monomer and if necessary, also the reactive diluent HEMA were weighed into a brown glass tube. Afterwards, the formulations were mixed with a vortex speed mixer for about one minute. For better handling and avoidance of undesired polymerization, the tubes were wrapped into aluminum foil. A broadband Hg-lamp was used with a 400-500 nm filter (Omnicure 3) to irradiate the samples. All measurements were performed in triplicates at room temperature (25 °C) with 1 W cm^{-2} light intensity at the end of the light guide. 150 µL sample volume was applied on a glass disk (+ PE tape) and a gap of 200 µm between the measuring system (PP25) and the disk was set. In order to determine the double bond conversion over the measuring period, the signal at ~ 6170 cm^{-1} was recorded and integrated over the measuring period related to the integral at t_0.

Photorheology experiments were performed with both synthesized monomers, the aliphatic methacrylate **VKMA** and the aromatic **T5MA**. In addition, different dilutions with HEMA were prepared. Due to the fact, that HEMA is a monofunctional methacrylate, twice the molar amount was necessary to provide double bond specific ratios of the dilutions. Three different formulations were prepared for each monomer. One formulation consisted of the photoinitiator with the pure monomer, 1:1 and 1:4 ratio of double bonds (DB-ratio) with the mono-functional reactive diluent HEMA were also desired. With these calculations, the formulations were prepared (Table 10). Unfortunately, these ratios were calculated without including the impurities. After including, different ratios were retained. The corrected values of **VKMA** would be 1:1.3 and 1:4.9 and for **T5MA** 1:1.1 and 1:4.4. In the Chapter Results and Discussion (Subchapter 2.3), the rounded ratios are used. The evaluated data of the photorheology measurements are summarized in Table 11.

Table 10: Formulation of VKMA and T5MA with different dilutions tested in photo-rheology experiments (1 mol% PI).

Sample:		m [mg]
VKMA	VKMA	840.6
	Ivocerin	10.3
VKMA:HEMA (1:1)	VKMA	446.4
	HEMA	356.5
	Ivocerin	16.6
VKMA:HEMA (1:5)	VKMA	191.9
	HEMA	608.4
	Ivocerin	20.9

Sample:		m [mg]
T5MA	T5MA	843.9
	Ivocerin	8.1
T5MA:HEMA (1:1)	T5MA	493.3
	HEMA	310.1
	Ivocerin	14.3
T5MA:HEMA (1:4)	T5MA	230.8
	HEMA	576.5
	Ivocerin	19.9

Table 11: Results (value ± sd) of Photo-Rheology measurements of the pure monomers VKMA and T5MA and the different dilutions.

Sample No.:	t_g [s]	DBC_g [%]	t_{95} [s]	DBC [%]	F_N [N]
VKMA	5.4 ± 0.0	12.5 ± 1.8	69.5 ± 3.1	88.3 ± 0.5	36.8 ± 1.5
VKMA:HEMA (1:1)	8.7 ± 0.2	17.5 ± 0.6	64.8 ± 4.8	90.9 ± 0.3	41.2 ± 1.4
VKMA:HEMA (1:5)	14.5 ± 0.2	29.8 ± 0.5	61.5 ± 3.5	92.3 ± 0.2	39.5 ± 1.5
T5MA	1.4 ± 0.0	23.8 ± 4.5	127.3 ± 17.9	78.3 ± 0.6	23.0 ± 0.4
T5MA:HEMA (1:1)	1.8 ± 0.0	14.3 ± 1.7	72.6 ± 1.0	88.2 ± 0.8	33.6 ± 0.5
T5MA:HEMA (1:4)	6.5 ± 0.1	20.3 ± 0.6	61.53 ± 2.4	91.5 ± 0.1	39.9 ± 0.6

2.3.2. Swelling and Degradation Behavior

2.3.2.1. Narrow meshed polymer networks (undiluted)

For the swelling tests, an aqueous HCl solution was prepared. The pH was adjusted to 4.4 with a pH electrode at 22.5 °C. Photopolymerized samples with a defined thickness of 200 µm (from Photorheology experiments) were cut using a scalpel and used in triplicates. The samples were weighed (Table 12) and afterwards placed into tissue culture dishes (Thermo Scientific, BioLite 35mm). These were immersed into 3 mL of the acidic solution and stored at room temperature. After defined periods, the samples were removed from the acidic solution, whiped with a paper towel, weighed (average values for **VKMA** and **T5MA** in Table 13**Error! Reference source not found.**) and again immersed into the medium. The dishes were sealed with laboratory film to avoid an evaporation of the aqueous solution.

Table 12: Mass of the close meshed polymers (triplicates) for the swelling tests.

	Sample:	m [mg]
VKMA	1	45.36
	2	52.51
	3	29.94
T5MA	1	23.95
	2	39.46
	3	51.02

Table 13: Average mass change (value ± sd) of the close meshed VKMA and T5MA (triplicates) for the swelling tests under acidic conditions (pH = 4.4).

Time [d]	Average mass change of VKMA [%]	Average mass change of T5MA [%]
0.0	0.00 ± 0.00	0.00 ± 0.00
0.0 (1 h)	-0.15 ± 1.85	-0.73 ± 1.20
0.7	0.47 ± 1.41	0.09 ± 1.43
1.8	1.48 ± 2.63	0.71 ± 1.06
2.8	1.49 ± 1.68	0.97 ± 1.12
3.8	1.27 ± 1.93	1.32 ± 0.94
5.8	0.81 ± 1.51	1.57 ± 0.82
6.7	1.06 ± 2.40	1.67 ± 0.98
8.0	0.61 ± 1.71	1.97 ± 1.08
9.1	1.28 ± 2.27	2.09 ± 0.96
12.9	-1.50 ± 1.14	2.75 ± 0.91
21.8	-5.42 ± 1.09	1.01 ± 0.76
32.8	-6.31 ± 0.46	-2.38 ± 1.23
38.7	-7.87 ± 1.28	-4.30 ± 0.49
53.6	-9.06 ± 1.93	-8.85 ± 2.12
71.2	-10.35 ± 3.19	-8.91 ± 0.41
104.3	-10.28 ± 4.80	-11.90 ± 1.39

2.3.2.2. Wide meshed polymer networks (diluted)

The networks with the reactive diluent HEMA were treated equally to the undiluted networks. However, for some formulations (DB-ratio of 1:5 for **VKMA** and 1:4 for **T5MA**), it was not possible to remove the disks from the disposable plates. Therefore, the disposable plates were weighed, then the rheology measurements were realized and the disposable plates with the adherent samples were weighed again to calculate the mass of the samples (Table 14). The plates with the samples were placed into the acidic solution. Overnight the samples separated from the disposable plates. Afterwards, those were removed and the samples were immersed again into the solution and sealed with laboratory film to avoid evaporation of the aqueous media. Table 15 shows the time ranges and masses of the swelled samples **VKMA** and **T5MA** for the 1:1 DB-ratio of monomer:HEMA and Table 16 for the 1:5 resp. 1:4 DB-ratio.

Table 14: Mass of the wide meshed polymers (triplicates) for the swelling tests.

	Sample:	m [mg]
VKMA:HEMA (1:1)	1	42.84
	2	29.90
	3	66.59
VKMA:HEMA (1:5)	1	154.60
	2	150.27
	3	151.19
T5MA:HEMA (1:1)	1	33.51
	2	55.75
	3	35.47
T5MA:HEMA (1:4)	1	160.88
	2	163.22
	3	161.74

Table 15: Average mass change (value ± sd) of the wide meshed ((DB-ratio (1:1)) VKMA and T5MA (triplicates) for the swelling tests under acidic conditions (pH = 4.4).

Time [d]	Average mass change for VKMA:HEMA (1:1) [%]	Average mass change for T5MA:HEMA (1:1) [%]
0.0	0.00 ± 0.00	0.00 ± 0.00
1.1	9.81 ± 0.93	8.11 ± 0.11
7.7	12.32 ± 1.74	9.19 ± 0.14
14.8	13.63 ± 0.69	6.69 ± 2.42
23.7	12.72 ± 3.05	6.35 ± 0.65
36.9	15.91 ± 1.07	5.79 ± 0.46
61.8	17.05 ± 0.93	4.92 ± 0.48

Table 16: Average mass change (value ± sd) of the wide meshed VKMA (DB-ratio (1:5)) and T5MA (DB-ratio (1:4)) (triplicates) for the swelling tests under acidic conditions (pH = 4.4).

Time [d]	Average mass change for VKMA:HEMA (1:5) [%]	Average mass change for T5MA:HEMA (1:4) [%]
0.0	0.00 ± 0.00	0.00 ± 0.00
1.7	13.84 ± 1.39	13.62 ± 3.91
8.8	20.42 ± 2.89	19.46 ± 0.55
17.7	22.25 ± 1.49	18.34 ± 1.81
30.9	27.40 ± 3.30	20.96 ± 0.91
55.8	23.32 ± 2.07	18.21 ± 1.96

SUMMARY

A longer lifetime of the human population, due to better medical care, entails certainly to an increase of age-related diseases. Such diseases affect e.g. joints and bones. Implanting of suitable temporary substitutes assist the healing process and treatment of those diseases. Tissue engineering (TE) concerns itself with the development of new materials e.g. for bone scaffolds. Essential properties like biomimetic, patient specificity, biocompatibility and degradability are required for those materials. The degradability is introduced by incorporation of cleavable moieties. For bone replacement materials, osteoclasts, the bone degrading cells, form an acidic microenvironment and therefore, functional groups are important in these polymers, which cleave in this environment. Polyesters, commonly used biomaterials cleave too slowly under these conditions and therefore, acetals were aimed as cleavable moieties in these materials. Furthermore, oligomeric building blocks were considered to design polymers with suitable mechanical properties. By addition of photopolymerizable groups, the polymers are processible by additive manufacturing technologies (AMTs) and are therefore suitable to generate patient specific parts.

In the first part of this work, the aim was to synthesize hydroxyl functional oligomers that exhibit an acetal moiety. The acetal unit implied the degradability and the oligomer itself should improve the mechanical properties, especially the toughness of the photopolymers. For this purpose, spiroglycol (**SPG**) building blocks were prepared. Figure 51 shows the successfully synthesized spiroacetals. The first **SPG** was formed with vanillin as staring material, as it is a renewable resource. In addition, 4-hydroxybenzalhdeyde (**4HB**) and 4-formylbenzoic acid (**4FBA**) are converted into the corresponding **SPG**s.

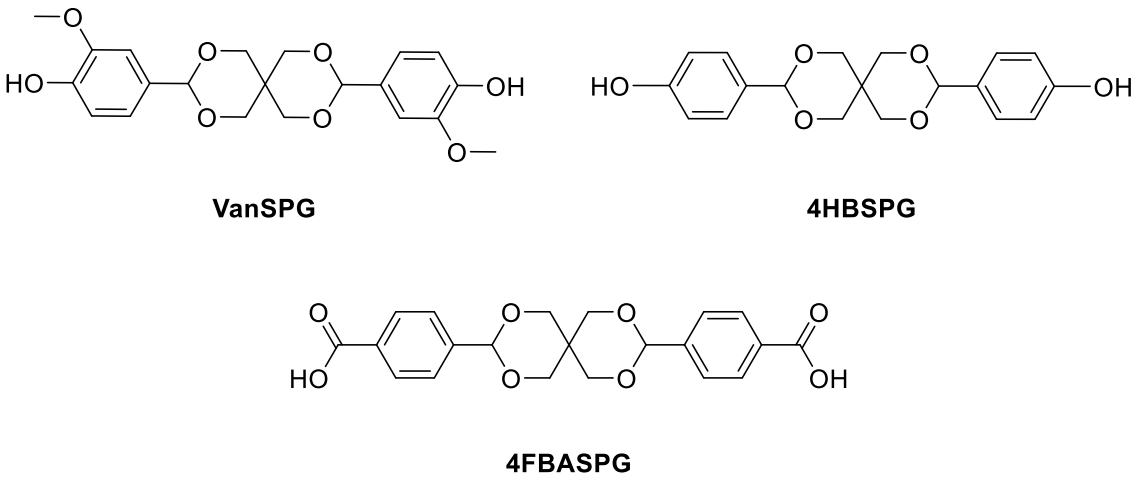

Figure 51: Structures of the synthesized aromatic spiroacetals.

During the synthesis of these spiroacetals, it was found that the solubility of the products were quite low which could be explained by the rather stiff structure as a consequence of the combination of the spiro-structure and the aromatic moieties. For this reason, this concept had to be rejected.

For further synthesis of more flexible oligomeric systems, a small spiroacetal-based model molecule, which is shown in Figure 52, was designed to study the optimal reaction conditions. An esterification reaction was considered for preparation of oligomers, because classical degradable polymers are typically based on the cleavage of ester groups.

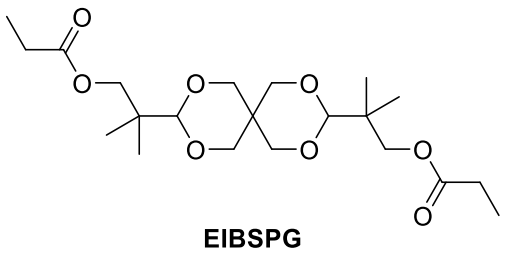

Figure 52: Structure of the synthesized and investigated esterified spiroacetal EIBSPG.

The molecule **EIBSPG** was synthesized from a commercial available diol and an appropriate acid chloride with a high conversion. Therefore, the synthesis of an oligomeric spiroacetal with terminal hydroxyl groups according to Figure 53 was carried out. As different strategies did not lead to the desired polyester, the concept of oligomeric building blocks was discontinued.

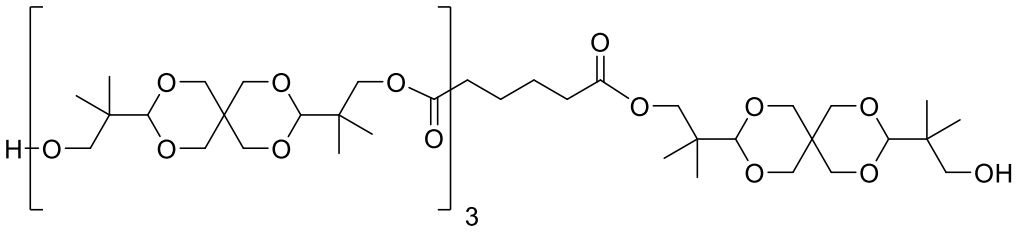

ACIBSPG

Figure 53: Desired polyester ACIBSPG.

To further evaluate the concept of spiroacetals regarding their degradation behavior compared to esters the before mentioned test molecule **EIBSPG** was examined. Hence, NMR studies with different pH-equivalents were conducted. Under basic conditions, only a fast cleavage of the ester was observed. At an acidic pH, both, the ester and the acetal moieties cleaved, however the latter degraded very slowly. As expected, this is a consequence of the rather stable spiroacetal moiety, which is therefore not appropriate for the designated application.

In the second part of this work, new acetals were designed, being less stable than the spiro-compounds. Therefore, low molecular weight test systems with different acetal moieties were investigated. To adjust the degradation behavior linear acetals based on aromatic (**VanKMA**) or aliphatic (**VKMA**) aldehydes were selected. Additionally cyclic acetals based on aromatic aldehydes (**T5MA** and **MB5**) were of interest.

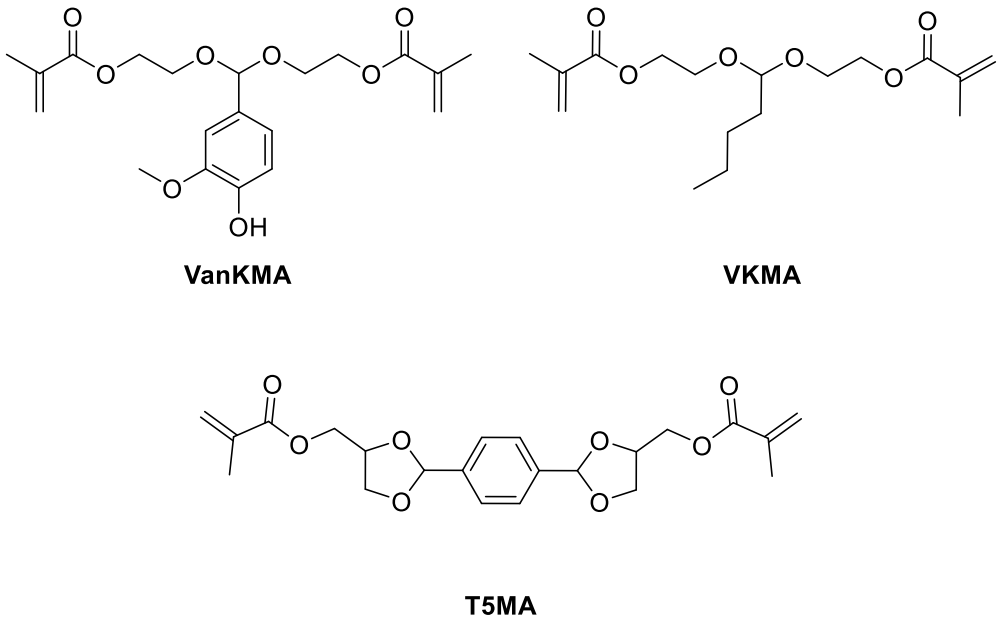

Figure 54: Structures of the synthesized and investigated low molecular weight polymerizable monomers with linear and cyclic acetal moiety.

As these model molecules should also subsequently used for photopolymerization experiments, appropriate methacrylate groups were included in the test molecules (Figure 54). In a first attempt for photopolymerizable acetals, vanillin was used as starting material, as it is a cheap and a natural product. However, the according linear acetal (**VanKMA**) could not be synthesized. The acetals **VKMA** and **T5MA** could be prepared in good yields, but there were some impurities, which were hard to remove due to the acid labile acetal moiety and the polymerizable functionalities.

The molecule in Figure 55 (**MB5**), with terminal hydroxyl groups, was designed, because this diol allows the functionalization of molecules with other photopolymerizable groups (e.g. vinyl carbonates). Moreover, it can be used as building block for oligomeric systems.

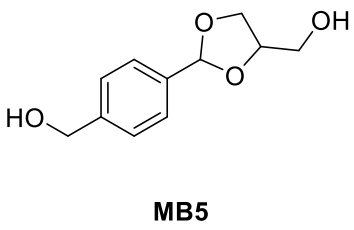

Figure 55: Structure of the acetal containing building block with terminal hydroxyl groups.

Small-scale synthesis resulted in two products, a 5- and 6-membered ring in a ratio of 60:40 in good yield, however, the scale-up to date was not successful.

The degradability of the acetal containing systems in solution was examined *via* ^{1}H-NMR spectroscopy and compared with the esterified spiroacetal (**EIBSPG**). Figure 56 shows the degradation velocity linear approximated with mol%/h for the first three hours of the experiments.

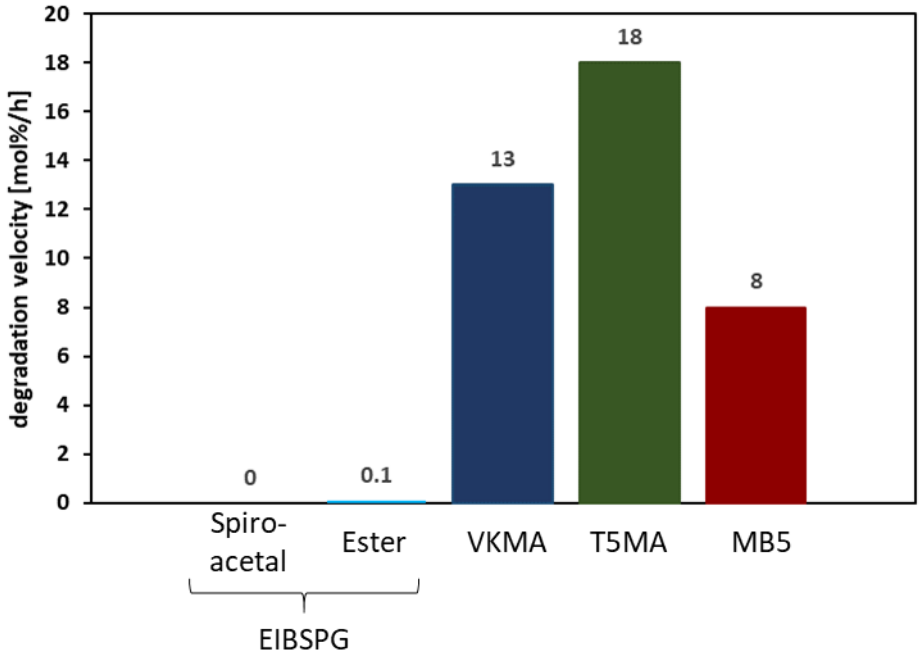

Figure 56: Degradation velocity (linear approximated with [mol%/h]) of EIBSPG and the alternative acetals (VKMA, T5MA and MB5) under acidic environment (pH equivalent of 2.1), determined in the first three hours by ^{1}H-NMR spectroscopy.

Overall, it can be concluded that the aromatic bicyclic methacrylate **T5MA** is the fastest and the aromatic and cyclic **MB5** (hydroxyl terminated) in total is the slowest degrading acetal (apart from the spiroacetal). In comparison to the esterified spiroacetal (**EIBSPG**), all alternative acetals degrade faster by a factor of 80-200 compared to the ester moiety.

RT-FTIR-Photorheology experiments were performed to determine the reactivity of the acetal containing systems regarding crosslinking reaction. To adjust the network density synthesized acetals **VKMA** and **T5MA** were investigated in bulk and with a reactive diluent to form more wide meshed polymer networks. HEMA was used as reactive diluent, as it is known as monomer for hydrogels in medical applications like bone implants. [160]

The RT-FTIR-Photorheology experiments showed that the aromatic cyclic acetal **T5MA** reacted faster than the aliphatic linear **VKMA**. However, the final DBC is for the aliphatic one higher.

The rigidity of the formed polymer network from **T5MA** and therefore limited diffusion can explain those results. By using HEMA as reactive diluent, the time until gelation and the DBC at the gel point increased. In addition, the overall DBC could be increased by using HEMA as reactive diluent.

By comparing the density of the crosslinked bulk polymer networks of **VKMA** and **T5MA**, initial swelling of the latter one is more slowly due to the rigid system. Afterwards, the degradation and mass loss itself is much faster for **T5MA** due to the lower hydrolytic stability of the cyclic acetal.

The diluted polymer networks show a higher mass change than the narrow meshed polymer networks, as it is easier to swell, due to the wider network (Figure 57). Moreover, HEMA is able to bind a high amount of water and therefore, the mass erosion cannot compensate the swelling behavior. Compared to **VKMA**, the network density for **T5MA** is lower and more hydrophobic, which can explain lower swelling. Furthermore, after water-uptake the degradation of the aromatic systems is faster and therefore, the mass change shows also lower values for swellability.

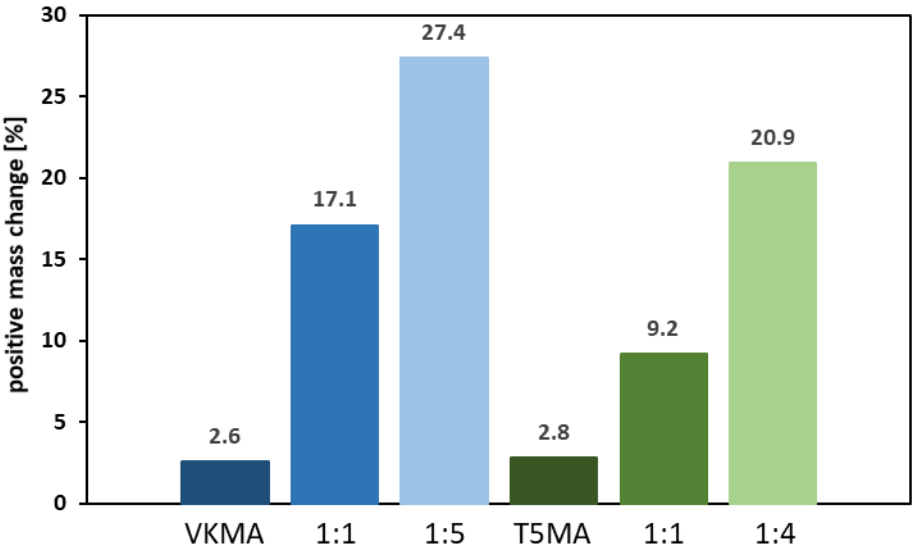

Figure 57: Highest positive mass change of the narrow meshed polymer network of the pure monomers VKMA (blue) and T5MA (green) and the wide meshed polymer networks with the reactive diluent HEMA in a DB-ratio of 1:1 and 1:5 for VKMA and a 1:1 and 1:4 for T5MA.

Further degradability studies have to consider the swellability and the mass erosion separately.

It can be concluded that all linear and cyclic acetals (except the spiroacetals) degraded faster than the ester moiety. Therefore, the concept of using acetals as degradable moieties for acid environment in TE could be proved.

MATERIALS AND GENERAL METHODS

Reagents and solvents- All reagents were applied without further purification, otherwise it is noted. The solvents were distilled before use and anhydrous solvents were absolutely dried with a PURESOLV-plant from *it-innovative technology inc*.

Thin layer chromatography (TLC)- For the thin layer chromatography aluminium foils, which were coated with silica 60 F254 (*Merck*) were used.

Light sources-

- UV chamber: *uvitron International INTELLI-RAY 600* with a Hg broad bond UV lamp (600 W, UV-A: 125 mW/cm², Vis: 125 mW/cm²)
- Omnicure-System: *Omnicure Series 200 EXFO* with a 200 W hg lamp and an installed filter with 400-500 nm

NMR spectroscopy- The NMR spectra were recorded on an *Avance DRX-400* with 400 MHz for ^{1}H (100 MHz for ^{13}C) Fourier transform spectrometer and are analyzed with the software TopSpin (version 3.5) by *Bruker*.

The data for ^{1}H- and ^{13}C- spectra are declared as described below:

- The chemical shifts are in parts per million (ppm) and related to trimethylsilane (TMS, δ = 0 ppm). The signals are referenced to the solvent (^{1}H: $CDCl_3$ δ = 7.26 ppm, D_2O δ = 4.79 ppm, DMSO-d_6 δ = 2.50 ppm; ^{13}C: $CDCl_3$ δ = 77.16 ppm, DMSO-d_6 δ = 39.52 ppm).
- The multiplicity is described as follows: ^{1}H: s = singlet, bs = broad singlet, d = doublet, dd = doublet of doublets t = triplet, q = quartet and m = multiplet; ^{13}C: s = quaternary C, d = CH, t = CH_2, q = CH_3, classification from APT-experiments.

Orange light lab- all weightings, reactions and measurements of light sensitive substances are carried out in an orange light lab. The windows are laminated with Asmetec metolight SF-UV-foils (type ASR-SF-LY5) and all lamps were type Osram lumix with chip controlled light color 62.

FTIR-RT-NIR-Photorheology- All measurements were performed on an *Anton Paar MCR 302 WESP*. A borosilicate glass plate with 60 mm diameter and 6 mm thickness and a PP25 stamp were used. The rheometer was coupled with a FTIR spectrometer (*Bruker Vertex 80*) with external mirrors to guide the IR beam through the sample during the rheology measurements. After passing the glass plate, the IR beam is reflected by the PP25 measuring system and returns to the MCT- detector. For UV curing an Omnicure lamp (see above, with *Ocean Optics* USB 200+ spectrometer 10 mW/cm² at the surface of the glass plate was measured) was used. The initiator Ivocerin® (1 mol%) and a broadband Hg-lamp was used with a 400-500 nm filter to irradiate the samples. All measurements were performed in triplicates at room temperature (25 °C) with 1 W cm^{-2} light intensity at the end of the light guide. 150 µL sample volume was applied on a glass disk (+ PE tape) and a gap of 200 µm between the measuring system (PP25) and the disk was set. The analyzing of the rheology measurements were done with the Software Rheoplus V3.62 by *Anton Paar* and for the data of the IR spectra, the software Opus 7.0 by Bruker was used.

Melting points- an OptiMelt automated melting point system from SRS Stanford Research System was used for determination of the melting points. The heating rate was conducted of 2 °C/min.

HR-MS- the analysis was carried out from acetonitrile solutions (concentration: 10 µM) by using an HTC PAL system autosampler (CTC Analytics AG, Zwingen, Switzerland), an Agilent 1100/1200 HPLC with binary pumps, degasser and column thermostat (Agilent Technologies, Waldbronn, Germany) and Agilent 6230 AJS ESI–TOF mass spectrometer (Agilent Technologies, Palo Alto, United States). Data evaluation was performed using Agilent MassHunter Qualitative Analysis B.07.00. Identification was based on peaks obtained from extracted ion chromatograms (extraction width ± 20 ppm).

HPLC- The analysis was carried out with a modular HP Agilent 1100 device, equipped with a HP photodiode array detector and a quaternary gradient pump. For the separation an OUT LipoMare C18 (105 Å; 5 µm, 150 x 4 mm) reversed phase column was used at a flow rate of 0.7 ml/min (H_2O:ACN = 42:58 (labeled as **A**); or H_2O:ACN = 70:30 (labeled as **B**)). The device was equipped with an auto sampler and the software ChemStation for LC 3D systems form Ailent Technologies (vB03.02-SR2 [341]).

ABBREVIATIONS

In addition to common short forms as well as chemical element symbols, the abbreviations below are used:

AMT	Additive Manufacturing Technology
BTE	Bone Tissue Engineering
CAD	Computer Aided Design
DBC	Double Bond Conversion
DBC_g	Double Bond Conversion at Gel Point
DCM	Methylene Chloride
DLP	Digital Light Processing
DMSO	Dimethyl Sulfoxide
EA	Ethyl Acetate
ECM	Extracellular Matrix
Et_3N	Trimethylamine
Et_2O	Diethyl Ether
F_N	Normal Force
FTIR	Fourier Transformation Infrared Spectroscopy
G’	Storage Modulus
G’’	Loss Modulus
HEMA	2-Hydroxyethyl methacrylate
MeOH	Methanol
NMR	Nuclear Magnetic Resonance
PE	Petroleum ether
PI	Photoinitiator
rf	Reflux
rt	Room Temperature
RT-FTIR	Real Time Fourier Transformation Infrared Spectroscopy
SLA	Stereolithography
TE	Tissue Engineering
t_{95}	Time to reach 95 % Overall Conversion

t_g	Time to Reach the Gel Point
THF	Tetrahydrofuran
TLC	Thin Layer Chromatography
3D	Three-Dimensional

REFERENCES

(1) Clarke, B. "*Normal bone anatomy and physiology*"; Clin. J. Am. Soc. Nephrol. 2008**, 3** (Suppl. 3), S131-S139.

(2) SEER https://training.seer.cancer.gov/anatomy/skeletal/tissue.html.

(3) Hadjidakis, D. J.; Androulakis, I. I. "*Bone remodeling*"; Ann. N. Y. Acad. Sci. 2006**, 1092** (Women's Health and Disease), 385-396.

(4) Huch, R.; Jürgens, K. D. "*Mensch Körper Krankheit*". 2015.

(5) Alghazali, K. M.; Nima, Z. A.; Hamzah, R. N.; Dhar, M. S.; Anderson, D. E.; Biris, A. S. "*Bone-tissue engineering: complex tunable structural and biological responses to injury, drug delivery, and cell-based therapies*"; Drug Metab. Rev. 2015**, 47** (4), 431-454.

(6) Henkel, J.; Woodruff, M. A.; Epari, D. R.; Steck, R.; Glatt, V.; Dickinson, I. C.; Choong, P. F. M.; Schuetz, M. A.; Hutmacher, D. W. "*Bone Regeneration Based on Tissue Engineering Conceptions - A 21st Century Perspective*"; Bone research 2013**, 1** (3), 216-248.

(7) Buckwalter, J. A.; Glimcher, M. J.; Cooper, R. R.; Recker, R. "*Bone biology. I: Structure, blood supply, cells, matrix, and mineralization*"; Instr. Course Lect. 1996**, 45**, 371-86.

(8) Stevens, M. M.; George, J. H. "*Exploring and Engineering the Cell Surface Interface*"; Science 2005**, 310** (5751), 1135-1138.

(9) Silver, I. A.; Murrills, R. J.; Etherington, D. J. "*Microelectrode studies on the acid microenvironment beneath adherent macrophages and osteoclasts*"; Exp. Cell Res. 1988**, 175** (2), 266-276.

(10) Eriksen, E. F. "*Normal and Pathological Remodeling of Human Trabecular Bone: Three Dimensional Reconstruction of the Remodeling Sequence in Normals and in Metabolic Bone Disease**"; Endocr. Rev. 1986**, 7** (4), 379-408.

(11) Schindeler, A.; McDonald, M. M.; Bokko, P.; Little, D. G. "*Bone remodeling during fracture repair: The cellular picture*"; Semin. Cell Dev. Biol. 2008**, 19** (5), 459-466.

(12) Raggatt, L. J.; Partridge, N. C. "*Cellular and Molecular Mechanisms of Bone Remodeling*"; J. Biol. Chem. 2010**, 285** (33), 25103-25108.

(13) Lian, J. B.; Stein, G. S.; van Wijnen, A. J.; Stein, J. L.; Hassan, M. Q.; Gaur, T.; Zhang, Y. "*MicroRNA control of bone formation and homeostasis*"; Nature reviews. Endocrinology 2012**, 8** (4), 212-227.

(14) Miller, S. C.; de Saint-Georges, L.; Bowman, B. M.; Jee, W. S. "*Bone lining cells: structure and function*"; Scanning Microsc. 1989**, 3** (3), 953-60; discussion 960-1.

(15) Dobnig, H.; Turner, R. T. "*Evidence that intermittent treatment with parathyroid hormone increases bone formation in adult rats by activation of bone lining cells*"; Endocrinology 1995**, 136** (8), 3632-3638.

(16) Langer, R.; Vacanti, J. P. "*Tissue Engineering*"; Science 1993**, 260** (5110), 920-926.

(17) Albrektsson, T.; Johansson, C. "*Osteoinduction, osteoconduction and osseointegration*"; Eur. Spine J. 2001**, 10** (2), S96-S101.

(18) Giannoudis, P. V.; Dinopoulos, H.; Tsiridis, E. "*Bone substitutes: An update*"; Injury 2005**, 36** (3, Supplement), S20-S27.

(19) Vögelin, E.; Jones, N. F.; Huang, J. I.; Brekke, J. H.; Lieberman, J. R. "*Healing of a Critical-Sized Defect in the Rat Femur with Use of a Vascularized Periosteal Flap, a Biodegradable Matrix, and Bone Morphogenetic Protein*"; JBJS 2005**, 87** (6), 1323-1331.

(20) Keating, J. F.; McQueen, M. M. "*Substitutes for autologous bone graft in orthopaedic trauma*"; J. Bone Joint Surg. Br. 2001**, 83** (1), 3-8.

(21) Laurencin, C. T.; Ambrosio, A. M. A.; Borden, M. D.; J. A. Cooper , J. "*Tissue Engineering: Orthopedic Applications*"; Annu. Rev. Biomed. Eng. 1999**, 1** (1), 19-46.

(22) Ikada, Y. "*Challenges in tissue engineering*"; Journal of The Royal Society Interface 2006**, 3** (10), 589-601.

(23) Nerem, R. M.; Sambanis, A. "*Tissue Engineering: From Biology to Biological Substitutes*"; Tissue Eng. 1995**, 1** (1), 3-13.

(24) Lutolf, M. P.; Hubbell, J. A. "*Synthetic biomaterials as instructive extracellular microenvironments for morphogenesis in tissue engineering*"; Nat. Biotechnol. 2005**, 23**, 47.

(25) Lee, K. Y.; Mooney, D. J. "*Hydrogels for Tissue Engineering*"; Chem. Rev. (Washington, D. C.) 2001**, 101** (7), 1869-1879.

(26) Hutmacher, D. W. "*Scaffold design and fabrication technologies for engineering tissues. State of the art and future perspectives*"; J. Biomater. Sci., Polym. Ed. 2001**, 12** (1), 107-124.

(27) Baudis, S. *Development and Processing of Materials for Vascular Tissue Regeneration*. Dissertation, TU Wien, 2010.

(28) Chen, H.; Yuan, L.; Song, W.; Wu, Z.; Li, D. "*Biocompatible polymer materials: Role of protein–surface interactions*"; Prog. Polym. Sci. 2008**, 33** (11), 1059-1087.

(29) Guo, H.; Su, J.; Wei, J.; Kong, H.; Liu, C. "*Biocompatibility and osteogenicity of degradable Ca-deficient hydroxyapatite scaffolds from calcium phosphate cement for bone tissue engineering*"; Acta Biomater. 2009**, 5** (1), 268-278.

(30) Miguel, B. S.; Kriauciunas, R.; Tosatti, S.; Ehrbar, M.; Ghayor, C.; Textor, M.; Weber, F. E. "*Enhanced osteoblastic activity and bone regeneration using surface-modified porous bioactive glass scaffolds*"; Journal of Biomedical Materials Research Part A 2010**, 94A** (4), 1023-1033.

(31) Li, W. J.; Laurencin, C. T.; Caterson, E. J.; Tuan, R. S.; Ko, F. K. "*Electrospun nanofibrous structure: a novel scaffold for tissue engineering*"; J. Biomed. Mater. Res. 2002**, 60** (4), 613-21.

(32) Henslee, A. M.; Gwak, D.-H.; Mikos, A. G.; Kasper, F. K. "*Development of a biodegradable bone cement for craniofacial applications*"; Journal of biomedical materials research. Part A 2012**, 100** (9), 2252-2259.

(33) Renno, A. C. M.; van de Watering, F. C. J.; Nejadnik, M. R.; Crovace, M. C.; Zanotto, E. D.; Wolke, J. G. C.; Jansen, J. A.; van den Beucken, J. J. J. P. "*Incorporation of bioactive glass in calcium phosphate cement: An evaluation*"; Acta Biomater. 2013**, 9** (3), 5728-5739.

(34) Chan, G.; Mooney, D. J. "*New materials for tissue engineering: towards greater control over the biological response*"; Trends Biotechnol. 2008**, 26** (7), 382-392.

(35) Orman, S. *Toughening of Photopolymers for Additive Manufacturing of Bone Replacements*. Dissertation, TU Wien, 2018.

(36) Hench, L. L.; Boccaccini, A. R.; Day, R. M.; Gabe, S. M. "*Third-Generation Gene-Activating Biomaterials*"; Mater. Sci. Forum 2003**, 426-432**, 179-184.

(37) Heinemann, S.; Gelinsky, M.; Worch, H.; Hanke, T. "*Resorbierbare Knochenersatzmaterialien*"; Der Orthopäde 2011**, 40** (9), 761-773.

(38) Moore, W. R.; Graves, S. E.; Bain, G. I. "*Synthetic bone graft substitutes*"; ANZ J. Surg. 2001**, 71** (6), 354-361.

(39) Kuehn, K.-D.; Berberich, C.; Bösebeck, H. "*Knochenersatzwerkstoffe als lokale Wirkstoffträger: Aktueller Stand bei Ersatzstoffen verschiedenen Ursprungs*". 2017; Vol. 47.

(40) Williams, D., Biomaterials Science: An Introduction to Materials in Medicine, Buddy D. Ratner, et al.(Eds.), Academic Press (2004),(864pp., $95/£ 49.99), ISBN: 0-12-582463-7. Elsevier: 2005.

(41) Wang, Y.; Wang, K.; Li, X.; Wei, Q.; Chai, W.; Wang, S.; Che, Y.; Lu, T.; Zhang, B. "*3D fabrication and characterization of phosphoric acid scaffold with a HA/β-TCP weight ratio of 60:40 for bone tissue engineering applications*"; PLoS One 2017**, 12** (4), e0174870-e0174870.

(42) Rezwan, K.; Chen, Q. Z.; Blaker, J. J.; Boccaccini, A. R. "*Biodegradable and bioactive porous polymer/inorganic composite scaffolds for bone tissue engineering*"; Biomaterials 2006**, 27** (18), 3413-3431.

(43) Staiger, M. P.; Pietak, A. M.; Huadmai, J.; Dias, G. "*Magnesium and its alloys as orthopedic biomaterials: A review*"; Biomaterials 2006**, 27** (9), 1728-1734.

(44) Hartwig, A. "*Role of magnesium in genomic stability*"; Mutation Research/Fundamental and Molecular Mechanisms of Mutagenesis 2001**, 475** (1), 113-121.

(45) Witte, F.; Kaese, V.; Haferkamp, H.; Switzer, E.; Meyer-Lindenberg, A.; Wirth, C. J.; Windhagen, H. "*In vivo corrosion of four magnesium alloys and the associated bone response*"; Biomaterials 2005**, 26** (17), 3557-3563.

(46) Sedelnikova, M.; Komarova, E.; Sharkeev, Y.; V. Tolkacheva, T.; Khlusov, I.; Sheikin, V. "*Bioactive calcium phosphate coatings on metallic implants*". 2017; Vol. 1882, p 020062.

(47) Horowitz, R.; Leventis, M.; D Rohrer, M.; S Prasad, H. "*Bone grafting: History, rationale, and selection of materials and techniques*". 2014; Vol. 35, p 1-6;quiz7.

(48) Lee, S.-H.; Shin, H. "*Matrices and scaffolds for delivery of bioactive molecules in bone and cartilage tissue engineering*"; Adv. Drug Del. Rev. 2007**, 59** (4), 339-359.

(49) Cai, S.; Liu, Y.; Zheng Shu, X.; Prestwich, G. D. "*Injectable glycosaminoglycan hydrogels for controlled release of human basic fibroblast growth factor*"; Biomaterials 2005**, 26** (30), 6054-6067.

(50) Rossi, C. A.; Flaibani, M.; Blaauw, B.; Pozzobon, M.; Figallo, E.; Reggiani, C.; Vitiello, L.; Elvassore, N.; Coppi, P. D. "*In vivo tissue engineering of functional skeletal muscle by freshly isolated satellite cells embedded in a photopolymerizable hydrogel*"; The FASEB Journal 2011**, 25** (7), 2296-2304.

(51) Zhang, Y.; Heher, P.; Hilborn, J.; Redl, H.; Ossipov, D. A. "*Hyaluronic acid-fibrin interpenetrating double network hydrogel prepared in situ by orthogonal disulfide cross-linking reaction for biomedical applications*"; Acta Biomater. 2016**, 38**, 23-32.

(52) Matsumoto, Y.; Arai, K.; Momose, H.; Kuroyanagi, Y. "*Development of a Wound Dressing Composed of a Hyaluronic Acid Sponge Containing Arginine*"; J. Biomater. Sci. Polym. Ed. 2009**, 20** (7-8), 993-1004.

(53) S. Nair, L.; T. Laurencin, C. "*Biodegradable Polymers as Biomaterials*". 2007; Vol. 32, p 762-798.

(54) George, M.; Abraham, T. E. "*Polyionic hydrocolloids for the intestinal delivery of protein drugs: Alginate and chitosan — a review*"; J. Controlled Release 2006**, 114** (1), 1-14.

(55) Sutter, M.; Siepmann, J.; Hennink, W. E.; Jiskoot, W. "*Recombinant gelatin hydrogels for the sustained release of proteins*"; J. Controlled Release 2007**, 119** (3), 301-312.

(56) Hori, K.; Sotozono, C.; Hamuro, J.; Yamasaki, K.; Kimura, Y.; Ozeki, M.; Tabata, Y.; Kinoshita, S. "*Controlled-release of epidermal growth factor from cationized gelatin hydrogel enhances corneal epithelial wound healing*"; J. Controlled Release 2007**, 118** (2), 169-176.

(57) Changhong, Y.; Xiongwei, L.; Xiaoli, C.; Danqing, W.; Dachang, Z.; Tianzhi, T.; Kitano, H. "*Anticancer gelatin microspheres with multiple functions*"; Biomaterials 1991**, 12** (7), 640-644.

(58) Egger, M.; Tovar, G. E. M.; Hoch, E.; Southan, A. "*Gelatin methacrylamide as coating material in cell culture*"; Biointerphases 2016**, 11** (2), 021007.

(59) Salgado, A. J.; Coutinho, O. P.; Reis, R. L. "*Bone Tissue Engineering: State of the Art and Future Trends*"; Macromol. Biosci. 2004**, 4** (8), 743-765.

(60) Katti, D. S.; Lakshmi, S.; Langer, R.; Laurencin, C. T. "*Toxicity, biodegradation and elimination of polyanhydrides*"; Adv. Drug Del. Rev. 2002**, 54** (7), 933-961.

(61) Tangpasuthadol, V.; Pendharkar, S. M.; Kohn, J. "*Hydrolytic degradation of tyrosine-derived polycarbonates, a class of new biomaterials. Part I: Study of model compounds*"; Biomaterials 2000**, 21** (23), 2371-2378.

(62) Rainbolt, E. A.; Washington, K. E.; Biewer, M. C.; Stefan, M. C. "*Recent developments in micellar drug carriers featuring substituted poly(ε-caprolactone)s*"; Polymer Chemistry 2015**, 6** (13), 2369-2381.

(63) Xiao, Y.; Yuan, M.; Zhang, J.; Yan, J.; Lang, M. "*Functional Poly(ε-caprolactone) Based Materials: Preparation, Self-assembly and Application in Drug Delivery*"; Curr. Top. Med. Chem. 2014**, 14** (6), 781-818.

(64) Yang, P.; Zhu, G.; Xu, S.; Zhang, X.; Shen, X.; Cui, X.; Gao, Y.; Nie, J. "*A novel shape memory poly(ε-caprolactone) network via UV-triggered thiol-ene reaction*"; J. Polym. Sci., Part B: Polym. Phys. 2017**, 55** (8), 692-701.

(65) Siparsky, G. L.; Voorhees, K. J.; Miao, F. "*Hydrolysis of Polylactic Acid (PLA) and Polycaprolactone (PCL) in Aqueous Acetonitrile Solutions: Autocatalysis*"; J. Environ. Polymer Degradation 1998**, 6** (1), 31-41.

(66) S, S.; YT, K.; T, S.; M, G.; E, P.; P, K.; P, R. "*Immune response to polyglycolic acid implants*"; The Journal of Bone and Joint Surgery. British volume 1990**, 72-B** (4), 597-600.

(67) Jandt, K. D. "*Evolutions, Revolutions and Trends in Biomaterials Science – A Perspective*"; Adv. Eng. Mater. 2007**, 9** (12), 1035-1050.

(68) Mautner, A.; Qin, X.; Kapeller, B.; Russmueller, G.; Koch, T.; Stampfl, J.; Liska, R. "*Efficient Curing of Vinyl Carbonates by Thiol-Ene Polymerization*"; Macromol. Rapid Commun. 2012**, 33** (23), 2046-2052.

(69) Heller, C.; Schwentenwein, M.; Varga, F.; Stampfl, J.; Liska, R. "*Additive Manufacturing Technologies for the 3D Fabrication of Biocompatible and Biodegradable Photopolymers*"; MRS Proceedings 2009**, 1239**, 1239-VV08-05.

(70) Schüller-Ravoo, S.; Feijen, J.; Grijpma, D. W. "*Flexible, elastic and tear-resistant networks prepared by photo-crosslinking poly(trimethylene carbonate) macromers*"; Acta Biomater. 2012**, 8** (10), 3576-3585.

(71) Anseth, K. S.; Shastri, V. R.; Langer, R. "*Photopolymerizable degradable polyanhydrides with osteocompatibility*"; Nat. Biotechnol. 1999**, 17**, 156.

(72) Guo, B.; Ma, P. X. "*Synthetic biodegradable functional polymers for tissue engineering: a brief review*"; Science China Chemistry 2014**, 57** (4), 490-500.

(73) Betz, M. W.; Modi, P. C.; Caccamese, J. F.; Coletti, D. P.; Sauk, J. J.; Fisher, J. P. "*Cyclic acetal hydrogel system for bone marrow stromal cell encapsulation and osteodifferentiation*"; Journal of Biomedical Materials Research Part A 2008**, 86A** (3), 662-670.

(74) Gebhardt, A. "*Rapid Prototyping- Werkzeuge für die schnelle Produktentstehung*". 2 ed.; Carl Hanser Verlag: München-Wien: 2000.

(75) Leong, K. F.; Cheah, C. M.; Chua, C. K. "*Solid freeform fabrication of three-dimensional scaffolds for engineering replacement tissues and organs*"; Biomaterials 2003**, 24** (13), 2363-2378.

(76) Hutmacher, D. W.; Sittinger, M.; Risbud, M. V. "*Scaffold-based tissue engineering: rationale for computer-aided design and solid free-form fabrication systems*"; Trends Biotechnol. 2004**, 22** (7), 354-362.

(77) Guvendiren, M.; Lu, H. D.; Burdick, J. A. "*Shear-thinning hydrogels for biomedical applications*"; Soft Matter 2012**, 8** (2), 260-272.

(78) Yeong, W.-Y.; Chua, C.-K.; Leong, K.-F.; Chandrasekaran, M. "*Rapid prototyping in tissue engineering: challenges and potential*"; Trends Biotechnol. 2004**, 22** (12), 643-652.

(79) Gibas, I.; Janik, H. "*Review: Synthetic polymer hydrogels for biomedical applications*". 2010; Vol. 4, p 297-304.

(80) Ligon, S. C.; Liska, R.; Stampfl, J.; Gurr, M.; Mülhaupt, R. "*Polymers for 3D Printing and Customized Additive Manufacturing*"; Chem. Rev. 2017**, 117** (15), 10212-10290.

(81) Faber, J.; Berto, P. M.; Quaresma, M. "*Rapid prototyping as a tool for diagnosis and treatment planning for maxillary canine impaction*"; Am. J. Orthod. Dentofacial Orthop. 2006**, 129** (4), 583-589.

(82) Kim, M.-J.; Lee, S.-R.; Lee, M.-Y.; Sohn, J. W.; Yun, H. G.; Choi, J. Y.; Jeon, S. W.; Suh, T. S. "*Characterization of 3D printing techniques: Toward patient specific quality assurance spine-shaped phantom for stereotactic body radiation therapy*"; PLoS One 2017**, 12** (5), e0176227-e0176227.

(83) custompartnet Jetted Photopolymer. http://www.custompartnet.com/wu/jetted-photopolymer (accessed 23.04.2019).

(84) Billiet, T.; Vandenhaute, M.; Schelfhout, J.; Van Vlierberghe, S.; Dubruel, P. "*A review of trends and limitations in hydrogel-rapid prototyping for tissue engineering*"; Biomaterials 2012**, 33** (26), 6020-6041.

(85) Tesavibul, P.; Felzmann, R.; Gruber, S.; Liska, R.; Thompson, I.; Boccaccini, A. R.; Stampfl, J. "*Processing of 45S5 Bioglass (R) by lithography-based additive manufacturing*"; Mater. Lett. 2012**, 74**, 81-84.

(86) Bakhtina, N. A.; Loeffelmann, U.; MacKinnon, N.; Korvink, J. G. "*Two-Photon Nanolithography Enhances the Performance of an Ionic Liquid–Polymer Composite Sensor*"; Adv. Funct. Mater. 2015**, 25** (11), 1683-1693.

(87) Zerobin, E. "*Two-Photon Structured Hydrogels based on Hyaluronic Acid for Applications in Tissue Engineering*"; 2017.

(88) Formlabs Formlabs Ultimate guide to stereolithography (SLA) 3D prining. https://formlabs.com/blog/ultimate-guide-to-stereolithography-sla-3d-printing/#sla-systems (accessed 06.04.2019).

(89) Schwentenwein, M.; Schneider, P.; Homa, J. "*Lithography-Based Ceramic Manufacturing: A Novel Technique for Additive Manufacturing of High-Performance Ceramics*"; Advances in Science and Technology 2014**, 88**, 60-64.

(90) Xing, J.-F.; Zheng, M.-L.; Duan, X.-M. "*Two-photon polymerization microfabrication of hydrogels: an advanced 3D printing technology for tissue engineering and drug delivery*"; Chem. Soc. Rev. 2015**, 44** (15), 5031-5039.

(91) Wang, W.-K.; Sun, Z.-B.; Zheng, M.-L.; Dong, X.-Z.; Zhao, Z.-S.; Duan, X.-M. "*Magnetic Nickel–Phosphorus/Polymer Composite and Remotely Driven Three-Dimensional Micromachine Fabricated by Nanoplating and Two-Photon Polymerization*"; The Journal of Physical Chemistry C 2011**, 115** (22), 11275-11281.

(92) Kawata, S.; Sun, H.-B.; Tanaka, T.; Takada, K. "*Finer features for functional microdevices*"; Nature 2001**, 412** (6848), 697-698.

(93) Liska, R.; Schuster, M.; Inführ, R.; Turecek, C.; Fritscher, C.; Seidl, B.; Schmidt, V.; Kuna, L.; Haase, A.; Varga, F.; Lichtenegger, H.; Stampfl, J. "*Photopolymers for rapid prototyping*"; Journal of Coatings Technology and Research 2007**, 4** (4), 505-510.

(94) Göppert-Mayer, M. "*Elementary processes with two quantum transitions*"; Annalen der Physik 2009**, 18** (7-8), 466-479.

(95) Hageman, H. J. "*Photoinitiators for free radical polymerization*". 1985; Vol. 13, p 123–150.

(96) Davis, K. A.; Burdick, J. A.; Anseth, K. S. "*Photoinitiated crosslinked degradable copolymer networks for tissue engineering applications*"; Biomaterials 2003**, 24** (14), 2485-2495.

(97) Gorsche, C.; Seidler, K.; Knaack, P.; Dorfinger, P.; Koch, T.; Stampfl, J.; Moszner, N.; Liska, R. "*Rapid formation of regulated methacrylate networks yielding tough materials for lithography-based 3D printing*"; Polymer Chemistry 2016**, 7** (11), 2009-2014.

(98) Fouassier, J.-P.; Rabek, J. F. "*Radiation curing in polymer science and technology*". Elsevier Applied Science: London; New York, 1993.

(99) Hufendiek, A.; Lingier, S.; Du Prez, F. E. "*Thermoplastic polyacetals: chemistry from the past for a sustainable future?*"; Polymer Chemistry 2018.

(100) Bulmus, V.; Chan, Y.; Nguyen, Q.; Tran, H. L. "*Synthesis and Characterization of Degradable p(HEMA) Microgels: Use of Acid-Labile Crosslinkers*"; Macromol. Biosci. 2007**, 7** (4), 446-455.

(101) Liu, B.; Thayumanavan, S. "*Substituent Effects on the pH Sensitivity of Acetals and Ketals and Their Correlation with Encapsulation Stability in Polymeric Nanogels*"; J. Am. Chem. Soc. 2017**, 139** (6), 2306-2317.

(102) Li, S. "*Hydrolytic degradation characteristics of aliphatic polyesters derived from lactic and glycolic acids*"; J. Biomed. Mater. Res. 1999**, 48** (3), 342-353.

(103) Delaissé, J.-M.; Andersen, T. L.; Engsig, M. T.; Henriksen, K.; Troen, T.; Blavier, L. "*Matrix metalloproteinases (MMP) and cathepsin K contribute differently to osteoclastic activities*"; Microsc. Res. Tech. 2003**, 61** (6), 504-513.

(104) Qin, A.; Cheng, T. S.; Pavlos, N. J.; Lin, Z.; Dai, K. R.; Zheng, M. H. "*V-ATPases in osteoclasts: Structure, function and potential inhibitors of bone resorption*"; The International Journal of Biochemistry & Cell Biology 2012**, 44** (9), 1422-1435.

(105) IUPAC, Acetals. in *Compendium of Chemical Terminology, 2nd ed. (the "Gold Book")*, Wilkinson, C. b. A. D. M. a. A., Ed. Online version (2019-) created by S. J. Chalk.: Blackwell Scientific Publications, Oxford (1997).

(106) IUPAC, Ketals. in *Compendium of Chemical Terminology, 2nd ed. (the "Gold Book")*, Wilkinson, C. b. A. D. M. a. A., Ed. Online version (2019-) created by S. J. Chalk: Blackwell Scientific Publications, Oxford (1997).

(107) Marrian, S. F. "*The Chemical Reactions of Pentaerythritol and its Derivatives*"; Chem. Rev. 1948**, 43** (1), 149-202.

(108) Bograchov, E. "*Exchange Reactions between Aldehydeacetals and Aldehydes. I*"; J. Am. Chem. Soc. 1950**, 72** (5), 2268-2270.

(109) Jin, T.-S.; Wang, H.-X.; Wang, K.-F.; Li, T.-S. "*Synthesis of diacetals from aldehydes and ketones with pentaerythritol catalyzed by silica sulfate under microwave irradiation*"; Synth. Commun. 2004**, 34** (16), 2993-2999.

(110) Lee, K. S.; Kim, H. M.; Rhee, J. M.; Lee, S. M. "*Synthesis and properties of processable rigid polymers containing spiroacetal moieties*"; Makromol. Chem. 1991**, 192** (5), 1033-40.

(111) Shaabani, A.; Maleki, A. "*Cellulose sulfuric acid as a bio-supported and recyclable solid acid catalyst for the one-pot three-component synthesis of α-amino nitriles*"; Applied Catalysis A: General 2007**, 331**, 149-151.

(112) Shaterian, H. R.; Rigi, F. "*Acetalization of Carbonyl Compounds as Pentaerythritol Diacetals and Diketals in the Presence of Cellulose Sulfuric Acid as an Efficient, Biodegradable and Reusable Catalyst*"; Chin. J. Chem. 2012**, 30** (3), 695-698.

(113) Pawar, R. R.; Gosai, K. A.; Bhatt, A. S.; Kumaresan, S.; Lee, S. M.; Bajaj, H. C. "*Clay catalysed rapid valorization of glycerol towards cyclic acetals and ketals*"; RSC Adv. 2015**, 5** (102), 83985-83996.

(114) Jermy, B. R.; Pandurangan, A. "*Efficient synthesis of diacetal of pentaerythritol under microwave irradiation using heteropoly acid H3PW12O40*"; Catal. Commun. 2006**, 7** (12), 921-925.

(115) Jin, T.-S.; Ma, Y.-R.; Li, T.-S.; Wang, J.-X. "*A practical and efficient procedure for preparation of diacetals from 2,2-bis(hydroxymethyl)-1,3-propanediol with aldehydes and ketones catalyzed by anhydrous ferrous sulfate*"; J. Chem. Res., Synop. 1999**,** (4), 268-269.

(116) Ummadisetti, C.; Rachapudi, B. N. P.; Bethala, L. A. P. D. "*Glycerol-based SO3H-Carbon Catalyst: A green recyclable catalyst for the chemoselective synthesis of pentaerythritol diacetals*"; European Journal of Chemistry 2014**, 5** (3), 536-540.

(117) Lingier, S.; Espeel, P.; Suarez, S. S.; Türünç, O.; De Wildeman, S.; Du Prez, F. E. "*Renewable thermoplastic polyurethanes containing rigid spiroacetal moieties*"; Eur. Polym. J. 2015**, 70**, 232-239.

(118) Gillies, E. R.; Goodwin, A. P.; Fréchet, J. M. J. "*Acetals as pH-Sensitive Linkages for Drug Delivery*"; Bioconjugate Chem. 2004**, 15** (6), 1254-1263.

(119) Ulbrich, K.; Šubr, V. r. "*Polymeric anticancer drugs with pH-controlled activation*"; Adv. Drug Del. Rev. 2004**, 56** (7), 1023-1050.

(120) Shenoi, R. A.; Lai, B. F. L.; Imran ul-haq, M.; Brooks, D. E.; Kizhakkedathu, J. N. "*Biodegradable polyglycerols with randomly distributed ketal groups as multi-functional drug delivery systems*"; Biomaterials 2013**, 34** (25), 6068-6081.

(121) Gillies, E. R.; Fréchet, J. M. J. "*A new approach towards acid sensitive copolymer micelles for drug delivery*"; Chem. Commun. 2003**,** (14), 1640-1641.

(122) Paramonov, S. E.; Bachelder, E. M.; Beaudette, T. T.; Standley, S. M.; Lee, C. C.; Dashe, J.; Fréchet, J. M. J. "*Fully Acid-Degradable Biocompatible Polyacetal Microparticles for Drug Delivery*"; Bioconjugate Chem. 2008**, 19** (4), 911-919.

(123) Wei, H.; Zhuo, R.-X.; Zhang, X.-Z. "*Design and development of polymeric micelles with cleavable links for intracellular drug delivery*"; Prog. Polym. Sci. 2013**, 38** (3), 503-535.

(124) Binauld, S.; Stenzel, M. H. "*Acid-degradable polymers for drug delivery: a decade of innovation*"; Chem. Commun. 2013**, 49** (21), 2082-2102.

(125) Wang, Y.; Morinaga, H.; Sudo, A.; Endo, T. "*Synthesis of amphiphilic polyacetal by polycondensation of aldehyde and polyethylene glycol as an acid-labile polymer for controlled release of aldehyde*"; J. Polym. Sci., Part A: Polym. Chem. 2011**, 49** (3), 596-602.

(126) Lee, A. S. Y.; Cheng, C. L. "*A novel and selective method for hydrolysis of acetals and ketals*"; Tetrahedron 1997**, 53** (42), 14255-14262.

(127) Moreau, J. L.; Kesselman, D.; Fisher, J. P. "*Synthesis and properties of cyclic acetal biomaterials*"; Journal of Biomedical Materials Research Part A 2007**, 81A** (3), 594-602.

(128) Falco, E. E.; Roth, J. S.; Fisher, J. P. "*EH Networks as a Scaffold for Skeletal Muscle Regeneration in Abdominal Wall Hernia Repair*"; J. Surg. Res. 2008**, 149** (1), 76-83.

(129) Sachlos, E.; Czernuszka, J. T. "*Making tissue engineering scaffolds work. Review: the application of solid freeform fabrication technology to the production of tissue engineering scaffolds*"; European cells & materials 2003**, 5**, 29-39; discussion 39-40.

(130) Falco, E. E.; Patel, M.; Fisher, J. P. "*Recent Developments in Cyclic Acetal Biomaterials for Tissue Engineering Applications*"; Pharm. Res. 2008**, 25** (10), 2348-2356.

(131) Hu, X.; Yang, T.; Gu, R.; Cui, Y.; Yuan, C.; Ge, H.; Wu, W.; Li, W.; Chen, Y. "*A degradable polycyclic cross-linker for UV-curing nanoimprint lithography*"; Journal of Materials Chemistry C 2014**, 2** (10), 1836-1843.

(132) Amato, D. V.; Amato, D. N.; Blancett, L. T.; Mavrodi, O. V.; Martin, W. B.; Swilley, S. N.; Sandoz, M. J.; Shearer, G.; Mavrodi, D. V.; Patton, D. L. "*A bio-based pro-antimicrobial polymer network via degradable acetal linkages*"; Acta Biomater. 2018**, 67**, 196-205.

(133) Kaihara, S.; Matsumura, S.; Fisher, J. P. "*Synthesis and Properties of Poly[poly(ethylene glycol)-co-cyclic acetal] Based Hydrogels*"; Macromolecules 2007**, 40** (21), 7625-7632.

(134) Patel, M.; Patel, K.; Caccamese, J.; P Coletti, D.; Sauk, J.; Fisher, J. "*Characterization of cyclic acetal hydroxyapatite nanocomposites for craniofacial tissue engineering*"; Journal of biomedical materials research. Part A 2010**, 94**, 408-18.

(135) Bryant, S. J.; Nuttelman, C. R.; Anseth, K. S. "*Cytocompatibility of UV and visible light photoinitiating systems on cultured NIH/3T3 fibroblasts in vitro*"; J. Biomater. Sci. Polym. Ed. 2000**, 11** (5), 439-57.

(136) Heller, C.; Schwentenwein, M.; Russmueller, G.; Varga, F.; Stampfl, J.; Liska, R. "*Vinyl esters: Low cytotoxicity monomers for the fabrication of biocompatible 3D scaffolds by lithography based additive manufacturing*"; J. Polym. Sci., Part A: Polym. Chem. 2009**, 47** (24), 6941-6954.

(137) Heller, C.; Schwentenwein, M.; Russmüller, G.; Koch, T.; Moser, D.; Schopper, C.; Varga, F.; Stampfl, J.; Liska, R. "*Vinylcarbonates and vinylcarbamates: Biocompatible monomers for radical photopolymerization*"; J. Polym. Sci., Part A: Polym. Chem. 2011**, 49** (3), 650-661.

(138) Orman, S.; Hofstetter, C.; Aksu, A.; Reinauer, F.; Liska, R.; Baudis, S. "*Toughness enhancers for bone scaffold materials based on biocompatible photopolymers*"; J. Polym. Sci., Part A: Polym. Chem. 2019**, 57** (2), 110-119.

(139) Patnaik, P. "*A Comprehensive Guide to the Hazardous Properties of Chemical Substances*". Wiley: 2007.

(140) Cohen, S. M.; Lavin, E. "*Polyspiroacetal resins. Part I. Initial preparation and characterization*"; J. Appl. Polym. Sci. 1962**, 6** (23), 503-507.

(141) Engell, K. M.; McClelland, R. A.; Sørensen, P. E. "*The decomposition of methyl hemiacetals of benzaldehyde in aqueous solution: a study of the effect of aromatic substitution*"; Can. J. Chem. 1999**, 77** (5-6), 978-989.

(142) Hirose, S.; Hatakeyama, T.; Hatakeyama, H. "*SYNTHESIS AND THERMAL ANALYSIS OF POLYESTERS HAVING SPIRO-DIOXANE RINGS AND GUAIACYL UNITS*"; Sen'i Gakkaishi 1982**, 38** (11), T507-T511.

(143) Liang, Y.; Guo, J.-j.; Liu, X.-m.; Wei, R.-b. "*Chiral Separation of Spiro-compounds and Determination Configuration*"; Chem. Res. Chin. Univ. 2008**, 24** (4), 441-444.

(144) Zakharova, E.; Martinez de Ilarduya, A.; Leon, S.; Munoz-Guerra, S. "*Sugar-based bicyclic monomers for aliphatic polyesters: a comparative appraisal of acetalized alditols and isosorbide*"; Des. Monomers Polym. 2017**, 20** (1), 157-166.

(145) Fischer Esterification. https://www.organic-chemistry.org/namedreactions/fischer-esterification.shtm.

(146) Schotten-Baumann Reaction. https://www.organic-chemistry.org/namedreactions/schotten-baumann-reaction.shtm.

(147) Wang, Z., Einhorn Acylation. in *Comprehensive Organic Name Reactions and Reagents*, 2010; pp 967-970.

(148) Zhao, Y.-C.; Zhang, L.-M.; Wang, T.; Han, B.-H. "*Microporous organic polymers with acetal linkages: synthesis, characterization, and gas sorption properties*"; Polymer Chemistry 2014**, 5** (2), 614-621.

(149) Kwon, Y. J.; Standley, S. M.; Goodwin, A. P.; Gillies, E. R.; Fréchet, J. M. J. "*Directed Antigen Presentation Using Polymeric Microparticulate Carriers Degradable at Lysosomal pH for Controlled Immune Responses*"; Mol. Pharm. 2005**, 2** (1), 83-91.

(150) Murthy, N.; Xu, M.; Schuck, S.; Kunisawa, J.; Shastri, N.; Fréchet, J. M. J. "*A macromolecular delivery vehicle for protein-based vaccines: Acid-degradable protein-loaded microgels*"; Proceedings of the National Academy of Sciences 2003**, 100** (9), 4995.

(151) Fife, T. H.; Jao, L. K. "*Substituent Effects in Acetal Hydrolysis*"; The Journal of Organic Chemistry 1965**, 30** (5), 1492-1495.

(152) Deslongchamps, P.; Dory, Y. L.; Li, S. "*The Relative Rate of Hydrolysis of a Series of Acyclic and Six-Membered Cyclic Acetals, Ketals, Orthoesters, and Orthocarbonates*"; Tetrahedron 2000**, 56** (22), 3533-3537.

(153) Wuts, P. G. M.; Editor "*Greene's Protective Groups in Organic Synthesis, 5th Edition*". Wiley: 2014; p 1400 pp.

(154) Vohr, H. W. "*Toxikologie: Band 2 - Toxikologie der Stoffe*". Wiley: 2012.

(155) Ratcliffe, L. P. D.; Ryan, A. J.; Armes, S. P. "*From a Water-Immiscible Monomer to Block Copolymer Nano-Objects via a One-Pot RAFT Aqueous Dispersion Polymerization Formulation*"; Macromolecules 2013**, 46** (3), 769-777.

(156) Leibler, L.; Nicolay, R.; Rottger, M. Polymer compositions comprising cross-linked polymers comprising boronic ester functions enabling exchange reactions, process for preparing them and their use. 2017.

(157) Zheng, Z.; Luo, M.; Yu, J.; Wang, J.; Ji, J. "*Novel Process for 1,3-Dihydroxyacetone Production from Glycerol. 1. Technological Feasibility Study and Process Design*"; Ind. Eng. Chem. Res. 2012**, 51** (9), 3715-3721.

(158) Wildling, L.; Unterauer, B.; Zhu, R.; Rupprecht, A.; Haselgrübler, T.; Rankl, C.; Ebner, A.; Vater, D.; Pollheimer, P.; Pohl, E. E.; Hinterdorfer, P.; Gruber, H. J. "*Linking of Sensor Molecules with Amino Groups to Amino-Functionalized AFM Tips*"; Bioconjugate Chem. 2011**, 22** (6), 1239-1248.

(159) Blake, M. E.; Bartlett, K. L.; Jones, M. "*A m-Benzyne to o-Benzyne Conversion through a 1,2-Shift of a Phenyl Group*"; J. Am. Chem. Soc. 2003**, 125** (21), 6485-6490.

(160) Wichterle, O.; LÍM, D. "*Hydrophilic Gels for Biological Use*"; Nature 1960**, 185**, 117.

(161) Corkhill, P. H.; Hamilton, C. J.; Tighe, B. J. "*Synthetic hydrogels VI. Hydrogel composites as wound dressings and implant materials*"; Biomaterials 1989**, 10** (1), 3-10.

(162) Netti, P. A.; Shelton, J. C.; Revell, P. A.; Pirie, G.; Smith, S.; Ambrosio, L.; Nicolais, L.; Bonfield, W. "*Hydrogels as an interface between bone and an implant*"; Biomaterials 1993**, 14** (14), 1098-1104.

(163) Gorsche, C.; Harikrishna, R.; Baudis, S.; Knaack, P.; Husar, B.; Laeuger, J.; Hoffmann, H.; Liska, R. "*Real Time-NIR/MIR-Photorheology: A Versatile Tool for the in Situ Characterization of Photopolymerization Reactions*"; Anal. Chem. 2017**, 89** (9), 4958-4968.

(164) Vivadent, I. *State of the Art: Photopolymerization in dentistry*; 19; July 2013, 2013.

(165) Orman, S. *Biocompatible Composite Photopolymers for 3D Printing*. TU Wien, 2015.

(166) Tamada, J. A.; Langer, R. "*Erosion kinetics of hydrolytically degradable polymers*"; Proc. Natl. Acad. Sci. U. S. A. 1993**, 90** (2), 552-556.

(167) Göpferich, A. "*Mechanisms of polymer degradation and erosion*"; Biomaterials 1996**, 17** (2), 103-114.

(168) Jermy, B. R.; Pandurangan, A. "*H3PW12O40 supported on MCM-41 molecular sieves: An effective catalyst for acetal formation*"; Appl. Catal., A 2005**, 295** (2), 185-192.

(169) https://www.alfa-chemistry.com/glycerol-monomethacrylate-mixture-of-isomers-cas-5919-74-4-item-283272.htm (accessed 24.06.2019).